UNIVERSITAT DE BARCELONA

CPEB4 regulation of vasculogenic mimicry in liver cancer: mechanisms and therapeutic implications

Beatriz Iralde Cárdenas

UNIVERSITAT DE BARCELONA

FACULTAT DE FARMÀCIA I CIÈNCIES DE L'ALIMENTACIÓ

CPEB4 regulation of vasculogenic mimicry in liver cancer: mechanisms and therapeutic implications

BEATRIZ IRALDE CÁRDENAS 2024

Faculty of Pharmacy and Food Sciences

Doctoral program in Biomedicine, University of Barcelona

CPEB4 regulation of vasculogenic mimicry in liver cancer: mechanisms and therapeutic implications

This thesis was conducted by Beatriz Iralde Cárdenas under the supervision of Dr. Mercedes Fernández Lobato at the Institut d'Investigacions Biomèdiques August Pi i Sunyer (IDIBAPS) in Barcelona, within the research group "Translational Control of Liver Disease and Cancer".

This thesis is submitted in pursuit of the Doctoral degree from the University of Barcelona.

Mercedes Fernández Lobato	Albert Tauler Girona	Beatriz Iralde Cárdenas
Thesis director	*Thesis tutor*	*Doctoral student*

Barcelona September 2024

Table of content

Abbreviations

4E-BPs: 4E-binding proteins

ABC: ATP-binding cassette

AFP: alpha-fetoprotein

AGM: aorta-gonad-mesonephros

ALD: alcohol-related liver disease

APPs: acute phase proteins

APS: ammonium persulfate

ASD: autism spectrum disorders

ATGL: adipose triglyceride lipase

ATP: adenosine triphosphate

AU: arbitrary units

BCLC: Barcelona Clinic Liver Cancer

BSA: bovine serum albumin

C/EBP: CCAAT/enhancer-binding protein

CCNA2: cyclin-A2

CCNE1: G1/S-specific cyclin-E1

CCR2: C-C chemokine receptor type 2

CD133: prominin-1

CD31: platelet endothelial cell adhesion molecule

cDNA: complementary deoxyribonucleic acid

CEs: cholesterol esters

CLD: chronic liver disease

c-myc: MYC proto-oncogene

CMV: cytomegalovirus

CPE: cytoplasmic polyadenylation elements

CPEB: cytoplasmic polyadenylation element-binding protein

CPEB4: Cytoplasmic Polyadenylation Element Binding Protein 4

CPSF: cleavage and polyadenylation specificity factor

CRC: colorectal cancer

CSC: cancer stem cell

CSF1R: colony-stimulating factor 1 receptor

CT: computed tomography

CTD: C-terminal RNA-binding domain

CTLA-4: cytotoxic T-lymphocyte protein 4

DAAs: direct-acting antiviral

DAB: 3,3'-diaminobenzidine

DAMPs: damage-associated molecular patterns

DAPI: 4',6-diamidino-2-phenylindole

DCs: dendritic cells

ddH_2O: double-distilled water

DEB: drug-eluting beads

DEN: diethylnitrosamine

DGAT1: diacylglycerol O-acyltransferase 1

DMEM/F-12: Dulbecco's Modified Eagle Medium: Nutrient Mixture F-12

DNA: deoxyribonucleic acid

DNL: *de novo* lipogenesis

dNTPs: deoxynucleotide triphosphates

E-cadherin: epithelial-cadherin

ECs: endothelial cells

ECM: extracellular matrix

E. coli: *Escherichia coli*

eEF2K: eukaryotic elongation factor 2 kinase

EGFR: epidermal growth factor receptor

eIFs: eukaryotic translation initiation factors

eIF4E: translation initiation factor 4E

eIF4G: translation initiation factor 4G

EMEM: Eagle's Minimum Essential Medium

EMT: Epithelial-to-Mesenchymal Transition

ENV: envelope protein gene

EPCs: endothelial progenitor cells

ER: endoplasmic reticulum

FAO: fatty acid oxidation

FcγRIIb2: Fc gamma receptor IIb2

FGF-2: fibroblast growth factor-2

FGFRs: fibroblast growth factor receptors

Gag: group-specific antigen

GALT: gut-associated lymphoid tissue

GFP: green fluorescent protein

GTP: guanosine triphosphate

H&E: hematoxylin & eosin

HBV: Hepatitis B Virus

HCC: Hepatocellular Carcinoma

HCV: Hepatitis C Virus

HDLs: high-density lipoproteins

HDV: Hepatitis delta virus

HFD: high-fat diet

HIF1α: hypoxia-inducible factor 1-alpha

HRP: horseradish peroxidase

Hs: *Homo sapiens*

HSCs: Hepatic stellate cells

HuNu: Human Nuclei

IA: intussusceptive angiogenesis

ICIs: immune checkpoint inhibitors

IHC: immunohistochemistry

IF: immunofluorescence

IL-1β: interleukin-1 beta

IL-2: interleukin-2

IL-6: interleukin-6

IL-15: interleukin-15

IL-22: interleukin-22

INF-γ: interferon gamma

INT: iodonitrotetrazolium chloride

IRB: Institute for Research in Biomedicine

IRES: internal ribosome entry site

KCs: Kupffer cells

KD: knockdown

KO: knockout

LDs: lipid droplets

LDLs: Low-density lipoproteins

LDLR: low-density lipoprotein receptor

LPS: lipopolysaccharide

LRAT: lecithin retinol acyltransferase

LSECs: liver sinusoidal endothelial cells

LTR: long terminal repeat

Luc-GFP: Luciferase-GFP

Ly6C: lymphocyte antigen 6C

MAFLD: metabolic associated fatty liver disease

MAPK: mitogen-activated protein kinase

MASH: metabolic associated steatohepatitis

MASLD: metabolic dysfunction-associated steatotic liver disease

MCS: multiple cloning site

MFBs: myofibroblasts

Mm: *Mus musculus*

MMPs: matrix metalloproteinases

MOI: multiplicity of infection

mRNA: messenger ribonucleic acid

MRI: magnetic resonance imaging

mTOR: mammalian target of rapamycin

NAFLD: non-alcoholic fatty liver disease

NASH: non-alcoholic steatohepatitis

N-cadherin: neural cadherin

ND: normal diet

NK: natural killer

NKT: natural killer T

NLRP3: NOD-, LRR-, and pyrin domain-containing protein 3

Notch1: Notch receptor 1

NTD: N-terminal regulatory domain

O_2: oxygen

Ori: origin of replication

ORR: objective response rates

OS: overall survival

PABP: poly(A)-binding protein

PAMPs: pathogen-associated molecular patterns

PARN: poly(A) ribonuclease

PAS: Periodic Acid-Schiff

PB: phenobarbital

PBS: phosphate-buffered saline

PCR: polymerase chain reaction

PD-1: programmed cell death protein 1

PDGFR: platelet-derived growth factor receptor

PD-L1: programmed death-ligand 1

PFKFB3: 6-phosphofructo-2-kinase/fructose-2,6-bisphosphatase 3

PFS: progression-free survival

PGLYRP2: peptidoglycan recognition protein 2

Pol: polymerase

PRR: pattern recognition receptor

RBP: RNA-binding protein

RCTs: randomized controlled trials

REs: retinyl esters

REHs: retinyl ester hydrolases

RFA: radiofrequency ablation

RME: receptor-mediated endocytosis

RNA: ribonucleic acid

RNAi: RNA interference

ROI: region of interest

ROS: reactive oxygen species

RRMs: RNA-recognition motifs

RT-qPCR: real-time quantitative pcr

SCID: severe combined immunodeficiency

SCR: scramble

SDS: sodium dodecyl sulfate

SDS-PAGE: sodium dodecyl sulfate polyacrylamide gel electrophoresis

shRNA: short hairpin RNA

slug: Snail family transcriptional repressor 2

SRs: scavenger receptors

STAT3: signal transducer and activator of transcription 3

SVR: sustained virological response

TACE: transarterial chemoembolization

TAGs: triacylglycerols

TAMs: tumor-associated macrophages

TARE: transarterial radioembolization

TBS-T: tris buffered saline with tween-20

TEMED: tetramethylethylenediamine

TERT: telomerase reverse transcriptase

TfR: transferrin receptor

TGF: transforming growth factor

TGF-β: transforming growth factor-beta

Th: T helper

TME: tumor microenvironment

TNF-α: tumor necrosis factor-alpha

tRNA: transfer RNA

uORFs: upstream open reading frames

UPR: unfolded protein response

UTR: untranslated region

VE-cadherin: vascular endothelial cadherin

VEGF: vascular endothelial growth factor

VEGFR: vascular endothelial growth factor receptor

VEGFR2: anti-Vascular endothelial growth factor receptor 2

VLDLs: very low-density lipoproteins

VM: vasculogenic mimicry

WHO: World Health Organization

WT: wild type

Abstract

Background: Hepatocellular carcinoma (HCC) poses a significant clinical challenge due to its complex vascular abnormalities and the regulatory mechanisms underlying tumor progression. Vasculogenic mimicry (VM), a neovascularization process where cancer cells form vessel-like structures, remains poorly understood in HCC. Cytoplasmic polyadenylation element binding protein 4 (CPEB4) is a critical regulator of mRNA translation. This study aims to elucidate the role of CPEB4 in VM and its potential impact on resistance to anti-angiogenic therapies in HCC.

Objectives: The objectives of this research were (1) to investigate the capacity of liver cancer cells to perform VM both *in vitro* and *in vivo*. (2) To explore the role and underlying mechanisms of CPEB4 in regulating VM. (3) To determine whether CPEB4 affects the pro-angiogenic profile of liver cancer cells. (4) To assess the role of VM in mediating resistance to anti-angiogenic therapies in liver cancer.

Methods: This study utilized a combination of *in vitro* and *in vivo* approaches. *In vitro*, liver cancer cells were modified to be deficient for CPEB4. Matrigel assays were employed to assess VM formation of liver cancer cells. Furthermore, proliferation, anchorage-independent growth and anoikis death resistance were assessed using CPEB4 wild type (WT) and knockout (KO) or knockdown (KD) liver cancer cells. The effects of the anti-angiogenic treatment bevacizumab were evaluated to determine its impact on VM *in vitro*. *In vivo*, $CPEB4^{WT}$ and $CPEB4^{KO}$ liver cancer mouse model was analysed for detection of VM and angiogenesis through histological techniques. Xenograft studies with human HepG2 cells, $CPEB4^{SCR}$ and $CPEB4^{KD}$, were conducted to evaluate tumor vascularization.

Results: *In vitro* matrigel assays revealed that CPEB4 deficient cells formed significantly more VM structures compared to $CPEB4^{WT}$ cells, indicating that CPEB4 protects against VM. The CPEB4 regulation of VM is potentially through regulating epithelial-to-mesenchymal transition (EMT) mechanisms. Mechanistically, CPEB4 deficiency was associated with reduced expression of epithelial markers and increased expression of

mesenchymal markers, suggesting a shift to a mesenchymal phenotype, which could be mediated by transcription factors regulated by CPEB4. Treatment with bevacizumab *in vitro* showed reduced efficacy in $CPEB4^{KO}$ cells, suggesting that VM may contribute to resistance to anti-angiogenic therapies. *In vivo*, tumors developed in $CPEB4^{KO}$ mice exhibited higher VM vessel density without changes in angiogenic vessel density compared to tumors developed in $CPEB4^{WT}$ mice. Xenograft studies showed increased angiogenic vessel density in $CPEB4^{KD}$ tumors, with a trend toward more VM structures in the perinecrotic region compared to $CPEB4^{SCR}$ tumors.

Conclusion: *In vitro* liver cancer cells exhibit enhanced VM formation in the absence of CPEB4, suggesting that CPEB4 functions as a suppressor of VM. The regulation of EMT by CPEB4 likely mediates its effects on VM, with CPEB4 absence resulting in a more mesenchymal phenotype. *In vivo*, xenograft studies further reveal that CPEB4 deficiency leads to more aggressive tumor behaviour with increased angiogenesis. Additionally, $CPEB4^{KO}$ animals of liver cancer protocol showed heightened tumor aggressiveness and VM density compared to $CPEB4^{WT}$ controls. The study also highlights the role of VM in mediating resistance to anti-angiogenic therapies, with $CPEB4^{KO}$ tumor cells showing increased participation in VM structures in response to bevacizumab treatment *in vitro*. These findings suggest that a therapeutic strategy combining the simultaneous targeting of endothelial vessels and VM might be more effective in treating liver cancer. Furthermore, these results underscore the significance of CPEB4 in liver cancer progression and therapeutic resistance, offering valuable insights for future research and treatment development in the field of oncology.

Introduction

Liver anatomy and physiology

The liver, with an average weight of 1500 grams, is the largest gland in the body and the second most extensive tissue after the skin, comprising approximately 2-3% of total body weight in humans. It performs over 500 vital functions that play crucial roles in maintaining homeostasis as well as in the onset and progression of various pathologies (1).

In humans, the liver is located beneath the diaphragm on the right side of the abdominal cavity and is composed of four interconnected lobes. The anterior portion includes the large right lobe and the smaller left lobe, while the visceral surface features the caudate lobe above and the quadrate lobe below, positioned between the right and left lobes. The liver is encased in the Glisson's capsule, a collagenous sheath that extends into the liver's internal stroma and is stabilized by various ligaments. Beneath the right lobe lies the gallbladder (2).

In mice, which are frequently used in liver research studies, the liver has a subtle different structure and is proportionally larger, representing 3-5% of the mouse's total body weight. It occupies most of the upper abdominal cavity. Mice liver consists of four main lobes not separated by ligaments: right, left, caudate and middle lobes. The right and middle lobes each have two segments connected by a small tissue area. The gallbladder is situated between the two segments of the middle lobe, marking a notable feature at the central convergence of all lobes (3).

Despite these differences in macroscopic anatomy, both species share comparable blood supply routes and microanatomy, which are essential for the liver's functions. The hepatic artery supplies oxygen (O_2) to support the liver's high metabolic activity, receiving blood from two primary sources: approximately 80% of this blood is venous, while the remaining 20% is arterial, delivering vital O_2 and nutrients to the tissues. Venous blood exits the liver through the hepatic vein, while lymphatic fluid drains into the thoracic duct. The liver's role in the circulatory system is fundamental for metabolite

collection, transformation, storage and detoxification of harmful substances (3). These detoxification processes are mediated by bile, which is critical for lipid digestion (2).

Within the portal triads, hepatocytes are separated from endothelial cells (ECs) by the space of Disse, which contains hepatocyte microvilli that facilitate the exchange of macromolecules between the sinusoidal lumen and hepatocytes. This mechanism allows hepatocytes to release and metabolize essential macromolecules in the bloodstream. The liver sinusoids also house Kupffer cells (KCs), specialized macrophages responsible for processing aged erythrocytes, eliminating residual circulation components, digesting haemoglobin and secreting molecules crucial for hepatic immune functions (4). Hepatic stellate cells (HSCs) are also located in the space of Disse. HSCs are responsible for the storage of dietary vitamin A as retinyl esters (REs) in lipid droplets (LDs) and play a significant role in immune responses (5,6). Activation of HSCs and KCs in response to stress stimuli can induce changes in tissue microanatomy, potentially impacting liver functionality.

Nutrients from ingested food are absorbed into the venous blood of the small intestine, except for most lipids, which are typically transported through lymphatic vessels. This nutrient-rich but O_2-poor blood is then directed to the liver via the portal vein before entering systemic circulation. The liver carries out its functions by utilizing these digestion products and synthesizing new molecules (7).

As a key metabolic organ, the liver plays a central role in energy production. Its metabolic pathways are intricately regulated by signals from nutrients, hormones and neurons. In the liver, lipid metabolism is particularly critical; the liver converts lipids into ketone bodies, triacylglycerols (TAGs), phospholipids or cholesterol. During development, fat stored in the fetal liver is crucial for providing energy necessary for the growth of other tissues (8). Furthermore, liver glucose metabolism through glycolysis is vital for energy production throughout the body. Under well-fed conditions, glycolysis products are used to synthesize new fatty acids, which are then either stored as LDs in hepatocytes or released into the bloodstream as very low-density lipoproteins (VLDLs). Conversely, during periods of insufficient nutrition, the liver breaks down glycogen and

synthesizes new glucose molecules to release into the bloodstream.

Given its constant exposure to toxins, the liver has developed mechanisms for immune tolerance. Additionally, it can also initiate apoptotic or autophagic processes to maintain tissue homeostasis. Autophagy plays a protective role by removing damaged macromolecules and organelles via lysosomes, thereby maintaining energy balance and recycling nutrients. However, excessive or uncontrolled autophagy can significantly contribute to the progression of liver diseases at various stages (e.g. non-alcoholic fatty liver disease, non-alcoholic steatohepatitis and hepatocellular carcinoma) (9).

Cell types

The subsequent sections will examine the different cell types found in the liver, detailing their specific characteristics and functions. Attention will be given to hepatocytes, KCs, HSCs and sinusoidal endothelial cells, among others. This analysis aims to provide a thorough understanding of the liver's cellular composition and its role in maintaining physiological balance.

Hepatocytes

Hepatocytes, constituting approximately 80% of the liver's cellular population, are primarily responsible for capturing and filtering blood from the sinusoids. These cells' functions are spatially differentiated within the liver. Hepatocytes in the periportal regions specialize in oxidative processes such as glycogen metabolism, gluconeogenesis, fatty acid oxidation (FAO) and urea synthesis. Conversely, those in the perivenular regions are involved in anaerobic glycolysis, lipogenesis, ketogenesis and the synthesis of lipoproteins and glutamine.

Hepatocytes possess specialized transport systems supported by their unique cellular structure. This specialization involves intricate vesicle formation and the activity of transmembrane proteins (10). The hepatocyte plasma membrane features distinct apical and basolateral domains, each with specific surface proteins, channels and receptors. In the basolateral (sinusoidal) domain, intrinsic kinase receptors like the epidermal growth factor receptor (EGFR) and receptors for lipid and iron uptake, such

as the low-density lipoprotein receptor (LDLR) and the transferrin receptor (TfR), are present. This domain also includes transporters for bile acid uptake. The apical (canalicular) domain, in contrast, is equipped with ATP-binding cassette (ABC) transporters and other transporters facilitating bile acid excretion (11).

The specialized structure of hepatocytes is essential for their function. These cells can display multiple basolateral and apical domains in close proximity, which is critical for maintaining the integrity of their secretory, excretory and endocytic systems. Hepatocytes exhibit polyploidy due to incomplete cytokinesis, resulting in multiple centriole pairs and numerous microtubule-organizing centers (12,13). This polyploidy implies that Golgi apparatuses near these centers may represent distinct sites for protein import and export (14). Hepatocyte polarization, achieved through the selective presence of membrane proteins in sinusoidal or canalicular domains, is vital for function. For example, bile acid production depends on the precise composition and coordination between the apical and basolateral domains. Components synthesized within the hepatocyte are transported to the apical membrane, where they enter the bile canaliculus formed between adjacent hepatocytes. Conversely, components of bile acids circulating in the bloodstream are taken up by hepatocytes via the sinusoidal membrane (11).

Hepatocytes secrete several important proteins, including alpha-fetoprotein (AFP), albumin, transferrin, plasminogen, fibrinogen and various coagulation factors (15). These proteins are secreted through various endocytic mechanisms including caveolae-mediated endocytosis, fluid-phase endocytosis and receptor-mediated endocytosis (RME), with RME being the most active and well-characterized (16). This endocytic activity is closely linked to metabolic functions, including glucose homeostasis.

In addition to endocytosis, hepatocytes perform transcytosis to transport fluids or proteins between membrane domains, from basolateral to apical or *vice versa*. A specialized transcytosis system is involved in moving newly synthesized proteins from the Golgi to the sinusoidal membrane before directing them to the canalicular membrane (17).

The liver, and hepatocytes in particular, play a critical role in lipid metabolism, including the absorption, storage, digestion and secretion of lipids. Hepatocytes secrete dietary lipids into the bloodstream as VLDLs (10). Fatty acids in VLDLs originate from various sources, including fatty acids bound to albumin from adipose tissue lipolysis, remnants of dietary lipoproteins, high-density lipoproteins (HDLs) derived from cholesterol esters (CEs), and TAGs synthesized through *de novo* lipogenesis (DNL) (18). While proteins like TANGO1 may aid in the secretion of large-volume loads like VLDLs by forming transport channels, the exact mechanisms are not fully elucidated (19,20). Lipoprotein internalization occurs through RME, mediated by LDLRs (21). Low-density lipoproteins (LDLs), which display ApoB100 and ApoE on their surface, are recognized by LDLRs and internalized, after which the receptor is recycled back to the membrane (22).

Beyond lipid metabolism, hepatocytes are essential for storing TAGs in LDs, which act as cytosolic organelles for lipid storage. While this storage mechanism is advantageous, excessive lipid accumulation due to high carbohydrate and fat intake can lead to hepatocyte dysfunction and conditions such as non-alcoholic steatohepatitis (NASH), potentially progressing to liver cancer (23). LDs are catabolized for energy production and degraded through lipophagy (24,25).

In addition to metabolic functions, hepatocytes are crucial for immune defense. They contribute to pathogen clearance and immune regulation through the secretion and detection of innate immune system molecules (26). In response to infection or inflammation, hepatocytes secrete acute phase proteins (APPs) that either directly kill pathogens or orchestrate an appropriate immune response. The production of APPs is regulated by cytokines such as interleukin-6 (IL-6), interleukin-22 (IL-22), interleukin-1 beta (IL-1β), interferon gamma (INF-γ) and tumor necrosis factor-alpha (TNF-α), which activate transcription factors like signal transducer and activator of transcription 3 (STAT3) and NF-kβ (27). Regulatory proteins, including members of the CCAAT/enhancer-binding protein (C/EBP) family, are also crucial for this regulation and are highly abundant in the liver (28).

Additionally, hepatocytes secrete humoral immune components and maintain the complement system to ensure pathogen clearance while promoting immune tolerance (29). Hepatocytes are the primary producers of fibrinogen, essential for blood clot formation and immune cell adhesion, and produce protease inhibitors to neutralize proteases from pathogens and dying cells (30,31).

Moreover, hepatocytes also produce chemokines to attract immune cells, such as CCL2 for macrophages and CXCL1 for neutrophils (32). They also secrete immunoregulatory molecules like peptidoglycan recognition protein 2 (PGLYRP2), which breaks down peptidoglycans into smaller fragments to prevent their recognition (28). Hepatocytes also contribute to immune tolerance by downregulating markers like programmed death-ligand 1 (PD-L1), which decreases T cell survival.

Immune component

The liver harbours a specialized immune microenvironment and possesses the ability to capture circulating immune cells, which enables it to mount a rapid and targeted immune response when necessary. As the organ responsible for filtering blood from the digestive tract before it enters systemic circulation, the liver must carefully balance its immune reactions. It is tasked with both, rejecting harmful substances and maintaining tolerance to harmless external molecules and macromolecules. This ability to switch between an immunotolerant state and a responsive immunologically active state equips the liver with unique and crucial immunological characteristics.

Macrophages are the predominant immune cells in the liver, essential for phagocytizing pathogens, dead cells, cellular debris and extracellular matrix (ECM) components. Beyond their phagocytic functions, these cells are integral to the stromal architecture of various tissues and organs, influencing homeostasis and tissue remodelling. In the liver, specialized macrophages known as KCs are predominantly located in the hepatic sinusoids and are the most extensively studied and prevalent within the liver's diverse immune cell population (33).

KCs can originate from multiple sources, including the yolk sac, bone marrow or hematopoietic stem cells from the ventral aorta in the mesonephric region (aorta-gonad-mesonephros, AGM) (34). Yolk sac-derived and AGM-derived macrophages are often considered functionally equivalent. By the fifth week of fetal development, hematopoietic stem cells migrate to the liver and differentiate into functional cells identifiable by specific markers (35). Yolk sac-derived macrophages express the colony-stimulating factor 1 receptor (CSF1R), which supports the development of KCs during fetal development. In contrast, bone marrow-derived macrophages express C-C chemokine receptor type 2 (CCR2) and lymphocyte antigen 6C (Ly6C) and are recruited to the liver, where they transition into KCs (36).

KCs main tasks are capturing aged or senescent erythrocytes and performing critical functions necessary for tissue development and regeneration, such as stimulating angiogenesis through the secretion of proteases and growth factors (37). KCs equipped with Toll receptors serve as a primary defence mechanism against hepatic pathogens. To perform their functions, KCs employ a pattern recognition receptor (PRR) system to identify and degrade pathogen-associated molecular patterns (PAMPs) and damage-associated molecular patterns (DAMPs) (38).

Monocyte recruitment to the liver generally occurs in response to inflammatory stimuli or hepatic damage to restore tissue homeostasis, with these cells undergoing apoptosis after fulfilling their role.

There are other minor immune components that also play significant roles in maintaining homeostasis or contributing to disease in the liver. These include neutrophils, which resolve liver damage by degrading collagen through matrix metalloproteinases (MMPs) secretion, and dendritic cells (DCs), which, along with some T helper (Th) cells such as Th2 cells, promote fibrosis through interleukin secretion or NOD-, LRR-, and pyrin domain-containing protein 3 (NLRP3) inflammasome activation (39–41). Conversely, Th1 lymphocytes exhibit anti-fibrotic effects through IFN-γ secretion, and natural killer (NK) cells contribute to anti-fibrotic responses by killing senescent HSCs via IFN-γ or inducing apoptosis through interleukin-15 (IL-15).

Nonetheless, these effects can be counteracted by CD4+ T lymphocytes, which can suppress NK cells, thereby aiding the survival of activated HSCs (42). B lymphocytes are also involved in fibrosis formation (43). NKT cells, distinct from NK cells, are large granular cells with a defined protective phenotype against various diseases or liver damage. They can recognize lipid antigens and are present in the liver's microvascular compartments, playing either pro-inflammatory or anti-inflammatory roles and shaping subsequent immune responses. Two subgroups with opposing functions have been identified (44). CD8+ T lymphocytes, which detect and lyse tumor cells, are tightly regulated to maintain tolerance and prevent excessive damage. The primary mechanism for the resolution of immune components post-damage involves exhaustion through the expression of programmed cell death protein 1 (PD-1) and its ligand PD-L1, as well as TIM-3 (45).

Hepatic stellate cells (HSCs)

HSCs are a resident, non-parenchymal cell population within the liver that play a central role in liver pathology, particularly in hepatic fibrosis. These cells are predominantly involved in the formation of myofibroblasts (MFBs) which are key contributors to fibrosis (6).

In a healthy liver, HSCs constitute approximately 10% of the hepatic cell population and are located in the space of Disse, functioning as pericytes between hepatocytes and liver sinusoidal endothelial cells (LSECs) (46). Their cellular extensions encircle the sinusoidal endothelium, which, due to its fenestrated structure, ensures continuous exposure of HSCs to the blood flow (46,47).

HSCs maintain a quiescent, non-proliferative state under normal conditions, regulated by both chemical and mechanical stimuli (48). In this quiescent state, HSCs are the primary storage sites for retinol (vitamin A), accounting for 60-95% of the body's vitamin A reserves (49,50). Dietary retinol is esterified, transported and hydrolysed by hepatocytes (51,52). After hydrolysis, retinol is transferred to HSCs for long-term storage, where it undergoes re-esterification by the enzyme lecithin retinol acyltransferase (LRAT) to form REs, stored in cytoplasmic LDs (53–55). These droplets,

consisting mainly of TAGs, REs and LRAT, accumulate around the nucleus in quiescent HSCs (56,57). During activation, these LDs decrease in size, relocate to the cell periphery, and their content shifts from RE to TAG, a process regulated by diacylglycerol O-acyltransferase 1 (DGAT1) and adipose triglyceride lipase (ATGL) (58). Stabilized RE is released from LDs by retinyl ester hydrolases (REHs) for fatty acid catabolism and β-oxidation (50). Consequently, activated HSCs lack cytoplasmic LDs as they are utilized for energy during activation (49,56,59).

HSCs undergo activation, in response to liver injury, which is triggered by various factors such as chronic inflammation, oxidative stress and toxic insults. These injuries, including chronic viral hepatitis, non-alcoholic fatty liver disease (NAFLD) and exposure to hepatotoxic substances, lead to persistent inflammatory responses and oxidative stress that activate HSCs (60). This activation is characterized by a loss of retinol storage capacity, increased proliferation, and the acquisition of a myofibroblastic phenotype (60). Activated HSCs then produce ECM components such as collagen types I and III, fibronectin and proteoglycans, which contribute to liver fibrosis. This accumulation of ECM components leads to a disrupted liver architecture and impairs liver function (60).

Understanding the regulation of HSCs activation and their transition from a quiescent to an activated state is crucial for developing therapeutic strategies to prevent or reverse liver fibrosis.

Liver sinusoidal endothelial cells (LSECs)

LSECs are highly specialized ECs that form a crucial permeable barrier between the bloodstream and hepatocytes in the liver, comprising approximately 15% of liver cells. These cells are distinguished by their unique structural features, including the absence of a basal membrane, a lack of diaphragm and the presence of fenestrations. These fenestrations are organized into clusters that vary in size and number based on their location within the liver, being larger but less numerous in peri-portal regions and smaller but more numerous in centrilobular areas (61). The fenestrations facilitate the exchange of substances between the blood and hepatocytes, with small molecules and gases diffusing freely while larger molecules pass through by forming pores in the LSECs'

membrane. Additionally, LSECs can dynamically adapt to the nutritional and health status of the organism. This distribution may be explained by the progressive decrease in O_2 along the liver lobule, which increases the need for blood exchange, or it could relate to the maturation of LSEC along the lobule. Additionally, the cytoskeleton, with VEGF playing a key role, is critical for fenestration formation (61,62).

LSECs are predominantly found lining the liver sinusoids, a network of small blood vessels within the liver. They are integral to the liver's vascular architecture and contribute to its overall function. LSECs originate from mature LSECs, intrahepatic progenitor LSECs, and, less commonly, progenitors from the bone marrow, with the latter playing a significant role in LSEC renewal during liver damage (63).

Under physiological conditions, LSECs maintain a balance of blood components, retaining erythrocytes while permitting the entry of other blood constituents into the Disse's space. They are involved in the regulation of vascular tone, helping to maintain low portal pressure and influencing other liver cell types, such as HSCs, to remain in a quiescent state, thereby preventing excessive fibrosis and vasoconstriction (64).

LSECs possess significant endocytic capacity, aided by key receptors including scavenger receptors (SRs), the mannose receptor, and Fc gamma receptor IIb2 (FcγRIIb2), which facilitate the clearance of pathogens and waste products from the bloodstream (65). They play a crucial role in hepatic immune regulation, participating in the clearance of pathogens and apoptotic cells and maintaining tolerance to harmless antigens.

In response to liver injuries, LSECs can become capillarized, losing their fenestrated structure and contributing to pathological conditions such as increased fibrosis and impaired liver function. This capillarization promotes angiogenesis and vasoconstriction, which exacerbate liver disease progression. The interaction between LSECs and other hepatic cell types, such as HSCs, significantly influences the fibrotic response and overall pathological outcomes in liver diseases.

LSECs are also involved in regulating immune responses within the liver by expressing various cell surface proteins and receptors that facilitate antigen presentation and T cell tolerance. They modulate immune activity through mechanisms such as the expression

of PD-L1 which interacts with PD-1 receptors on naïve T cells to induce tolerance. This process involves a complex interplay of immune signalling pathways and cytokines, including interleukin-2 (IL-2) and IL-6, which are essential for transitioning from tolerance to an effective immune response (66,67).

Liver pathology

Metabolic Associated Fatty Liver Disease (MAFLD), formerly known as NAFLD, is an increasing concern in hepatology and metabolic medicine. MAFLD is the most common liver disease in Western countries, affecting approximately 25% of adults, with a projected prevalence of 27.6% in Spain by 2030 (68–70). This condition progresses from simple hepatic steatosis to Metabolic Associated Steatohepatitis (MASH), characterized by inflammation and liver cell injury, and is associated with metabolic dysfunctions such as obesity and type 2 diabetes (68).

The progression from MAFLD to MASH is explained by the "two-hit" hypothesis, where the initial accumulation of triglycerides (the first hit) is followed by oxidative stress (the second hit), leading to increased inflammation and liver damage (71,72). Hepatic fibrosis, resulting from chronic liver injury, can advance to cirrhosis, which is associated with severe complications such as portal hypertension and hepatocellular carcinoma (HCC) (73–76).

HCC, accounting for approximately 90% of liver cancer cases, arises from the malignant transformation of damaged hepatocytes and is one of the leading causes of cancer-related deaths globally (77–79).

The following section will provide a detailed exploration of these topics, examining the progression of liver disease from MAFLD to MASH, fibrosis, cirrhosis, and ultimately to HCC (**Figure 1**).

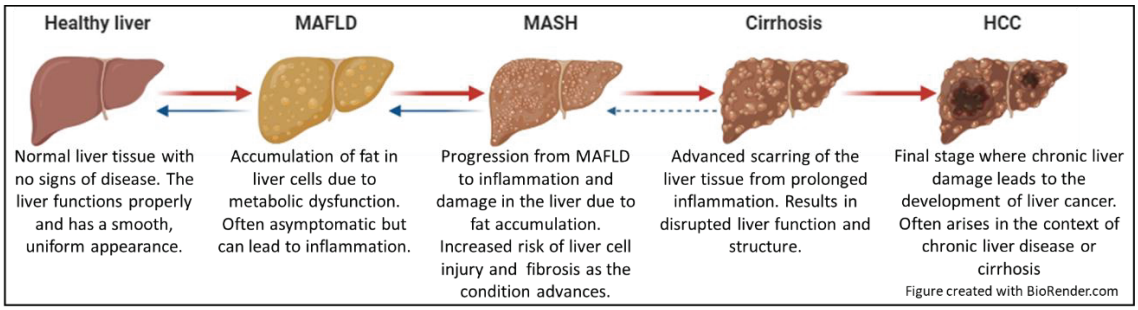

Figure 1. Progression of liver disease from healthy liver to HCC. The diagram illustrates the sequential stages in the progression of liver disease: healthy liver, MAFLD, MASH, cirrhosis and HCC. Each stage is depicted with corresponding visual elements to highlight key pathological changes and disease advancement. The progression is characterized by increasing liver damage and dysfunction, ultimately leading to the development of liver cancer. The figure was created with BioRender.com.

Metabolic associated fatty liver disease (MAFLD)

MAFLD, formerly known as NAFLD, represents a growing concern in hepatology and metabolic medicine. This reclassification reflects a broader understanding of the condition's association with metabolic dysfunction, irrespective of alcohol consumption (68). MAFLD is the most prevalent cause of liver disease in Western countries and is expanding in developed nations, with a prevalence of approximately 25% in adults. This rise in prevalence parallels the growing rates of diabetes and obesity (69). The global burden of MAFLD has risen considerably, with its prevalence in Spain predicted to reach 27.6% by 2030, and the more severe form, MASH, affecting nearly 6% of the population (70).

MAFLD encompasses a spectrum of hepatic manifestations, from simple steatosis to more severe conditions such as MASH, characterized by inflammation and liver cell injury (68). The etiology of MAFLD is intrinsically linked to metabolic syndrome, including obesity, insulin resistance, type 2 diabetes and dyslipidemia, all of which promote lipid accumulation in hepatocytes. This accumulation triggers oxidative stress and inflammation, creating a chronic inflammatory environment that contributes to hepatic injury and fibrosis, which can progress to cirrhosis or HCC (80).

Liver steatosis in MAFLD is primarily marked by the accumulation of TAGs in more than 5% of the liver parenchyma without the need for hepatocellular injury, disrupting

hepatocyte function and promoting tissue inflammation (81). The key metabolic processes involved in lipid homeostasis, which become dysregulated in MAFLD, include increased uptake of circulating lipids and enhanced DNL. Meanwhile, FAO is insufficient to mitigate the damage. Additionally, the export of VLDLs also plays a role in this imbalance (82). This pathophysiology leads to further metabolic disturbances, including appetite dysregulation, gut dysbiosis, insulin resistance and the activation of pro-inflammatory pathways, thereby exacerbating the condition (69).

The diagnosis of MAFLD involves clinical evaluation, imaging studies and biochemical markers. Although liver biopsy remains the gold standard for distinguishing between simple steatosis and MASH, non-invasive methods such as transient elastography and serum biomarkers are increasingly used for monitoring liver stiffness, fat content, and disease progression (83). These methods are critical for assessing the extent of fibrosis and guiding clinical management. Non-invasive measures such as TAGs levels, gamma-glutamyl transferase, serum insulin, aminotransferases, waist circumference and the presence of metabolic syndrome or type 2 diabetes are also employed to assess liver health (84).

In terms of pathophysiology, hepatocytes and HSCs are both critically involved in disease progression. TAGs accumulation in hepatocytes activates HSCs through increased transforming growth factor (TGF) production, contributing to the fibrogenic process. This activation is further exacerbated by mitochondrial dysfunction and the production of reactive oxygen species (ROS), which induces cell death and enhances fibrosis (85,86).

Management of MAFLD focuses primarily on lifestyle modifications, including weight loss through dietary changes and increased physical activity, which are shown to improve liver histology and metabolic health (87). In cases where lifestyle modifications are insufficient, pharmacological interventions may be considered, though no specific therapies for MAFLD have yet been widely approved.

In conclusion, MAFLD presents a significant public health challenge due to its strong link with metabolic dysfunction. The shift from NAFLD to MAFLD underscores the importance of metabolic factors in the disease's pathogenesis. Early detection and a

comprehensive management strategy combining lifestyle changes with potential pharmacological treatments are critical to preventing disease progression and its associated complications.

Metabolic associated steatohepatitis (MASH)

As MAFLD progresses, it can advance to MASH, which was previously referred to as NASH. MASH represents a more severe form than MAFLD characterized by the presence of necro-inflammatory changes in the liver. Unlike MAFLD, which involves fat accumulation without significant hepatocellular damage, MASH is marked by both fat deposition and hepatocellular injury, resulting in a microenvironment of steatosis and inflammation (71).

The progression to MASH is often described by the "two-hit" hypothesis. The first "hit" involves the accumulation of TAGs in the liver, while the second "hit" is associated with oxidative stress, primarily through ROS. This oxidative stress induces lipid peroxidation, inflammation and endoplasmic reticulum (ER) stress, which further exacerbates liver injury (72).

As the disease progresses, immune cells, including CD8+ T lymphocytes and NKT cells, contribute to the metabolic reprogramming of hepatocytes. These immune cells induce a cytokine-secreting phenotype in hepatocytes, which supports the development of MASH and potentially HCC. Platelets also play a role in MASH by promoting immune activation through interactions with KCs and the recruitment of cytotoxic T lymphocytes (88). In MASH, there is a notable increase in pro-inflammatory cytokines such as TNF-α, IL-1β and IL-6. These cytokines activate KCs, HSCs and inflammatory cascades, leading to liver fibrosis (72).

Fibrosis and cirrhosis

Liver fibrosis is characterized by an excessive and disproportionate deposition of fibrous ECM, predominantly composed of crosslinked collagens (type I and type III), fibronectin, elastin fibers, glycoproteins and mucopolysaccharides, among other components (73,74). This process is primarily driven by activated MFBs that, in response to liver

injury, replace normal liver tissue and remodel the organ's physiological architecture (75). Chronic liver injuries that lead to hepatic fibrosis can generally be classified into two categories: hepatotoxic injuries, which result from chronic hepatocyte damage (e.g., viral infections, alcohol consumption or metabolic syndromes) and cholestatic injuries, which stem from bile flow obstruction (e.g., in biliary cholangitis and biliary atresia) (76).

Historically, viral infections, particularly those caused by hepatitis B virus (HBV) and hepatitis C virus (HCV), were the predominant causes of liver fibrosis. In 2017, these viral infections accounted for approximately 50% of all cirrhosis and HCC cases globally (89). However, with the rising obesity epidemic, NAFLD and its more severe form, NASH, have emerged as the leading precursors of fibrosis and liver failure (90,91). The global prevalence of these obesity-related conditions has prompted experts to propose the term MAFLD, which more accurately describes a cluster of fatty liver diseases linked to metabolic dysfunction (68). This reclassification is also considered to improve the identification of patients with significant fibrosis through non-invasive methods (92). Other, less common diseases that may lead to excessive fibrosis and eventual cirrhosis include autoimmune hepatitis, hemochromatosis, Wilson's disease and primary and secondary biliary cholangitis (93).

Fibrosis is inherently a tissue repair mechanism that aids in isolating the injury site and supporting the dissemination of growth factors and cytokines, thereby facilitating the renewal of damaged cells (94). Given the liver's unique regenerative capacity, fibrosis is a potentially reversible process. When the source of injury is removed, fibrosis regression may occur. However, if the fibrosis process fails to resolve, it can lead to severe consequences. The critical threshold is reached when excessive ECM accumulation causes significant architectural distortion, resulting in vascular collapse and portal hypertension, at which point substantial regression is unlikely (95). Chronic liver disease (CLD), characterized by persistent ECM accumulation and the formation of fibrous scar tissue, disrupts normal hepatic functions. Cirrhosis, a severe form of fibrosis, increases the risk of life-threatening complications such as portal hypertension, hepatic failure and HCC (96). Despite its severity, cirrhosis can still be reversible in some cases (97,98), particularly when the underlying cause is addressed and eliminated (99).

Advances in treatment and vaccination against HBV, along with new antiviral therapies for HCV, have significantly reduced the prevalence of liver fibrosis and cirrhosis due to these infections, particularly in Western countries (95). However, lifestyle changes necessary to combat the metabolic syndrome associated with MAFLD/MASH and obesity remain challenging to implement, and the global incidence of fibrosis due to these metabolic conditions continues to rise.

Hepatocellular carcinoma (HCC)

Epidemiology

Liver cancer is the sixth most commonly diagnosed cancer and the third leading cause of cancer-related deaths globally, with over 860,000 new cases and more than 750,000 deaths reported in 2022 (77,78). HCC, which accounts for approximately 90% of liver cancer cases, results from the malignant transformation of hepatocytes damaged by various agents (79).

Risk factors

HCC predominantly arises in the context of CLD, with cirrhosis being the strongest risk factor (100). Cirrhosis condition heightens the risk of HCC by 1-6% annually and is a major cause of death among those affected (101). Key risk factors for HCC include obesity, HBV or HCV infections and excessive alcohol consumption.

Global health initiatives, such as HBV vaccination programs and HCV antiviral therapies, have significantly altered the landscape of HCC risk factors (102,103). However, a significant lifestyle shift towards increased overweight and obesity has emerged as a major risk factor for CLD, which can ultimately lead to liver cancer. The World Health Organization (WHO) reported that in 2022, 43% of adults worldwide were overweight and 16% were obese. This marks a doubling of the at-risk population between 1990 and 2022, with projections indicating further increases (104,105).

Overweight and obesity are strongly associated with an increased risk of developing HCC. High-fat diet (HFD) can lead to liver steatosis, which may progress to MAFLD. These

conditions contribute to chronic inflammation, liver cell damage and fibrosis, thereby accelerating hepatocarcinogenesis through elevated rates of hepatocyte replication and subsequent genetic alterations (106).

HBV infection is a major contributor to HCC. It is particularly prevalent in Asia and Africa, where it is responsible for about 60% of HCC cases (107). HBV, a DNA virus, can integrate into the host genome, inducing insertional mutagenesis that activate oncogenes (108). Although HBV can lead to HCC even in the absence of cirrhosis, most patients present with both HBV and cirrhosis. Universal HBV vaccination has reduced HCC incidence in some areas, though many regions still lack vaccination programs (109).

HCV infection, an RNA virus that does not integrate into the host genome, poses a significant HCC risk in North America, Europe and Japan (107). However, the risk has decreased with the advent of direct-acting antiviral (DAA) therapies, which have achieved a sustained virological response (SVR) in many patients (110). SVR is associated with a 50-80% reduction in HCC risk, although patients with HCV-induced cirrhosis continue to face a persistent risk of over 2% annually, highlighting the need for ongoing surveillance, especially among underserved populations (111,112).

Hepatitis delta virus (HDV), an RNA virus that requires HBV for replication, aggravates liver disease severity. Co-infection with HBV and HDV significantly increases the risk of HCC compared to HBV infection alone. Studies show that acute and chronic HDV infections substantially heighten HCC risk (113).

Chronic excessive alcohol consumption leads to alcoholic liver disease, cirrhosis and HCC. Alcohol-related cirrhosis accounts for 15-30% of HCC cases, with the risk exacerbated by alcohol's interaction with other factors such as HBV infection (114,115).

NASH, increasingly prevalent due to rising obesity rates, has become a major cause of cirrhosis and HCC, especially in Western countries. Representing 15-20% of HCC cases in these regions, NASH is associated with a lower annual incidence of HCC compared to viral cirrhosis but still warrants surveillance due to its high population attributable fraction (116,117). A significant proportion of NASH-related HCC occurs without cirrhosis, complicating surveillance efforts (118,119).

Age is a robust risk factor for HCC, with higher incidence observed in individuals over 70 years (120). According to sex, HCC predominantly affects men (male to female ratio of 2–3:1), likely due to higher exposure to risk factors and sex hormones differences (121). Racial and ethnic disparities exist, with higher incidence among Hispanics, potentially linked to single nucleotide variants in PNPLA3 (associated with NASH-HCC) (122) Smoking is associated with an increased risk of HCC (123), while the direct role of diet remains unclear, though coffee and aspirin may offer preventive benefits (124,125).

Symptoms, diagnosis and screening

HCC is often detected through surveillance in high-risk populations such as those with chronic hepatitis B or cirrhosis (126,127). However, up to 50% of cases may be diagnosed incidentally, particularly in areas with inconsistent screening practices. Diagnosis typically relies on non-invasive imaging, with computed tomography (CT) or magnetic resonance imaging (MRI) being used for lesions 1 cm or larger (128). These imaging techniques reveal key diagnostic features, such as the 'arterial enhancement and delayed washout' phenomenon, which indicates HCC with high sensitivity and specificity (129).

For lesions smaller than 1 cm, short-term follow-up with repeat ultrasonography is generally sufficient. For larger lesions, quadruple-phase CT or dynamic contrast-enhanced MRI is recommended. Despite the effectiveness of these imaging methods, biopsy remains crucial for atypical cases and for molecular characterization of the tumor. However, the accuracy of biopsy decreases with smaller lesions, and multiple biopsies may be necessary.

Prevention

Primary prevention of HCC focuses on addressing underlying causes such as HBV and HCV infections. HBV vaccination and antiviral therapies have proven effective in reducing HCC incidence (130,131). Similarly, antiviral treatments for HBV and SVR after DAA therapy for HCV are associated with reduced HCC risk (110).

Although alcohol cessation and management of MAFLD are recommended, evidence on their impact on HCC risk is limited. Various therapies, such as vitamin A, vitamin K and retinol analogues, have been explored for chemoprevention, but results have been inconclusive. For example, administering vitamin A has been explored as a therapeutic strategy to mitigate liver fibrosis, as vitamin A plays a crucial role in maintaining the quiescent state of HSCs. By maintaining their quiescence, vitamin A can potentially prevent HSCs from becoming activated, which is a key process in the development of liver fibrosis. Observational studies suggest that metformin, statins, coffee and aspirin may reduce HCC risk (132). Coffee consumption has shown a dose-dependent relationship with decreased HCC incidence (133), while aspirin has demonstrated potential benefits, especially in long-term use (125).

Molecular mechanisms involved in HCC

The pathophysiology of HCC is a complex and multi-step process. It involves the interaction of multiple factors that contribute to the early stages of malignant transformation of hepatocytes and the progression of HCC. These factors include genetic predispositions, interactions between viral and non-viral risk factors, the cellular microenvironment, various immune cells, and the severity of the underlying chronic liver disease. A disrupted microenvironment plays a crucial role in cancer development, influencing all phases of malignant progression, from the initial transformation to invasion and eventual metastasis (134). While the understanding of HCC's underlying mechanisms has advanced, translating this knowledge into effective clinical applications remains a challenge. Around 25% of HCC tumors present actionable mutations, but most of these mutations occur in fewer than 10% of cases, complicating proof-of-concept studies (135–137). Notably, key mutations such as telomerase reverse transcriptase (TERT), TP53, and CTNNB1 are currently undruggable (106). Additionally, research is still ongoing to convert molecular and immune classifications into practical biomarkers for guiding therapy. Recent progress has provided new insights into NASH-associated HCC, particularly regarding the role of the tumor microenvironment (TME), including the immune system and platelet activation (138,139).

The debate over the cell of origin for HCC continues. It could arise from liver stem cells, transit-amplifying populations or mature hepatocytes. Mature hepatocytes are long-lived and have significant proliferative potential, especially in response to injury. Some mouse models suggest that HCC originates from transformed mature hepatocytes, while others propose liver stem cells as the source (140). Additionally, intrahepatic cholangiocarcinomas and tumors with mixed HCC or cholangiocarcinoma morphology often appear to originate from mature hepatocytes, highlighting concepts of metaplasia and cell plasticity. This indicates that the tumor's morphology and epigenetic landscape might not always reflect its true cell of origin (141,142).

High-throughput next-generation sequencing has identified several cancer driver genes with recurrent alterations in HCC. TERT promoter mutations, leading to telomerase activation, viral insertions, chromosome translocation or gene amplification are the most common, occurring in approximately 80% of cases. These mutations prevent the normal erosion of chromosomes during cell division, thereby promoting cellular immortality. The Wnt–β-catenin signaling pathway is frequently activated in 30-50% of cases due to mutations in CTNNB1, AXIN1, or APC (135,143). Other prevalent mutations involve TP53, RB1, and genes related to cell cycle control, epigenetic regulation, oxidative stress, and various signaling pathways. Only about 20-25% of HCC patients have actionable mutations based on current standards (135–137). Specific genes are associated with HCC molecular subtypes, defined by transcriptomic profiles and histological features.

Viral infections contribute to HCC through molecular alterations. HBV infection often causes insertional mutagenesis in the TERT promoter, resulting in overexpression of telomerase (144). This activation prevents telomere erosion, protects cells from senescence and promotes transformation (145). HBV-induced mutations can activate oncogenes such as cyclin-A2 (CCNA2) and G1/S-specific cyclin-E1 (CCNE1), leading to replicative stress and genome rearrangements (146). Adeno-associated virus 2 has shown similar insertional mutagenesis effects (147). In contrast, HCV infection does not directly drive oncogenesis but induces mutations through oxidative stress associated with chronic inflammation.

Mutational signatures during CLD and cirrhosis contribute to HCC development. Exome sequencing has identified specific mutational signatures associated with various risk factors (135,148). For example, signature 22 is linked to aristolochic acid exposure, and signature 24 is associated with aflatoxin B1 exposure (135,149). Additionally, signature 4 and signature 16 correspond to tobacco smoking and alcohol intake, respectively (150). These signatures emphasize the liver's role in detoxifying metabolites, which can damage the hepatocyte genome and contribute to carcinogenesis.

Neovascularization processes in cancer

HCC relies on the formation of new blood vessels to meet its O_2 and nutrient demands; vascularization enables the tumor to grow and develop (151). Moreover, solid tumors with a diameter greater than 2 mm require the maintenance of blood supply through the creation of new blood vessels to prevent necrosis due to ischemia and hypoxia (152). Therefore, targeting the liver's vasculature to treat HCC could be a promising strategy. There are different paths to form new tumor blood vessels as are summarised in the following sections.

Angiogenesis

HCC is a highly vascularized tumor, distinguished by aberrant angiogenesis, which significantly contributes to its malignancy (153,154). The progression of tumor growth and metastasis is closely linked to the formation of a tumor vascular network that provides O_2 and nutrients. In the initial stages of tumorigenesis, the tumor relies on passive diffusion of O_2 and nutrients. However, as the tumor increases in size, the availability of these resources becomes insufficient (155). Under hypoxic conditions, tumor cells release angiogenic factors, such as vascular endothelial growth factor (VEGF), creating a concentration gradient toward the hypoxic center. This process results in an imbalance between pro-angiogenic and anti-angiogenic factors. ECs, stimulated by these angiogenic signals, secrete enzymes such as MMPs, which degrade the basement membrane of blood vessels. Subsequently, the ECs migrate through the degraded membrane and are directed toward the tumor tissue, following the angiogenic factor gradient (156,157). This process, known as angiogenesis, involves the sprouting

of new capillaries from existing ECs and represents the most widely studied form of tumor neovascularization, serving as a primary target for conventional anti-angiogenic therapies (158,159).

Angiogenesis remains the most extensively researched mechanism of new blood vessel formation in tumors. It refers to the sprouting of neoplastic capillaries from pre-existing ECs. Another process, intussusceptive angiogenesis (IA), occurs within the lumen of existing blood vessels and is mediated by the interstitial columnar structure, leading to the division of the original lumen and the formation of two new vessels (156,160). In pathological angiogenesis, tumor cells release angiogenic factors that alter the tumor's vascular microenvironment. Prolonged expression of these factors results in abnormal tumor vasculature, increasing interstitial pressure and vascular permeability (161). These angiogenic factors include VEGF, fibroblast growth factor-2 (FGF-2), tumor-associated macrophages (TAMs) and MMPs (162).

Thus, both sprouting angiogenesis and IA play critical roles in tumor vascularization, with each mechanism contributing to the abnormal and highly permeable vasculature observed in malignancies like HCC. These processes are central targets for anti-angiogenic therapies aimed at disrupting the tumor's blood supply and limiting its progression.

Vasculogenesis

Vasculogenesis occurs when endothelial progenitor cells (EPCs) differentiate into ECs, migrate to the tumor and participate in its blood supply by forming new blood vessels.

Vasculogenesis plays a critical role in the development and progression of HCC, contributing to its aggressive nature and resistance to conventional therapies. Unlike angiogenesis, which involves the sprouting of new blood vessels from existing ones, vasculogenesis in HCC is characterized by the formation of new blood vessels through the recruitment and differentiation of EPCs from the bone marrow. These EPCs are mobilized to the TME, where they contribute to the formation of new vascular networks, supporting the growth and survival of the tumor (163). This process is driven by various

signaling pathways, including VEGF, hypoxia-inducible factors (HIFs), and other pro-angiogenic factors that are often upregulated in HCC (164).

Vessel co-option

Vessel co-option is a neovascularization process that happens in several malignancies. This process involves the hijacking of the existing vasculature and tumor cells migrate along the existing or newly induced blood vessels to supply tumor growth and metastasis (157,165).

Vessel co-option is a significant mechanism by which HCC tumors sustain their blood supply, especially in the context of resistance to anti-angiogenic therapies. Unlike angiogenesis, which involves the growth of new blood vessels, vessel co-option occurs when cancer cells hijack pre-existing blood vessels in the surrounding normal liver tissue to ensure their growth and survival. This process allows HCC tumors to circumvent the need for new vessel formation and contributes to the development of a more invasive and therapy-resistant phenotype. Vessel co-option is particularly prominent in well-differentiated HCCs, where the tumor integrates with the liver's existing vascular architecture, maintaining blood flow and nutrient supply without inducing significant angiogenesis (166). This mechanism is often associated with poorer patient outcomes, as tumors relying on vessel co-option may not respond well to treatments targeting angiogenesis, such as VEGF inhibitors (167).

Vasculogenic mimicry

VM is a distinct form of neovascularization in tumors. It was first described by Maniotis *et al.* in 1999 in malignant human melanoma. Unlike angiogenesis, VM does not require ECs to provide sufficient blood supply for tumor growth. Instead, tumor cells undergo dedifferentiation into an endothelial-like phenotype and form canal-like structures through which blood can flow (168) (**Figure 2**). Since it was first described, VM has been closely associated with aggressive tumor behaviors, including increased invasiveness, higher tumor grade, metastasis, and poorer patient prognosis in several cancer types (169–172). Tumor cells situated along the inner surface of VM vessels are directly

exposed to blood flow, which enables them to preferentially infiltrate the microcirculatory environment, migrate with the bloodstream and metastasize to distant areas (173).

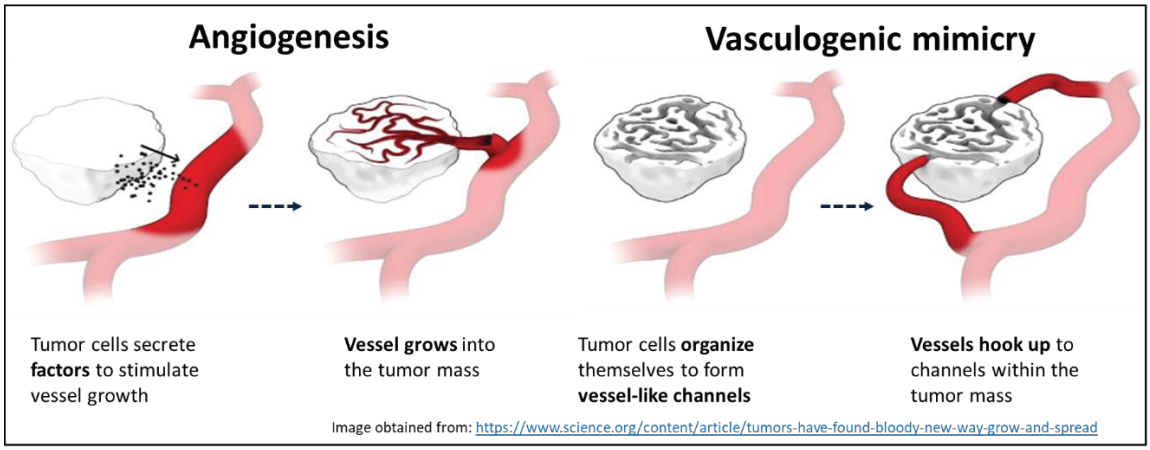

Figure 2. Neovascularization processes suggested in cancer. In hypoxic tumoral conditions, tumors release angiogenic factors like VEGF, promoting EC migration and capillary formation. Additionally, VM is another form of tumor vascularization, where cancer cells form vessel-like structures without endothelial cells. VM has been suggested to be part of the neovascularization processes of some malignant cancers.

In recent years, VM has been suggested to occur in different malignant tumors, including glioblastoma (174), melanoma (175,176), breast cancer (177), lung cancer (178,179), colorectal cancer (CRC) (180), prostate cancer (181), gastric cancer (182) and, what interest us the most in this doctoral thesis, HCC (183). However, despite VM being linked to HCC, the underlying mechanisms remain poorly understood. When this doctoral thesis began in 2021, little was known about VM in HCC, and, to date, the number of high-quality studies on this topic remains limited. While there has been growing interest in exploring VM in HCC, significant gaps and methodological weaknesses persist in the literature, leading to inconclusive findings and highlighting the urgent need for more comprehensive research.

The first study linking VM to HCC was published in 2006, and since then, only 88 publications have followed. Since January 2021, the start of this doctoral thesis, the number of papers published annually on VM and HCC has averaged eight per year (**Figure 3**). In comparison, if one searches for "VM" and "cancer," 936 results are

retrieved, with the first reference being Maniotis *et al.* from 1999 (**Figure 4**). Despite these numbers, VM research lags significantly behind other neovascularization mechanisms like angiogenesis. For example, searching for "angiogenesis" and "cancer" yields 60,076 articles since its first description in 1968, with 2,543 linking angiogenesis to HCC (**Figure 5**).

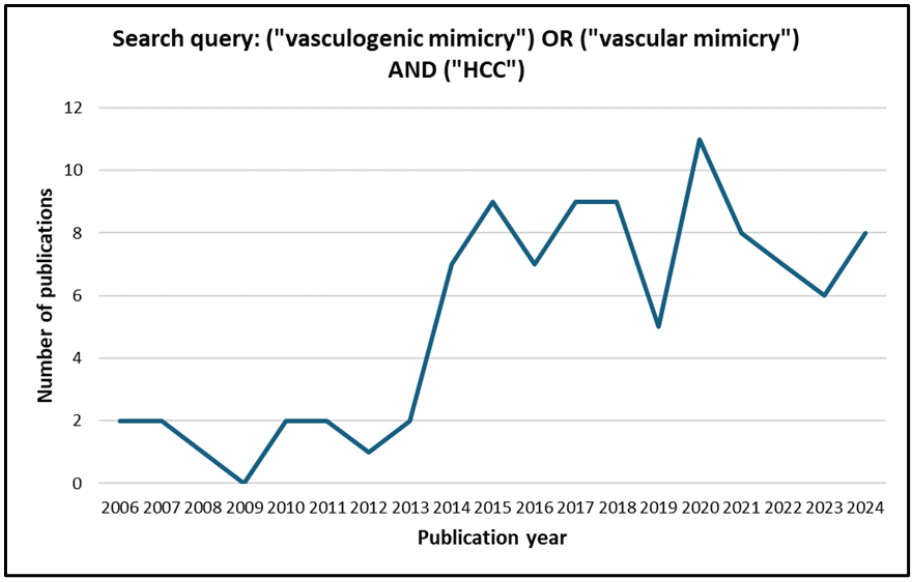

Figure 3. Publications per year on VM and HCC. The first publication on this topic was in 2006, and since the start of this doctoral thesis in 2021, there has been a steady but limited output of approximately 8 publications annually.

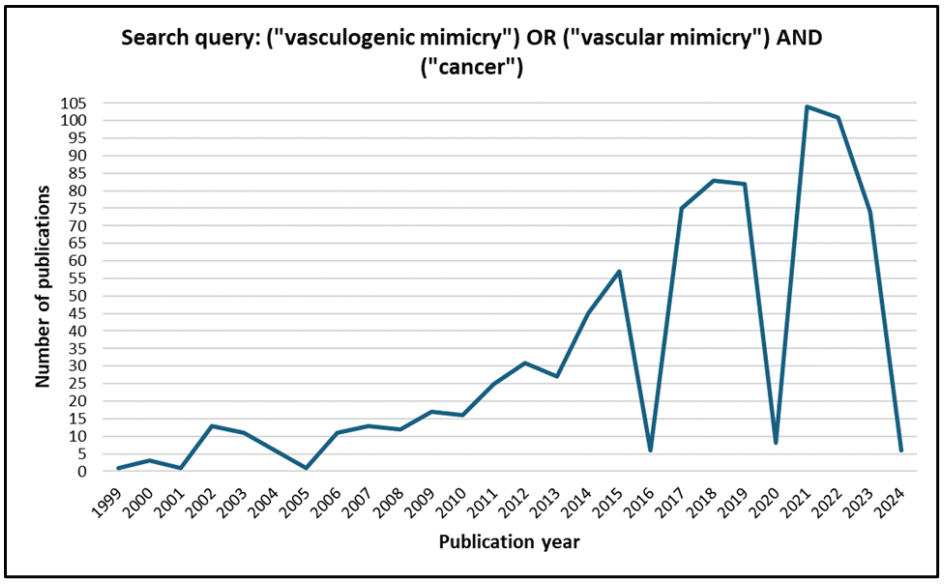

Figure 4. Publications per year on VM and cancer. VM research has shown an upward trend since 1999, but interest has significantly increased over the last 8-10 years.

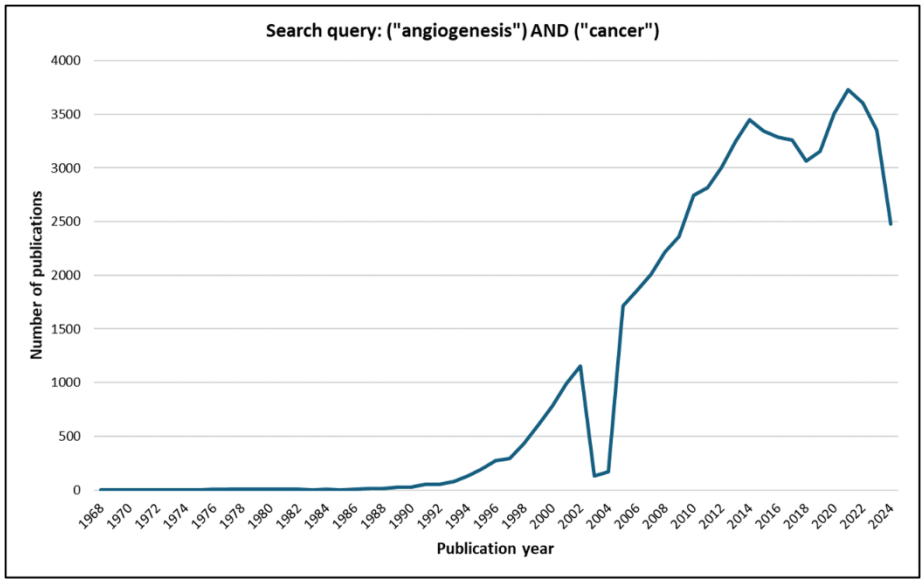

Figure 5. Publications per year on angiogenesis and cancer. Angiogenesis research has expanded considerably since 1968, with particular growth after 2000.

According to some researchers in the field, patients with VM-positive tumors have worse prognosis and a lower 5-year survival rate than patients without VM in their tumors (182,184) what highlights the plausible importance of VM as a prognosis marker in tumors.

According to its structure, there are two different types of VM suggested: patterned and tubular. Though this doctoral thesis the term VM encompasses both types. There are some differences between VM types. Patterned VM networks conduct fluids although it is not formed by a continuous lumen. Patterned VM is composed of ECM proteins positive for PAS as laminin, heparan sulfate proteoglycan and collagens (IV and VI) (185). Tubular VM is composed of tumoral cells mimicking endothelial channels to form tube-like structures covered by secretory glycoproteins that are hollowed and perfused (186).

Despite VM's suggested significance, there is ongoing debate about the detection criteria for VM structures in tumors. Although the full VM process is not yet well understood, some detection criteria have been proposed. Maniotis *et al.* defined the first criterion as the absence of vascular ECs on the inner wall of VM vessels, with the second being the presence of tumor cells lining the vascular-like structures. VM diagnosis typically relies on PAS-positive staining (PAS^{POS}) to detect glycoproteins

secreted by tumor cells, along with the absence of endothelial markers, like CD31-negativity ($CD31^{NEG}$). Additionally, the presence of red blood cells within the vascular-like channels is another key diagnostic feature (187,188). *In vitro*, VM is suggested by the ability of cell lines to form tubular structures on matrigel, and some researchers argue that the functionality of VM structures should be confirmed by demonstrating perfusion, either through dye perfusion assays *in vitro* or the presence of red blood cells in tumor biopsies (189,190).

Various mechanisms have been proposed to explain VM formation in cancer. These include self-deformation of highly malignant tumor cells, ECM remodeling and connections between VM structures and existing blood vessels to facilitate blood supply (168,191).

One of the mechanisms proposed to drive VM in cancer is the epithelial-to-mesenchymal transition (EMT). EMT is a biological process where epithelial cells, which are normally characterized by strong cell-cell adhesion and a non-motile phenotype, undergo molecular changes that give them mesenchymal features, including enhanced migratory capacity, invasiveness and resistance to apoptosis. In the context of VM, EMT will enable cancer cells to acquire a plastic phenotype, allowing them to form tubular structures resembling blood vessels. This transition is driven by key transcription factors such as Snail, Slug, Twist and ZEB1/2, which repress epithelial markers like E-cadherin while upregulating mesenchymal markers, including N-cadherin and vimentin (162,192). Furthermore, EMT involves plenty of signaling pathways as the transforming growth factor-beta (TGF-β) signaling pathway (183,192), Wnt signaling pathway (193,194) and Notch signaling pathway (195,196).

Hypoxia, or low O_2 levels in the TME, is another factor that has been suggested to promote VM in cancer. Hypoxia stabilizes HIFs, particularly hypoxia-inducible factor 1-alpha (HIF-1α), which in turn activates a variety of downstream genes that support tumor adaptation to hypoxic conditions. These genes include those involved in glycolysis, angiogenesis and survival pathways, which collectively enhance the ability of

cancer cells to engage in VM. Furthermore, HIF-1α contributes to the EMT process, further linking hypoxia to the promotion of VM (197).

The ECM plays a critical role in VM by providing the structural framework necessary for the formation of the pseudo-vascular channels. MMPs, particularly MMP-2 and MMP-9, are enzymes that degrade components of the ECM, facilitating its remodelling. This remodelling is thought to be essential for the formation of the VM channels, as it allows cancer cells to rearrange the ECM into patterns that resemble the lumen of blood vessels. The activity of MMPs is often upregulated in cancer including HCC, correlating with increased VM and tumor invasiveness (198). Moreover, the interaction between tumor cells and the ECM via integrins and other cell surface receptors further supports the structural integrity and function of these VM channels.

Another molecular pathway that seems to be implicated in VM is the PI3K/AKT/mTOR signalling axis. This pathway is frequently activated in HCC and is known to promote cell survival, proliferation and metabolic adaptation. The PI3K/AKT/mTOR pathway also influences the expression of EMT-related genes and could enhance the capacity of HCC cells to participate in VM. Inhibition of this pathway has been shown to reduce VM, suggesting its critical role in the maintenance of these vessel-like structures (198).

Finally, the presence of cancer stem cells (CSCs) within HCC has also been linked to VM. CSCs possess the ability to differentiate into various cell types, including those capable of forming VM structures. These cells are highly plastic and can adapt to the TME's demands, contributing to both VM and the overall heterogeneity and aggressiveness of HCC (199). Targeting CSCs has therefore been proposed as a potential strategy to disrupt VM and reduce tumor progression.

Treatment

HCC is typically diagnosed at late stages, at which point treatment options are limited. Early-stage HCC may be treated with tumor resection or liver transplantation, provided the tumor is localized, with few nodules and preserved liver function. Intermediate-stage HCC can be managed with locoregional treatments, while late-stage HCC often

requires palliative care. Standard treatment for late-stage HCC involves multikinase inhibitors such as sorafenib, which targets vascular endothelial growth factor receptor (VEGFR) and platelet-derived growth factor receptors (PDGFR), among others, to slow down tumor growth and disrupt blood supply, though these only extend median overall survival (OS) by 11-14 months (200). The limited efficacy of such therapies is attributed to the high tumor heterogeneity that facilitates the selection of resistant cells. Therefore, new therapeutic strategies are needed, focusing on identifying and targeting tumor-specific dependencies (201).

Surgical, locoregional and systemic therapies in HCC

In patients with HCC at early stages, curative interventions such as surgical resection, liver transplantation and radiofrequency ablation (RFA) are available and may offer the potential for long-term survival. For those with intermediate-stage HCC, transarterial chemoembolization (TACE) remains the standard therapeutic approach (202). However, a significant proportion of HCC cases are diagnosed at advanced stages, where systemic therapies are the only viable option for extending survival (203). Despite these treatments, clinical outcomes remain suboptimal (136,204), primarily due to resistance to conventional therapies, as well as tumor metastasis and recurrence (205).

The following section will provide a detailed examination of the various treatment options currently employed in the management of HCC.

HCC represents a significant challenge in oncology due to its complex nature and varied clinical presentations. Most patients of HCC are diagnosed at late stages when the clinical outcome is unfavourable. Anyway, there are different disease stages where treatment is scheduled in accordance. The treatment plan is determined based on the stage of the tumor and the anticipated benefits of significant interventions, in accordance with the Barcelona Clinic Liver Cancer (BCLC) staging system (100,206,207). The management of HCC involves a combination of surgical, locoregional and systemic therapies tailored to the disease stage, liver function and patient-specific factors. For patients with early-stage HCC, curative options include surgical resection, liver transplantation, or RFA, which can offer long-term survival benefits. In cases of

intermediate-stage HCC, TACE is the standard treatment (202). However, the majority of HCC patients are diagnosed at an advanced stage, where systemic therapy is the sole approach available to extend survival (203). Regrettably, the therapeutic outcomes observed in clinical practice remain unsatisfactory (136,204). These poor results are primarily due to resistance to conventional treatments, as well as tumor metastasis and recurrence (205).

Intermediate-stage HCC, classified as BCLC stage B, presents a heterogeneous clinical challenge, often managed through locoregional therapies such as TACE and transarterial radioembolization (TARE). TACE has long been established as the standard of care for this stage (100,208,209), supported by randomized controlled trials (RCTs) and meta-analyses demonstrating median OS ranging from 19 to 37 months in well-selected patients (210–213). Despite its effectiveness, TACE carries a treatment-related mortality risk of approximately 0.6%, primarily due to acute liver insufficiency (202).

TACE involves the selective delivery of chemotherapy agents to the tumor via the hepatic artery, causing tumor necrosis and reduced tumor burden. The advent of TACE with drug-eluting beads (DEB-TACE) has improved the safety profile by reducing systemic drug-related adverse events while maintaining similar oncological outcomes (214,215). A large meta-analysis reported that objective responses to TACE, achieved in roughly 50-70% of patients, are associated with improved OS (216). However, the combination of TACE with systemic therapies such as sorafenib or brivanib, which target angiogenesis, has not shown a significant OS benefit in RCTs (211).

TARE represents an alternative embolization technique, where yttrium-90 embedded glass or resin microspheres are delivered intra-arterially to the tumor. Compared to TACE, TARE has shown a longer time to disease progression in some studies but similar OS outcomes (217–219). Personalized dosimetry in TARE, targeting higher doses to the tumor, has demonstrated improved objective response rates (ORR) and prolonged OS compared to standard TACE dosimetry. Despite these advancements, TARE remains less widely adopted outside certain regions due to varying levels of evidence and clinical experience.

TARE has also been explored in patients with locally advanced disease unamenable to curative therapies or with disease progression after prior TACE. Early data from studies involving patients with portal vein thrombosis suggested potential benefits, but recent RCTs comparing TARE with systemic therapies such as sorafenib did not meet their primary endpoints of superior OS. The SARAH and SIRveNIB trials, which evaluated TARE against sorafenib, and the SORAMIC trial, which compared the combination of TARE and sorafenib to sorafenib alone, did not demonstrate a significant OS advantage for TARE (220–222).

Deciding when to transition from locoregional to systemic treatment is crucial. Emerging data indicate that patients with extensive intrahepatic disease burden may have lower responses to locoregional therapies and a higher risk of liver dysfunction. Such patients might benefit more from upfront systemic therapy. There is no consensus definition of 'TACE unsuitability' (223,224), but expert guidelines suggest transitioning to systemic therapy in cases of disease progression or development of contraindications during or after multiple rounds of TACE or TARE (100,225,226). Lack of an objective response after at least two rounds of TACE is often used as a predictor for systemic treatment (225,227).

Overall, approximately 20% of patients in phase III trials evaluating systemic therapies have intermediate-stage HCC unresponsive or unsuitable for locoregional therapies. This underscores the importance of identifying appropriate candidates for each treatment modality and the need for ongoing research to refine treatment strategies for intermediate-stage HCC (228–230).

Systemic therapies targeting angiogenesis: antiangiogenic therapies

Antiangiogenic therapies have become a cornerstone in the management of HCC, primarily targeting the VEGF signalling pathway, which is critical for tumor vascularization and growth. These therapies have significantly advanced the treatment paradigm for advanced-stage HCC, BCLC C disease, particularly when combined with other modalities.

Sorafenib was the first antiangiogenic agent to gain approval for HCC, following the demonstration of its efficacy in the phase III SHARP trial. As a multikinase inhibitor, sorafenib exerts its therapeutic effects by inhibiting several receptor tyrosine kinases, including VEGFRs. The trial results showed that sorafenib improved OS compared to placebo, establishing it as a new standard of care for advanced HCC (228,230,231). Subsequent patient-level meta-analyses indicated that patients with HCV-related HCC experienced greater survival benefits from sorafenib, highlighting its potential role in HCV-associated HCC subtypes (232).

In the following years, Lenvatinib emerged as a significant alternative to sorafenib. Lenvatinib, another multikinase inhibitor, targets VEGFRs and fibroblast growth factor receptors (FGFRs), which are involved in tumor angiogenesis and growth (230). The REFLECT trial, a phase III study, demonstrated that lenvatinib was non-inferior to sorafenib in terms of OS, with median survival durations of 13.6 months and 12.3 months, respectively. Notably, lenvatinib showed superior outcomes in secondary endpoints, including ORR and progression-free survival (PFS), indicating its effectiveness in controlling tumor progression and enhancing patient response (230).

Regorafenib and Cabozantinib, both second-line multikinase inhibitors, have also shown substantial benefits for patients who progress after initial antiangiogenic therapy. Regorafenib is a multikinase inhibitor used in HCC treatment that targets VEGFR, PDGFRs, FGFR, c-KIT (KIT), RET, RAF kinases and TIE2, thereby inhibiting tumor growth, angiogenesis and metastasis. Regorafenib demonstrated improved OS compared to placebo in patients who had previously been treated with sorafenib, offering a viable treatment option for those with progressive disease (233). Similarly, cabozantinib, with its multi-targeted mechanism, has proven effective in extending survival in advanced HCC, particularly in patients who have failed other systemic therapies (234). Cabozantinib is a multikinase inhibitor used in HCC treatment and targets VEGFR, MET, AXL, RET, KIT and TAM receptors.

Ramucirumab, an anti-vascular endothelial growth factor receptor 2 (VEGFR2) monoclonal antibody, has shown efficacy in a subset of patients with elevated serum

AFP levels, providing an additional therapeutic avenue for patients with specific biomarker profiles (235).

The introduction of immune checkpoint inhibitors (ICIs) has further revolutionized the management of advanced HCC. The combination of Atezolizumab, an anti-PD-L1 inhibitor and Bevacizumab, an anti-VEGF antibody, has demonstrated improved OS compared to sorafenib in the phase III IMbrave150 trial (228,236). This regimen not only extended median OS but also enhanced ORR and PFS, setting a new benchmark in first-line treatment for advanced HCC. The phase III HIMALAYA trial further expanded therapeutic options with the combination of Durvalumab, an anti-PD-L1 antibody, and a single priming dose of Tremelimumab, an anti-cytotoxic T-lymphocyte protein 4 (CTLA-4) antibody, showing significant improvements in OS compared to sorafenib (237).

Despite these advancements, the effectiveness of ICIs and antiangiogenic therapies in HCC varies according to the underlying aetiology of the disease. While some studies suggest differential responses based on disease aetiology, the current evidence does not robustly support changes in treatment strategies based solely on tumor aetiology.

In summary, antiangiogenic therapies have markedly improved the treatment landscape for HCC, offering various options for managing advanced disease and extending patient survival. Continued research into optimizing these therapies and identifying predictive biomarkers will be crucial in further enhancing patient outcomes in HCC treatment.

Potential therapeutic targeting of VM in cancer

Anti-angiogenic drugs, such as bevacizumab, sunitinib, sorafenib and regorafenib, have been widely employed to inhibit tumor growth through mechanisms that include blocking EC proliferation, inducing EC apoptosis and reducing vascular density, ultimately leading to tumor hypoxia. However, paradoxically, this hypoxia may stimulate the development of VM, which diminishes the therapeutic efficacy of these treatments (162). The insufficiency of current therapeutic strategies targeting aggressive tumors has become evident, as residual tumor cells can adapt and form VM structures, providing alternative blood supply routes that facilitate tumor survival and progression (238).

Additionally, angiogenesis inhibitors are ineffective against VM since VM is regulated by distinct molecular pathways (239).

Although there are some reports suggesting potential therapeutic agents that target VM, the quality of the available research is questionable. Many of these findings are based on low-quality studies, often involving traditional Chinese herbs and remedies, which lack rigorous scientific validation. For example, Melittin, derived from bee venom, has been proposed to inhibit hypoxia-induced VM and EMT by suppressing the Hif-1α/Akt pathway in liver cancer (240). Similarly, extracts from Celastrus orbiculatus and Luteolin, derived from Chinese herbal medicine, have been suggested to downregulate Notch1 signaling, inhibiting VM and tumor growth (241,242). However, these studies often suffer from inadequate experimental controls, lack of reproducibility and insufficient pharmacological profiling, limiting their translatability into effective clinical interventions.

CSCs play a crucial role in VM formation and are linked to the low survival rates seen in patients with aggressive tumors. Post chemo- and radiotherapy, a small subset of CSCs could drive tumor recurrence. Additionally, EMT contributes to the development of CSC characteristics. These insights suggest that targeting both EMT and CSCs could enhance anti-VM therapy, reducing invasion and metastasis while improving patient survival rates. Salinomycin is a potassium ionophore which has been reported to inhibit VM by selectively targeting CSCs. While CSCs are believed to play a critical role in VM formation and are associated with poor prognosis in aggressive tumors, most studies on salinomycin have been conducted *in vitro* or in animal models, without adequate clinical evidence supporting its efficacy in human patients (243).

Other manners suggested to target VM formation by tumor cells is addressing MMPs with MMPs inhibitors. This is the case of doxycycline, that acts inhibiting E-cadherin degradation and down-regulating the expression of vimentin protein (198). Yet again, these findings are based on limited preclinical studies that require further validation in large-scale clinical trials.

Plant-derived compounds have also been explored for their potential anti-VM effects in

HCC. For instance, polyphyllin I, a component of Rhizoma paridis, has been shown to inhibit VM by blocking the PI3K/AKT–Twist1–VE-cadherin pathway (244). Despite these promising results, the overall quality of this research is compromised by the preliminary nature of the studies. Critical pharmacological data, including pharmacokinetics and pharmacodynamics, remain underexplored, making it difficult to assess the real therapeutic potential of these compounds.

In summary, while there are some preliminary reports of agents targeting VM in liver cancer, most studies lack the scientific rigor required for high-impact clinical application. Much of the current knowledge is derived from poorly designed studies and speculative claims about traditional remedies, underscoring the urgent need for more robust, high-quality research in this area.

Post-transcriptional control of gene expression

Gene expression regulation is a highly intricate and multi-dimensional process involving DNA, RNA and proteins. Each phase of gene expression control is precisely managed to enable cells to respond effectively to environmental and physiological changes while maintaining stability against disruptions (245). The nucleotide sequence of a gene dictates the corresponding mRNA sequence and the mRNA sequence determines the amino acid sequence of the resulting protein. Despite this process, the correlation between transcript levels and protein concentrations is complex. Historically, research has concentrated on transcription regulation as the initial step in gene expression. However, recent studies that measure transcripts and proteins on a genomic scale have revealed the importance of additional processes in influencing protein expression (246). This highlights translational efficiency as a key predictor of protein levels, underscoring the significance of mRNA translation (247).

The process of mRNA translation involves several stages and has been the subject of extensive research. Initiation, elongation and termination are the three main stages, with initiation being the most complex and often the rate-limiting step. Initiation involves numerous proteins and is categorized into cap-dependent and cap-independent mechanisms. Cap-dependent initiation, which is more common, involves a

set of eukaryotic initiation factors (eIFs) that help recruit the 40S ribosomal subunit to the 5' untranslated region (5'UTR) of the mRNA, where the cap is localized. The 40S subunit then scans the mRNA until it locates the start codon, which is recognized and matched with the corresponding transfer RNA (tRNA), leading to the assembly of the complete ribosomal complex and progression to elongation. Alternatively, internal ribosome entry site (IRES)-mediated initiation, the alternative mechanism of translation initiation, allows translation to start without the need for 5'UTR recognition, by directly positioning the 40S subunit nearby the start codon.

During elongation, a conserved process across all life forms, the ribosome reads the mRNA sequence and sequentially adds amino acids to the growing polypeptide chain. This step is facilitated by elongation factors such as eEF1A-B, eEF2 and eIF5A, which ensure the accurate movement of aminoacyl-tRNAs through the ribosome's A- (acceptor), P- (peptidyl), and E- (exit) sites.

Termination occurs when the ribosome encounters a stop codon, triggering the release of the newly synthesized polypeptide. This process involves release factors eRF1 and eRF3, which, in conjunction with guanosine triphosphate (GTP), form a complex that facilitates peptide release (248). Following termination, the ribosomal complex disassembles, preparing its components for subsequent translation cycles.

Once the mRNA has fulfilled its role, it undergoes degradation via various exonuclease-mediated pathways, which are tightly regulated to ensure precise mRNA turnover (249). In eukaryotes, the primary degradation pathway begins with the shortening of the poly(A) tail by deadenylases, followed by removal of the 5' cap by mRNA decapping enzymes Dcp1 and Dcp2 (250). The resulting de-capped mRNA fragments are then degraded either by the 5' to 3' exonuclease Xrn1 or by the exosome complex, which acts in the 3' to 5' direction.

The poly(A) tail, consisting of 200–250 adenine residues at the 3' end of nuclear transcribed eukaryotic mRNAs, plays a crucial role in protecting mRNA from degradation. It also helps regulate mRNA stability by promoting circularization during

translation, a process facilitated by initiation factors eIF4E and eIF4G, and poly(A)-binding protein (PABP), which are involved in modulating mRNA translation (251).

Translational regulation of mRNAs

Gene expression has traditionally been associated with transcriptional control. However, recent advancements have highlighted the growing importance of translational regulation in eukaryotic cells. This aspect of gene expression is crucial for making rapid adjustments in protein levels across different biological contexts. Translational regulation primarily occurs during the initiation phase of mRNA translation, when the 40S ribosomal subunit binds to the mRNA. This process can be regulated through two main mechanisms: global control and specific control.

Global control involves modifications to translation initiation factors that affect most mRNAs in the cell. A key player in this process is eukaryotic translation initiation factor 4E (eIF4E), which must interact with eukaryotic translation initiation factor 4G (eIF4G) to facilitate ribosome assembly on the mRNA. The availability of eIF4E is regulated by the phosphorylation state of 4E-binding proteins (4E-BPs). When 4E-BPs are hypo-phosphorylated, they bind to eIF4E, preventing its interaction with eIF4G and thereby inhibiting the binding of the 40S ribosomal subunit to the mRNA and reducing translation. Conversely, when 4E-BPs are hyper-phosphorylated, often due to extracellular signals from the mammalian target of rapamycin (mTOR) pathway—a known regulator of 4E-BP—they release eIF4E, thus enabling translation initiation (252).

Specific control of translation is mediated by proteins that bind to particular sequences within the 5' or 3' UTRs of target mRNAs. These proteins regulate translation without broadly affecting general protein synthesis. Specific mRNA elements that influence translational control include canonical end modifications, IRES, upstream open reading frames (uORFs) and various RNA structures. For example, Maskin is a protein that inhibits eIF4E by binding to specific mRNA sequences. Maskin interacts with cytoplasmic polyadenylation element-binding protein (CPEB), which binds to cytoplasmic polyadenylation elements (CPE) on the mRNA, thus modulating translation through cytoplasmic polyadenylation (251).

Although less common, translational regulation can also occur during the elongation phase. For instance, the phosphorylation of eEF2 by eukaryotic elongation factor 2 kinase (eEF2K) reduces its affinity for ribosomes, thereby inhibiting elongation. The MAPK (mitogen-activated protein kinase) and mTOR signaling pathways can inactivate eEF2K, promoting the elongation function of eEF2. Recent studies have identified additional factors influencing elongation, including acyl-tRNA availability and modifications, ribosome composition and codon optimality (253).

Cytoplasmic polyadenylation element binding (CPEB)-family of proteins

The proteins eIF4E, eIF4G and PABP are part of the RNA-binding protein (RBP) family, which plays a crucial role in RNA metabolism by governing various stages of mRNA life, such as synthesis, processing, maturation, export, stability, transport and translation. RBPs are also pivotal in forming regulatory networks that link these processes, enabling the swift modulation or correction of disruptions within these pathways (254). A notable subset of RBPs is the CPEB family, which was first suggested to exist in the 1990s during studies on the involvement of $p34^{cdc2}$ kinase in cyclin-mediated polyadenylation (255). Researchers discovered that $p34^{cdc2}$ kinase phosphorylated another kinase, probably Aurora-A kinase, which then phosphorylated a CPE-binding protein, later identified as CPEB1.

CPEB-family functions and mechanisms

Among the four mammalian CPEB paralogs, CPEB1-4, there are variations in sequence affinity due to differences in their N-terminal regulatory domain (NTD) and C-terminal RNA-binding domain (CTD) (**Figure 6**). While the CTD is largely conserved, the NTD varies significantly in its RNA-recognition motifs (RRMs) and is subject to various post-transcriptional modifications (256–258). These variations result in distinct expression patterns for each CPEB on the same mRNA target. Additionally, some CPEBs, especially CPEB1 and CPEB4, have been shown to self-regulate their expression by utilizing CPE elements in their own mRNA (259,260). This ability, combined with observations from different tissues and disease states, indicates that CPEBs can finely tune spatial and

temporal signals. However, further research is needed to clarify the specific mechanisms and conditions governing CPEB function.

Recent genome-wide association studies indicate that about 20% of vertebrate transcripts possess CPE motifs, suggesting they could be targets for CPEBs (261). Despite this, the exact functions and regulatory mechanisms of each CPEB in adult tissues are not yet fully understood. CPEBs are particularly interesting due to their role in regulating cytoplasmic polyadenylation by binding to specific elements on target mRNAs and interacting with various proteins. They can modulate translation by either activating or repressing it through polyadenylation and deadenylation, respectively. This is achieved by binding to specific sequences on the 3'UTR of mRNAs, with the CPE (AU-rich domain) being the most common sequence (262). The binding strength and the effect on translation are influenced by factors like the number and type of sequences, their spatial arrangement and the interacting proteins and complexes.

Early studies on CPEB sequences revealed that CPEB2-4 are more closely related to each other than to CPEB1, leading to their classification into a separate subfamily (251,263). CPEB orthologs are better conserved across species compared to paralogs, likely due to their evolutionary importance, although the number of CPEBs varies among species (264) (**Figure 6**). Initial research on CPEBs utilized *Xenopus laevis* oocytes as a model for studying cytoplasmic polyadenylation-dependent translation. Over time, research expanded to other models and contexts, revealing distinct identities and functions for each CPEB member related to poly(A) tail regulation.

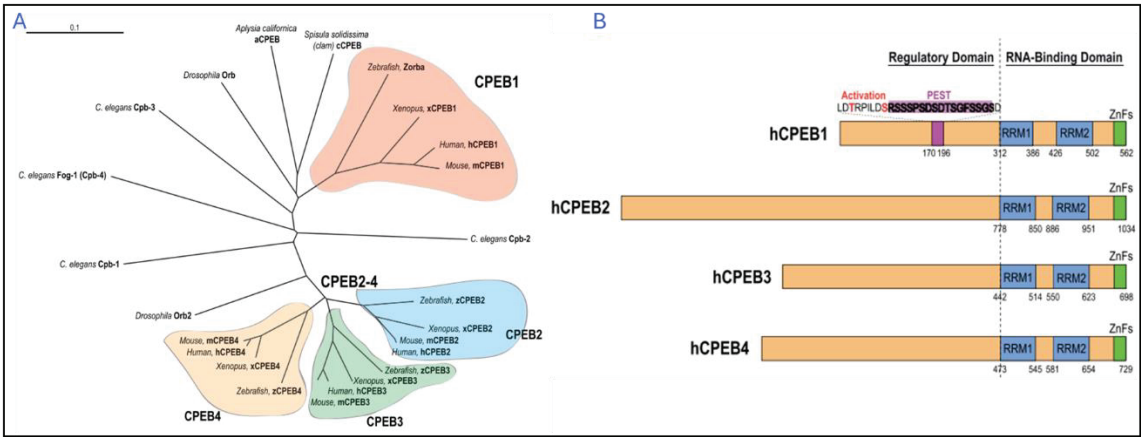

Figure 6. Phylogenetic and structural analysis of the family of RNA-binding proteins CPEB. (**A**) An unrooted phylogenetic tree illustrating the evolutionary relationships among representative CPEB proteins, derived from a comprehensive multiple sequence alignment of their full-length sequences. The tree indicates that orthologs of CPEB1 (colored red) are the most distantly related within the CPEB family, while CPEB2 (blue), CPEB3 (green), and CPEB4 (yellow) are more closely related and grouped in the same branch. (**B**) Schematic representation of human CPEB protein structures. The proteins feature a conserved RNA-binding domain at the C-terminal end and a variable regulatory domain at the N-terminal end. The RNA-binding domain includes two RRMs (shown in blue) and two zinc fingers (depicted in green). For CPEB1, the regulatory domain includes two residues (highlighted in red) that become phosphorylated by Aurora A to activate CPEB1, followed by a PEST-degradation motif (shown in purple). Image obtained from Fernández-Miranda, G. & Méndez, R. (2012) (251)**.**

CPEB1, the most extensively studied member, was the first identified and has been shown to act as both an activator and repressor of mRNA translation depending on its phosphorylation state (251). Although the activation mechanism is well understood, the repression mechanism involving unphosphorylated CPEB1 is still debated. Phosphorylation alters CPEB1's affinity for the cleavage and polyadenylation specificity factor (CPSF), leading to poly(A) ribonuclease (PARN) eviction and the initiation of polyadenylation by Gld2 during both meiotic (265) and mitotic stages (266). CPEB1 is also linked to cellular senescence (267), tumor development (268), inflammation (268), synaptic plasticity (269) and liver homeostasis (270).

In contrast, CPEB2 was initially thought to be a translational repressor during the elongation phase through interaction with eEF2 (271), though its activation mechanisms on specific mRNAs are less understood (272). CPEB2 is expressed in the liver, brain and testes. CPEB2 interacts with β-catenin and CaMKII, which are also targets of CPEB1 (273).

Additionally, CPEB2 has been implicated in regulating HIF-1α activity, particularly in neuroblastoma cells (272). More research is needed to fully understand CPEB2's roles in cancer and liver function.

CPEB3, studied mainly in synaptic contexts, has been shown to enhance mRNA activation and degradation through monoubiquitination (261) and cleavage by Calpain2 via prion-like aggregate formation (256,274,275). CPEB3 is also linked to tumorigenesis and may contribute to HCC progression (276).

CPEB4 exhibits both repression and activation roles in cytoplasmic polyadenylation depending on the context, including terminal erythroid differentiation (259), circadian rhythms (277,278), cellular stress responses (278–280), oocyte maturation, somatic cell cycle, tumor progression and pathological angiogenesis in the liver (266,281). While these functions suggest a pro-tumorigenic role for CPEB4 (282–285), some studies report contrasting findings (286).

CPEB4 functions

CPEB1, CPEB2 and CPEB3 are critical for proper mitotic cell division, while CPEB4 specifically plays a crucial role in cytokinesis (266,287). Beyond its developmental functions, CPEB4 is implicated in several pathological conditions. For instance, CPEB4 is often overexpressed in cancers like gliomas and pancreatic cancer (281). In these malignancies, CPEB4 contributes to the TME by modifying the stroma, enhancing tumor vascularization and promoting invasion. Additionally, CPEB4 has been associated with melanoma progression through the regulation of specific lineage drivers (288) and with breast cancer by facilitating cell migration and invasion via upregulation of the EMT marker vimentin (289). Furthermore, CPEB4 is involved in intestinal inflammation and CRC. CPEB4's expression in gut-associated lymphoid tissue (GALT) is crucial for managing inflammation and cancer development. In CPEB4-deficient mice, acute colitis symptoms were more severe and CRC progression was affected, illustrating CPEB4's role in intestinal inflammation and cancer (290).

CPEB4 has also been connected to autism spectrum disorders (ASD). Patients with autism show a higher percentage of a specific CPEB4 mRNA isoform with a shortened poly(A) tail, which leads to reduced expression of genes associated with autism risk (291). In the nervous system, CPEB4, alongside other CPEB family members, is highly expressed in the brain and is vital for the survival of hippocampal neurons. It likely plays a role in regulating mRNA processing necessary for neuroprotection against cellular stress (292).

In cardiac tissue, CPEB4's function is essential for managing pathological stress. CPEB4, regulated through ERK1/2 phosphorylation, inhibits mRNAs of transcription factors Zeb1 and Zbtb20, which are implicated in cell proliferation and cancer. In hypertrophied cardiomyocytes, CPEB4's repression of these targets correlates with pathological cell growth, suggesting that its phosphorylation status affects cardiac cell growth and may influence heart disease progression (280).

CPEB4's role in the immune system has also been elucidated in recent studies. CPEB4 is crucial for T-cell function within the TME. CPEB4 supports T-cell responses under ER stress, facilitating adaptive immunity and tumor surveillance. Its role in T-cells, particularly CD8+ T-cells, is vital for maintaining effective immune responses in stressed conditions (279).

In macrophages, CPEB4 stabilizes anti-inflammatory mRNAs, aiding in inflammation resolution post-stress. CPEB4 knockout ($CPEB4^{KO}$) mice exhibit higher levels of pro-inflammatory cytokines and reduced survival after lipopolysaccharide (LPS)-induced inflammation. CPEB4 is involved in managing inflammation and recovery from stress-induced damage (293).

In the context of obesity, CPEB4 mediates post-transcriptional reprogramming in adipocytes, which boosts pro-inflammatory factor production and enhances macrophage inflammation and migration. This highlights CPEB4's role in systemic inflammation linked to adipose tissue (294).

CPEB4 role in liver disease

CPEB4 plays a crucial role in cell autonomous effects in hepatocytes in cellular stress responses, particularly in the liver, where it significantly impacts both metabolic and pathological processes. In NAFLD, CPEB4 modulates the hepatic unfolded protein response (UPR) and regulates lipid metabolism, implicating it in obesity-related liver damage (278). CPEB4 mRNA exhibits a circadian rhythm, essential for regulating the UPR, maintaining ER function and overseeing glucose and lipid metabolism. Research has shown that in mice on a HFD, the absence of CPEB4 exacerbates liver steatosis and fibrosis due to disrupted lipid metabolism and compromised ER stress management. This deficiency impairs mitochondrial FAO and increases lipid toxicity, highlighting CPEB4's vital role in liver metabolic balance and stress adaptation (278).

Moreover, CPEB4 is critical in ECs for pathological angiogenesis in the liver and mesentery during conditions such as portal hypertension and CLD (295). It promotes the overexpression of the proangiogenic factor VEGF during cirrhosis through the phosphorylation of CPEB1. Increased CPEB4 expression in portal hypertension is associated with the expansion of vascular stem progenitor cells and neovascularization (296). Furthermore, studies from our research group have revealed that CPEB4 has a role in liver fibrogenesis regulating the glycolysis driver 6-phosphofructo-2-kinase/fructose-2,6-bisphosphatase 3 (PFKFB3) in activated HSCs through post-transcriptional mechanisms (297).

In summary, CPEB4 has a multifaceted and context-dependent role in cellular stress responses, regulating stress adaptation across various tissues by modulating mRNA stability and translation. Its diverse functions underscore its significance in both developmental processes and various pathological conditions. Further research is needed to fully comprehend its complex roles in different physiological and pathological contexts.

Hypothesis and objectives

Rationale: Investigating the role of CPEB4 in VM within liver cancer is of significant importance for several reasons. VM, where cancer cells adopt endothelial-like characteristics to form vessel-like structures, remains underexplored in liver cancer. By examining CPEB4's involvement, we aim to uncover novel insights into the regulatory mechanisms governing VM and its broader implications in liver cancer pathology. Understanding how CPEB4 influences VM could provide critical information on how it modulates translational control mechanisms that are key for tumor progression and vascularization.

CPEB4 plays a crucial role in regulating mRNA translation, a process integral to cellular functions relevant to cancer biology. Elucidating its role in VM will provide a clearer understanding of how translational control impacts tumor vascularization, progression and resistance to therapy. Furthermore, anti-angiogenic therapy, often used in treating liver cancer, has advantages over chemotherapy, as it does not directly kill cancer cells but inhibits new blood vessel formation—an occurrence rare outside of tumors. This makes it better tolerated by patients, with fewer side effects. However, anti-angiogenic therapies often create a hypoxic TME, leading to resistance through alternative vascularization pathways such as VM.

By exploring CPEB4's role in VM, this research could illuminate how tumors bypass the effects of anti-angiogenic therapies. Understanding the signaling pathways and molecular mechanisms of VM may help overcome the limitations of these therapies and lead to improved treatment outcomes. The findings from this study could also extend beyond liver cancer, contributing to the understanding of VM in other cancer types, and could uncover new therapeutic targets or biomarkers.

The overarching hypothesis is that CPEB4-dependent translational control modulates VM and contributes to the resistance of liver cancer to anti-angiogenic therapies. We propose that CPEB4 regulates liver cancer-associated neovascularization by influencing pathological angiogenesis, promoting VM and facilitating EMT in tumor cells. Through a

comprehensive investigation of these processes, this thesis seeks to advance our understanding of CPEB4's role in liver cancer progression and therapeutic resistance, ultimately contributing to more effective treatment strategies.

Our specific objectives are:

Investigate the ability of liver cancer cells to perform vasculogenic mimicry *in vitro* and *in vivo*.

This objective seeks to systematically assess the capacity of liver cancer cells to exhibit VM under controlled *in vitro* conditions and within *in vivo* tumor models. By characterizing the structural and functional aspects of VM, we aim to understand how liver cancer cells form vessel-like structures that mimic blood vessels without involving endothelial cells. We will identify key molecular markers associated with VM and quantify the extent of VM in liver cancer tissues.

Explore the role and mechanisms of CPEB4 in vasculogenic mimicry.

To define CPEB4's specific role in VM regulation, we will investigate how CPEB4 influences the formation and maintenance of VM structures. We aim to determine how CPEB4 modulates the transition of liver cancer cells to an endothelial-like phenotype and identify the relevant signaling pathways and gene expression profiles involved. This exploration will clarify the mechanistic role of CPEB4 in VM and evaluate its potential as a therapeutic target in liver cancer.

Determine if CPEB4 regulates the pro-angiogenic profile of cancer cells.

This objective will examine whether CPEB4 impacts the pro-angiogenic properties of liver cancer cells. We will evaluate changes in tumor vasculature in response to CPEB4 modulation. By correlating CPEB4 expression with angiogenic activity, we will gain insights into its role in promoting or inhibiting tumor blood vessel formation.

Assess if CPEB4 plays a role in the resistance to anti-angiogenic therapy in liver cancer.

To explore CPEB4's involvement in therapeutic resistance, we will assess how changes in CPEB4 expression influence the response of liver cancer cells to anti-angiogenic

treatments. This objective includes *in vitro* studies to evaluate whether modulating CPEB4 expression alters the effectiveness of anti-angiogenic agents. This investigation will provide critical insights into the molecular mechanisms driving resistance to anti-angiogenic therapies, with the goal of identifying strategies to overcome these limitations.

By addressing these objectives, this research will provide a deeper understanding of how CPEB4 influences VM, angiogenesis and therapy resistance in liver cancer, with potential implications for developing more effective treatments.

Materials and methods

In vitro models and molecular biology techniques

To investigate the role of CPEB4 in VM vessel formation, we utilized liver tumor cell lines of both human and murine origins. Our primary objective was to determine whether these liver cancer cells can form VM channels and to elucidate the role of CPEB4 in this tumoral mechanism. For this study, we employed wild type (WT) cells as well as knockdown (KD) or knockout (KO) cells for CPEB4, all of which express a luciferase-GFP (Luc-GFP) reporter plasmid. The expression of luciferase-GFP allows us to detect tumor growth through bioluminescence, thanks to luciferase, and to analyse the structures formed by the tumor cells *in vitro* by fluorescence, as they will be GFP-positive.

Initially, plasmids needed to generate the cells of interest were amplified and cells were infected. Once cells were successfully modified to express the desired plasmids, their ability to form tube-like structures in matrigel was assessed. Subsequently, cells were tested for different tumoral characteristics, including proliferation, soft agar colony formation and resistance to anoikis death. After constructing and evaluating the cells for various tumoral parameters, they were injected subcutaneously into mice. This allowed us to study their tumor-forming ability, the tumors' aggressiveness and the correlation between the tumor cells' capacity to form VM structures and tumor aggressiveness.

Bacterial DNA isolation

Transformation of competent cells

The One Shot® Stbl3™ Chemically Competent *Escherichia coli* (*E. coli*) (Invitrogen, C7373-03) was used to facilitate the transformation of plasmid DNA of interest into *E. coli*. This methodology involved several key steps designed to maximize transformation efficiency and plasmid stability. First, the chemically competent Stbl3™ *E. coli* cells were thawed on ice to maintain their competence. Plasmid DNA (**Table 1**) was then gently mixed with the cells and incubated 30 minutes on ice, allowing the DNA to adhere to the bacterial

cell membranes. Following this, a heat shock was applied at 42°C for 45 seconds, which induced the uptake of the plasmid DNA into the cells. The cells were then returned to ice briefly for 2 minutes before adding 250 µL pre-warmed S.O.C. medium (*provided by the kit*) to aid in the recovery and expression of antibiotic resistance genes. The mixture was incubated at 37°C with horizontal shaking, for one hour at 225 rpm, to allow for cell recovery and plasmid replication. Finally, the transformed cells were spread on pre-warmed selective agar plates containing 100 µg/mL ampicillin (Sigma-Aldrich, A5354) to select for colonies that had successfully taken up the plasmid and incubated overnight at 37°C. Plates were made *in house* using LB Broth (Lennox) (Sigma-Aldrich, L3022). For the preparation of plates, 20 grams of LB Broth were diluted in 1 litre of distilled water, heated to boiling while stirring to dissolve ingredients and autoclaved for 15 minutes at 121ºC. Once autoclaved and completely dissolved, antibiotic was added and the mixture was poured into plates in a sterile environment (under a Bunsen burner). Plates were let to solidify at room temperature and kept at 4ºC until needed.

Table 1. **Plasmids for cell lentiviral and retroviral infection experiments.**

<table>
<tr><th colspan="2">Lentiviral infection</th><th colspan="2">Retroviral infection</th></tr>
<tr><td rowspan="2">Lentiviral plasmid:</td><td>MISSION® pLKO.1-puro Non-Mammalian shRNA Control Plasmid DNA (Sigma-Aldrich, SCR SHC002)</td><td rowspan="2">Retroviral plasmid:</td><td rowspan="2">SIN40C.SFFV.Luciferase.IRES.GFP (Addgene, plasmid #169308)</td></tr>
<tr><td>pLKO shCPEB4.4 (Hs). shRNA sequence: 5’-GCGTTATGTGTTGAACAGTAT-3'</td></tr>
<tr><td>Envelope plasmid:</td><td>pCMV-VSV-G (Addgene, plasmid #8454)</td><td rowspan="2">Envelope plasmid:</td><td rowspan="2">pCMV-VSV-G (Addgene, plasmid #8454)</td></tr>
<tr><td>Packaging vector:</td><td>psPAX2 (Addgene, plasmid #12260)</td></tr>
</table>

Miniprep protocol

Plasmids obtained during this project were amplified in all cases by miniprep protocols. For miniprep, the desired bacterial colony was grown in 3 mL of LB medium with ampicillin (1 µg/mL) overnight at 37ºC and the commercial recommendations of the QIAprep® Spin Miniprep kit (Qiagen, 27104) were used.

Plasmid expression verification in colonies via restriction enzyme digestion

Restriction enzyme digestion was used to check if bacterial colonies expressed the plasmid of interest.

All digestions were carried out using 20 units of enzyme (New England BioLabs®), 1 µg of DNA, appropriate reaction buffer according to supplier recommendations (10X buffer, New England BioLabs®) and up to 50 µL nuclease free water (Thermo Fisher, AM9932). Digestions were performed at 37ºC for 1 hour. Digestion reactions were checked running DNA into 0.8% agarose gels by electrophoresis. For the 0.8% agarose gel, 0.8 grams of UltraPure™ agarose (Thermo Fisher, 16500500) per 100 mL of Invitrogen™ UltraPure™ TBE Buffer (Invitrogen™ 15581044) were used. DNA samples (with 1X loading dye, New England BioLabs®, B7025S) and a Quick-Load Purple 2-Log DNA Ladder (0.1-10Kb) (New England BioLabs®, N0550S) were loaded into the wells. Electrophoresis was run at 100 volts for 30-45 minutes, monitoring the progress by the migration of the dye.

Production of lentivirus, retrovirus and infection protocol

On Day 1, GP-293 packaging cells (for retrovirus) or 293T packaging cells (for lentivirus) were seeded onto 6 cm tissue culture plates (TPP Reactiva, 93060) that had been pre-treated for 1 hour at room temperature with 1% gelatine (Sigma-Aldrich, G1393), with the goal of achieving 70-80% confluency by the following day.

On Day 2, the media was replaced and transfections were conducted in the afternoon. For retrovirus, the transfection mixture included 2 µg of retroviral plasmid DNA and 1 µg of ENV plasmid DNA. For lentivirus, the transfection mixture consisted of 2.5 µg of

lentiviral plasmid DNA, 1.5 µg of packaging vector and 0.5 µg of envelope plasmid DNA (**Table 1**). To transfect cells, LipoD293™ DNA *In Vitro* Transfection Reagent (SignaGen® Laboratories, SL100668) was used. For each transfection, LipoD293 reagent was diluted in serum-free medium and gently mixed with the plasmid DNA solution, allowing the complex to form for a 15 minute incubation period at room temperature. DNA-LipoD293 complex was added dropwise to the cells, ensuring even distribution by gently swirling the plate. Cells were incubated at 37°C with 5% CO_2 overnight.

On Day 3, the media was changed in the morning to remove the transfection reagent and replaced with 3 mL of fresh DMEM (DMEM/F-12, Invitrogen 11320-074) supplemented with 10% bovine foetal serum (FBS) (Reactiva®, 04-001-1A) and penicillin/streptomycin (Gibco®, 15140122), taking care to avoid disturbing the transfected cells. Cells were then incubated at 37°C with 5% CO_2 for 24 hours. Simultaneously, target cells for infection were plated in 6 cm dishes to achieve a confluency of 40-50% by the following day.

On Day 4, the media was harvested from the transfected GP-293 or 293T cells and filtered through 0.22 µm filter (TPP Reactiva, 99722). The filtered media was diluted with 3 mL of fresh media and 2 mL were added to the 6 cm dishes containing the cells of interest. The target cells were then incubated at 37°C with 5% CO_2 for 24 hours.

On Day 5, the media from the GP-293 or 293T cells was again harvested and processed as described in day 4. The media from the infected target cells was removed and fresh media containing the virus was added. In the late afternoon, the virus-containing media was removed from the infected cells and replaced with fresh media.

By Day 8, the media of the infected cells was replaced with media containing the selection antibiotic as the retrovirus and lentivirus encoded an antibiotic selection gene (puromycin). Prior to this media change, cells of interest were checked for the toxic dose of puromycin.

Generation of stable CPEB4 knockdown human liver cancer cell lines.

On one hand, we have used the tumoral human commercial cell line HepG2 from an HCC origin (ATCC®, HB-8065™). Cells were grown on Eagle's Minimum Essential Medium (EMEM) (ATCC®, ATCC-30-2003) supplemented with 10% FBS (Reactiva®, 04-001-1A), 100 units/mL penicillin, 100 µg/mL streptomycin (Gibco®, 15140122) and 1% L-glutamine (Gibco®, 25030024) (complete EMEM medium). Incubation of cells took place at 37ºC, 5% CO_2 and 21% O_2 in a humid atmosphere. When cells reached confluence, they were split to avoid contact inhibition. First, complete EMEM medium was removed using a vacuum pump. Then, cells were washed with phosphate-buffered saline (PBS) (Reactiva, 02-023-1A) and incubated with trypsin-EDTA (Corning®, 25-051-CI) until they were close to be detached from the plate. Then, trypsin excess was removed, cells were resuspended in complete medium and the desired number of cells was transferred to a clean plate.

To generate human CPEB4 knockdown cell lines, short hairpin RNA (shRNA) encoding sequences were delivered to the HepG2 cell line through lentiviral infection. Lentivirus were produced by transfecting 293T packaging cells with the plasmid psPAX2 (Addgene, plasmid #12260) (**Figure 7**), the envelope plasmid ENV (pCMV-VSV-G, Addgene, plasmid #8454) (**Figure 8**) and pLKO shCPEB4.4 (pLKO.1 puro, Addgene, plasmid #8453) with the sequence 5'-GCGTTATGTGTTGAACAGTAT-3' (**Figure 9**) for knockdown experiments. For control conditions, the MISSION® pLKO.1-puro Non-Mammalian shRNA Control Plasmid DNA (Sigma-Aldrich, SCR SHC002) (**Figure 10**) was used. All transfections were performed using the liposome-based DNA transfection reagent LipoD293.

The pLKO shCPEB4.4 vector carried a shRNA sequence specific for CPEB4 (5'-GCGTTATGTGTTGAACAGTAT-3') and puromycin resistance marker. A scramble (SCR) control RNA, that does not recognize any region in the mammalian genome was used to obtain the WT cells for CPEB4 (MISSION® pLKO.1-puro Non-Mammalian shRNA Control Plasmid DNA from Sigma-Aldrich® was used). Media from transfected 293T cells was removed and replaced with fresh media every 24 hours. The media was harvested 48 and 72 hours post transfection, filtered through a 0.22 µm filter (to use only the lentiviral

particles) and used to infect HepG2 cells grown on 6 cm dishes. Efficiently infected HepG2 cells were selected with 4 µg/mL puromycin (Millipore, 540222-25MG) to create constitutive stable CPEB4 knockdown HepG2 cells. To test the phenotype of the cells, RNA and proteins were extracted from the cells to perform real-time quantitative PCR (RT-qPCR) and western blot analyses as described in the following sections.

These cells were then infected with retrovirus containing pRV luciferase-GFP plasmid (Addgene, Plasmid #169308) (**Figure 11**). To produce retrovirus, the pRV luciferase-GFP plasmid as well as the envelop pCMV-VSV-G plasmid (Addgene, plasmid #8454) (**Figure 12**) were transfected to GP-293 cells, as previously explained and retrovirus were used to infect the cells of interest. The number of GFP positive cells was determined by flow cytometry and GFP positive cells were sorted with a sorter using the BD FACSDiva™ Software (BD Biosciences) in the Flow Cytometry facility at IDIBAPs.

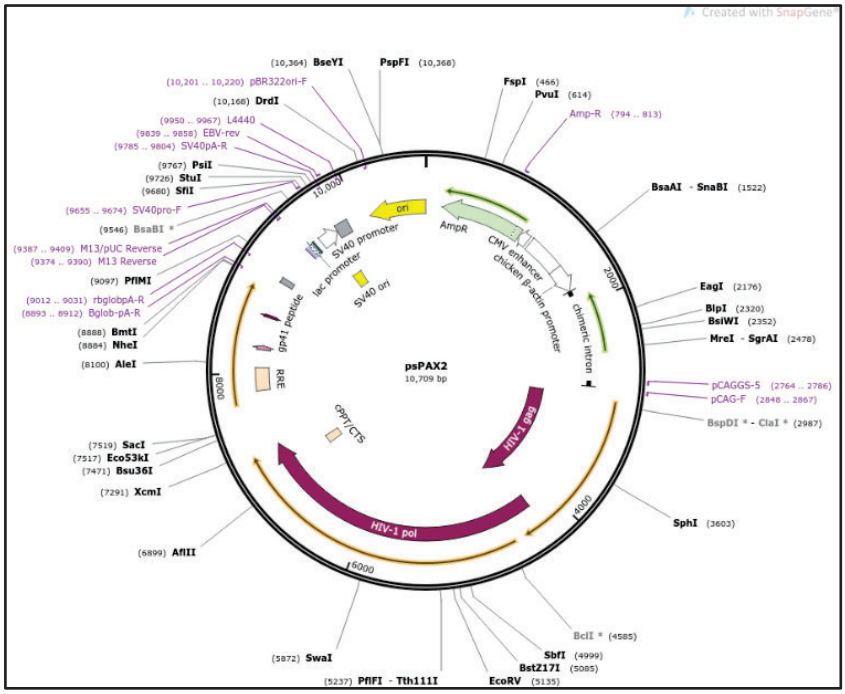

Figure 7. Plasmid map of psPAX2 (Addgene, plasmid #12260). Key elements of this plasmid include the 5' Long Terminal Repeat (LTR), which contains the U3 region critical for transcription initiation and the packaging signal (ψ), necessary for the incorporation of viral RNA into virions. Additionally, this plasmid contains the Gag/Pol coding region, responsible for the production of Gag (group-specific antigen) and Pol (polymerase) proteins essential for viral particle assembly and replication. The absence of the viral envelope protein gene (env) in psPAX2 enhances the safety profile of the plasmid by preventing the formation of replication-competent lentiviruses but requires the addition of another plasmid to the transfection.

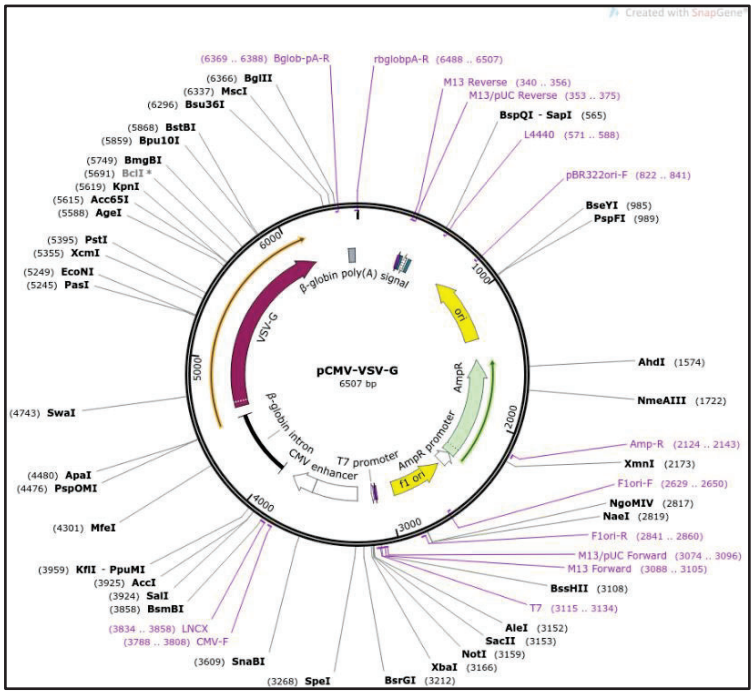

Figure 8. Plasmid map of envelop plasmid pCMV-VSV-G (Addgene, Plasmid #8454). This plasmid encodes the VSV-G (vesicular stomatitis virus glycoprotein) and was used to enhance the pseudotyping of lentiviral vectors. The map features the CMV (cytomegalovirus) promoter, which drives high-level expression of the VSV-G protein. The VSV-G coding sequence itself is shown, responsible for providing the **envelop protein** necessary for the efficient pseudotyping of lentiviral particles. This plasmid is a vital tool in gene delivery applications, facilitating the production of viral vectors with improved cell entry capabilities.

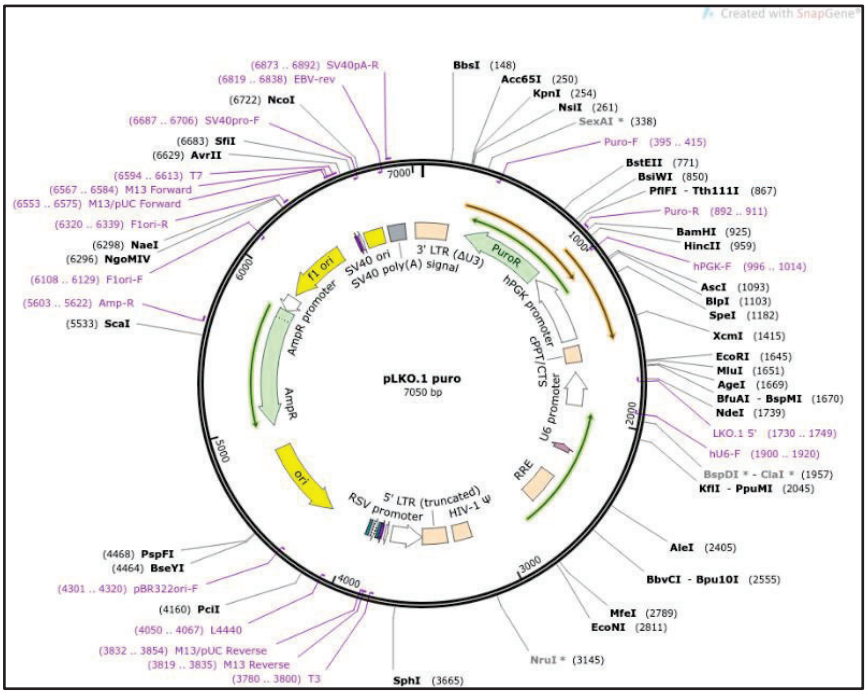

Figure 9. **Plasmid map of pLKO.1 puro (Addgene, Plasmid #8453).** This plasmid contains the U6 promoter, which drives the expression of shRNAs designed to target specific mRNAs for degradation. In this case we used a sequence targeting human CPEB4 (5'-GCGTTATGTGTTGAACAGTAT-3'). Additionally, the plasmid contains a puromycin resistance gene, allowing for the selection of successfully transfected cells through antibiotic selection. This vector is a valuable tool for functional genomics studies, enabling the targeted knockdown of gene expression in mammalian cells.

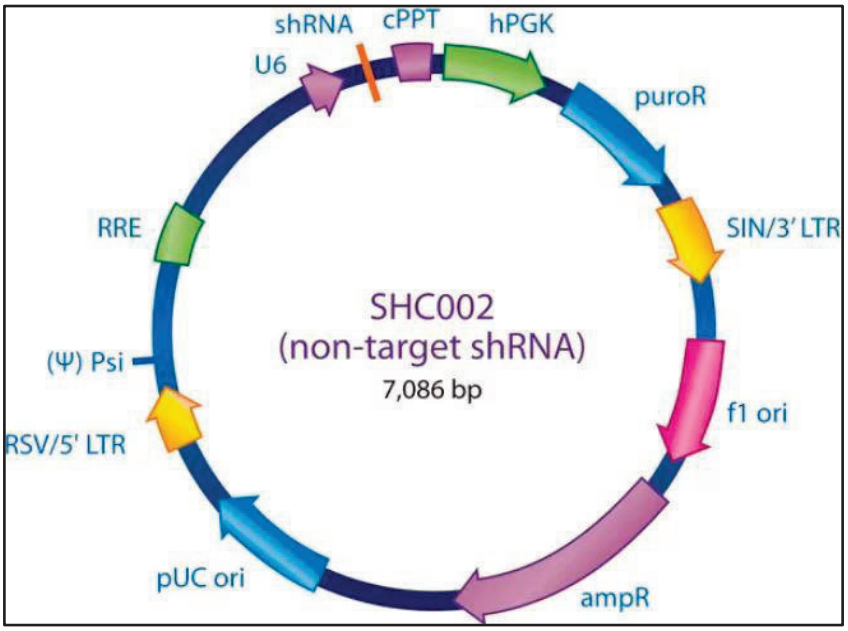

Figure 10. **Plasmid map of the MISSION® pLKO.1-puro Non-Mammalian shRNA Control Plasmid DNA (Sigma-Aldrich, SCR SHC002).** This vector was used as a negative control. This plasmid

includes a U6 promoter, which drives the expression of a non-mammalian shRNA sequence. The inclusion of a puromycin resistance gene allows for the selection of successfully transfected cells via antibiotic resistance. This control plasmid is utilized to assess the specificity and efficiency of shRNA-mediated gene silencing by providing a baseline measurement against which experimental shRNA constructs can be compared.

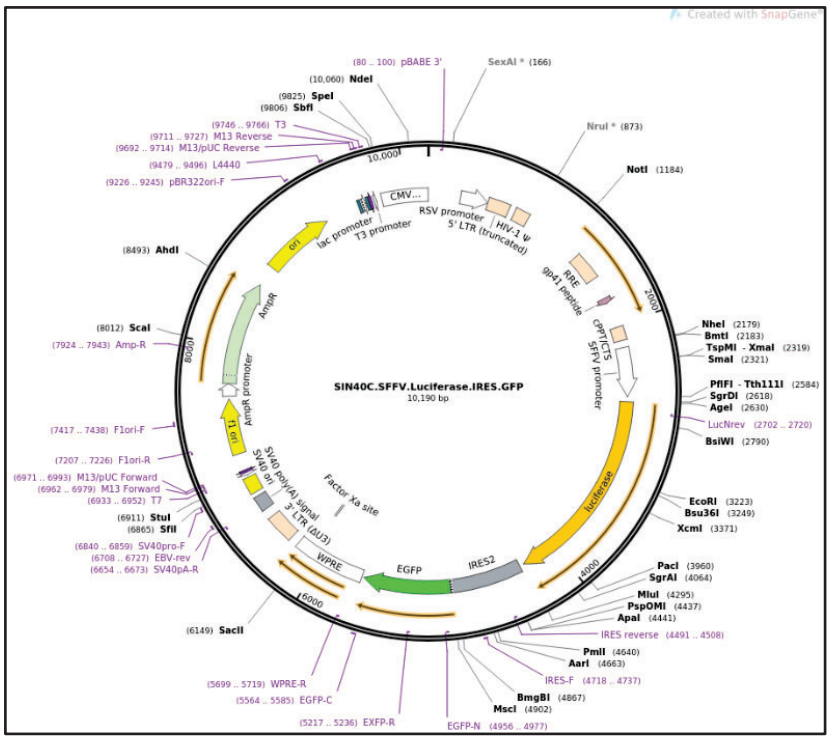

Figure 11. **Plasmid Map of SIN40C.SFFV.Luciferase.IRES.GFP (Addgene, plasmid #169308).** This plasmid includes the origin of replication (ori) necessary for plasmid propagation, a multiple cloning site (MCS) for gene insertion and a selection marker for antibiotic resistance. Additionally, the figure highlights the promoter region responsible for gene expression.

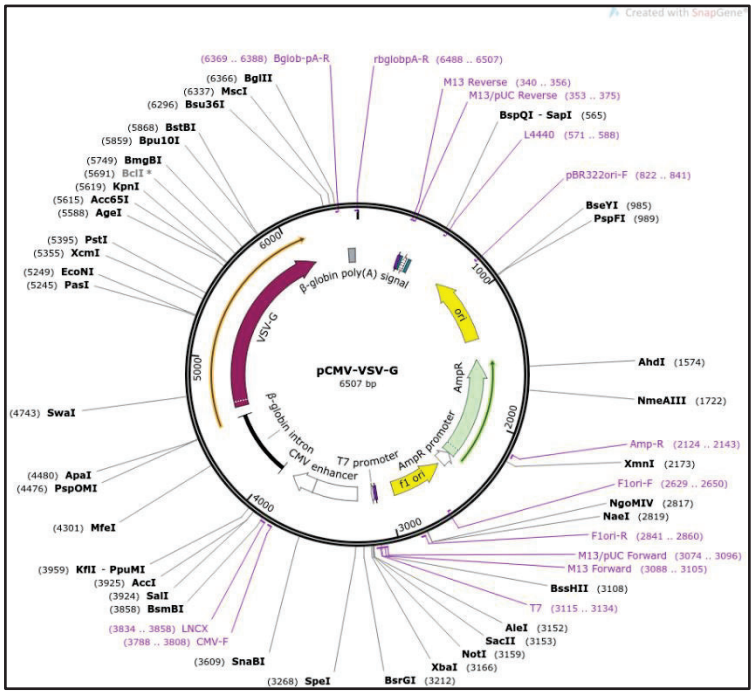

Figure 12. Plasmid map of pCMV-VSV-G (Addgene, plasmid #8454). This plasmid encodes the VSV-G envelope protein under the control of the CMV promoter. This plasmid contains the CMV promoter, the VSV-G coding sequence and relevant restriction enzyme sites. The pCMV-VSV-G plasmid is commonly used to enhance the production of viral particles by providing a functional envelope protein necessary for efficient viral entry into target cells.

Generation of stable CPEB4 knockout mouse liver cancer cell lines.

On the other hand, cells from murine origin were used. These cells, named 2020B3, were derived from liver tumors developed in inducible CPEB4^{KO} mice after 50 weeks of a liver carcinogenesis protocol including HFD and diethylnitrosamine (HFD+DEN) treatment, following the method described under "*In vivo* models and protocols" section.

To obtain mouse liver tumor cell line 2020B3, the animal bearing the liver tumors was first anesthetized and immobilized. A careful incision was made from the base of the tail to the neck along the abdomen, avoiding puncture of the peritoneum. The skin was retracted to expose the tumors, which were then cut free from the body, removing excess surrounding tissue. Tumors were stored in serum-free DMEM/F12 medium on ice until digestion, which occurred within one hour.

In a 10 cm Petri dish, tumors were minced into 1-2 mm pieces using a scalpel and placed into a 50 mL conical tube. Digestion medium (for a final volume of 50 mL: 25 mL accutase

(PAA laboratories, L11-007), 50 mg collagenase (Sigma, 10103578001), 0.5 mL 100x Penicillin/Streptomycin and 24.5 mL DMEM/F12) was added to the tube at a 10:1 ratio of medium to tumor volume. The mixture was incubated on a shaker at 37°C for 3-5 hours to ensure thorough digestion. After digestion, the mixture was diluted with DMEM/F12 containing 0.2% bovine serum albumin (BSA) (Ecogen, A1391,0100), filtered through a 40 µm nylon mesh and centrifuged at 200 g for 5 minutes. The pellet was resuspended in DMEM/F12 0.2% BSA, centrifuged again and washed repeatedly until the supernatant was clear. To remove red blood cells, the pellet was resuspended in a mixture of NH_4Cl and PBS supplemented with 1% BSA (adjusted based on pellet volume) and the process was repeated if necessary. After the final washing, clumped cells were treated with accutase, neutralized with DMEM/F12-0.2% BSA, centrifuged and washed with PBS. The cells were then resuspended in PBS and kept on ice until further processing.

Finally, lineage marker-negative (Lin-) epithelial cells were isolated using the EasySep™ Mouse Epithelial Cell Enrichment Kit II (STEMCELL Technologies, 19868) to obtain a purified epithelial sample, which was used immediately or stored in appropriate conditions for later use.

After the establishment of murine tumoral cells, they were cultured in Dulbecco's Modified Eagle Medium: Nutrient Mixture F-12 (DMEM/F-12, Invitrogen, 11320-074). The medium was supplemented with 10% FBS (Reactiva®, 04-001-1A), 100 units/mL penicillin, 100 µg/mL streptomycin (Gibco®, 15140122), 100 µg/mL non-essential amino acids (Gibco®, 11140050) and 100 µg/mL sodium pyruvate (Sigma-Aldrich®, S8636-100ML), constituting a complete DMEM medium. The cells were then maintained following the previously described protocol for human cells.

To obtain luciferase-GFP cells these cells were infected as in the case of HepG2 cells with a retrovirus containing the pRV luciferase-GFP plasmid (**Figure 11**) and selected with the aid of flow cytometry. In the case of murine cells, cells knockout for CPEB4 were stablished instead of knockdown. To obtain $CPEB4^{KO}$ cells, an adenovirus expressing CRE recombinase system (Tebu-Bio®, SL100707) was used as the cells contained the CPEB4

gene surrounded by loxP sequences (that when recognized by CRE, will be excised). Recombinant adenovirus was supplied in liquid form at the indicated titter, stored in DMEM/2.5% glycerol solution at -80°C. Upon arrival, the viral stock was aliquoted as needed and immediately stored at -80°C to prevent degradation, with care taken to avoid repeated freeze-thaw cycles. For 2020B3 infections, the viral stock was thawed on ice and the desired amount of virus diluted in complete DMEM media was added to the cell's media. For that, the original cell culture media was removed and 3 mL of the virus-containing media was added to each 6 cm 2020B3 Luc-GFP cell plate. Cells were incubated with the virus-containing media for 16 hours, after which the media containing virus was replaced with fresh media. To achieve optimal infection without cytotoxicity, the appropriate multiplicity of infection (MOI) was determined. 2020B3 Luc-GFP cells required a multiplicity of infection (MOI) of 1,000. Pilot testing with increasing MOI of virus was conducted to establish the optimal viral concentration for 2020B3 Luc-GFP cell line. Optimal viral concentration was validated by western blot and RT-qPCR being the optimal the one making CPEB4^{KO} cells with the lowest MOI. To test the phenotype of the cells, RNA and proteins were extracted from the cells to perform RT-qPCR and western blot analyses as described in the following sections.

Flow cytometry

To sort GFP-positive cells, cells stably expressing GFP were cultured in complete media until 70-80% confluent. Cells were detached with 0.05% trypsin-EDTA, trypsin neutralized with complete media and centrifuged at 300 g for 5 minutes. Cell pellet was washed twice with PBS and resuspended in PBS containing 2% FBS to a concentration of 5 x 10^6 cells/mL. To be able to discriminate live from dead cells, cells resuspended in PBS were incubated 7 minutes at room temperature in the dark with 1 µg/mL propidium iodide (Sigma-Aldrich, P4170). After incubation, cells were washed with two rounds of PBS and centrifuged. Prior to sorting, cells were filtered through a 40 µm cell strainer (Corning®, CLS431750) to remove cell clumps. Flow cytometer (BD FACSDiva™ Software) was calibrated for GFP detection using a 488 nm laser and a 530 nm filter. Cells were gated on forward scatter and side scatter to exclude debris and dead cells. GFP-positive

cells were identified by setting a gate on the GFP fluorescence channel based on control samples. Sorted cells were collected into sterile tubes, centrifuged and resuspended in an appropriate medium for further analysis.

Angiogenesis potential assay – 2D matrigel assay

To check if the studied cells were able to form tubular like structures *in vitro*, angiogenesis potential assay was performed. The name of the assay (angiogenesis potential) came after the fact that it is an assay used with ECs. In our case we expected the tumoral cells of interest to be able to form tubular like structures in 2D matrigel experiments so we had to optimize the assay for our tumoral cells. Growth factor reduced matrigel (Corning™, 356231) was thawed overnight in the cold room at 4ºC for slow thawing, the pipette tips and 24-well plate that would be used in the assay were also kept in the cold room overnight. The next day, 300 µL of matrigel were used to coat the wells of the 24-well plate (Thermo Scientific™, 142475) and the plate was incubated at 37ºC for at least 1 hour to allow matrigel solidification. Meanwhile, cells were detached using Trypsin-EDTA solution, counted using a Neubauer's chamber (Hirschmann®, BE718605) with the aid of the viability dye trypan blue (Sigma-Aldrich®, 93595). The same number of cells were seeded in each well in a final volume of 0.5 mL per well (volumes were adjusted using complete cell culture medium). Cells were kept in the incubator at 37ºC until the time points of interest. When reaching the time points of interest, cells were moved out of the incubator and placed under the invert microscope (Olympus IX51) to take pictures at 4X-10X magnification. The maximum time point used in these experiments is 24 hours as matrigel was toxic for the cells and affected viability and, therefore, might affect their ability to form the structures. Five images were obtained from each well of a 24-well plate, captured in random fields. Closed tubular structures were evaluated thanks to the ImageJ software (National Institutes of Health, USA. Software version 1.8.0).

Cell proliferation assay

To assess tumoral cell proliferation, two different procedures were performed. For cell proliferation assays involving cell counting, used for human tumoral cells (HepG2), cells were seeded in 6-well plates (TRPP Reactiva, 92006) and allowed to attach and proliferate at 37ºC, 5% CO_2 and 21% O_2 in a humid atmosphere. Every 24 hours during the following four days, cell counts were determined using a BRAND™ BLAUBRAND™ Neubauer Counting Chambers (BRAND™, 718605) and trypan blue (Sigma-Aldrich, 93595-50ML) exclusion method to differentiate between viable and non-viable cells.

For crystal violet assay (Sigma-Aldrich, C0775-25G) used with murine tumoral cells (2020B3), cells were seeded at specific concentrations in 12-well plates (Corning, 3513) and were incubated overnight at 37°C, 5% CO_2 and 21% O_2 in a humid atmosphere. Proliferation was quantified every 24 hours for the next 4 days. Each day, cells were washed with PBS and incubated with crystal violet (0.2% crystal violet in a 2% ethanol solution, Sigma-Aldrich®, CAS 64-17-5) for 15 minutes. Afterwards crystals were lysed with Sodium Dodecyl Sulfate 10% (SDS) (PanReacAppliChem, A0675,0250) in agitation on orbital shaker until color was uniform with no areas of dense coloration in bottom of wells. Absorbance was read at 520 nm in TECAN microplate spectrophotometer.

Soft agar colony formation assay

For soft agar colony formation assay, cells were seeded in 6 cm tissue culture plates and agar was used. Stock agar was prepared by making a 3.5% BD Difco™ Noble Agar (BD Biosciences, 214230) stock solution with Milli-Q water, which was then autoclaved. When needed, the agar was melted in a microwave and cooled to 50°C in a water bath, with the stock kept at room temperature when not in use. For use, the agar was mixed with complete cell medium to achieve a final concentration of 0.7% agar (base agar), prepared in a 50 mL tube and kept in a water bath set to approximately 50°C. 3 mL of the base agar mixture were poured into 6 cm tissue culture plates, taking care to avoid air bubbles and allowed to cool for 20 minutes.

Top agar was prepared by melting a 3.5% agar solution and cooling it to 50°C, ensuring the medium was warmed to the same temperature. Cells were trypsinized, counted and mixed with the agar and medium to achieve a final concentration of 0.5% agar and desired number of cells per plate (top agar). This mixture was added to 6 cm tissue culture plates pre-coated with base agar and incubated at 37°C in a humidified incubator for the weeks needed for colonies to grow. The cells were fed every 3 to 4 days with 1 mL of complete medium per plate and excess old medium was discarded. After incubation, colonies were stained overnight with 0.5 mg/mL iodonitrotetrazolium chloride (INT) solution (Sigma-Aldrich®, I10406-1G) diluted in PBS. The following day, colonies were scanned and subsequently quantified with ImageJ software (National Institutes of Health, USA).

Anoikis resistance assay

An anoikis resistance test was conducted to verify the potential metastatic capability of 2020B3 Luc-GFP CPEB4^{WT} and 2020B3 Luc-GFP CPEB4^{KO} cells.

Anoikis resistance was tested using two different 24-well plates. One of them allowed the attachment of cells into its surface that has been treated so the polystyrene surface of the plate is more hydrophilic, promoting maximum adhesion for cells (Thermo Scientific™, 142475). The other plates used were ultra-low attachment plates as they are treated to feature a covalently bound hydrogel layer that effectively inhibits cellular attachment (Corning, 3473).

The presence of metabolically active cells, indicative of anoikis resistant cells, was determined using the ATP measurement CellTiter-Glo® 2.0 Cell Viability Assay kit (Promega, G9242). This assay involved a reaction where ATP facilitated the conversion of luciferin to oxyluciferin reaction, catalysed by luciferase, producing a luminescent signal. The luminescent signal was measured with the luminometer BioTek Synergy HTX microplate reader.

The plate density was set at 50,000 cells per well in a total volume of 0.5 mL per well (complete DMEM medium and the cells). The plates (high and ultra-low attachment)

were incubated for 18 hours and 36 hours at 37ºC. At 18 hours and 36 hours, the plates were removed from the incubator and left at room temperature for 30 minutes to equilibrate the temperature. Subsequently, 0.5 mL of CellTiter-Glo® reagent was added to each well and the plates were incubated at room temperature on a shaker for 30 minutes. Luminescence was allowed to stabilize for 10 minutes without agitation before transferring the solution to the measurement plate. Plates used for measure were Nunc™ FluoroNunc™/LumiNunc™ flat bottom 96 well plate white (Thermo Scientific™, 437796). A volume of 100 µl from the high and ultra-low attachment plates was transferred to the measurement plate and quantified. To obtain the luminescence of the cells without interference, background luminescence was corrected by the luminescence results from wells containing only complete culture medium.

Western blot

Human HepG2 and murine 2020B3 liver cancer cell lines were homogenized and lysed in cold RIPA lysis buffer (Sigma®, R0278-500ML) supplemented with 1X Halt protease and phosphatase inhibitor cocktail and 1X EDTA (Thermofisher®, 78440). Lysates were incubated 30 minutes on ice and frequently vortexed to lyse cells and after incubation they were centrifuged for 20 minutes at maximum speed in a benchtop microcentrifuge (Eppendorf®, centrifuge 5415 R) to obtain cytoplasmic protein extracts. Protein concentration was measured using the BCA Protein assay (Thermofisher®, 23227). Equal amounts of total protein were heated (95°C, 10 min) in sample buffer containing lysis buffer, Laemli buffer (BioRad, 161-0747) and β-mercaptoethanol (Sigma®, G63689-25ML-F). Samples were resolved in SDS polyacrylamide gel electrophoresis (SDS-PAGE). SDS-PAGE gels for Western blotting consisted of acrylamide/bisacrylamide (Biorad, 161-0148) for the gel matrix, SDS for protein denaturation and imparting a negative charge, Tris-HCl for buffering, ammonium persulfate (APS) (Sigma-Aldrich, A3678-100G) and tetramethylethylenediamine (TEMED) (Sigma-Aldrich, T9281) to initiate and accelerate polymerization and distilled water for preparation. The gel setup includes a stacking gel (4% acrylamide) to concentrate proteins and a resolving gel (8-15% acrylamide) for separating proteins based on size. Samples were transferred to a previously activated

Immobilon-P PVDF membrane (Millipore®, IPVH00010). Activation of the PVDF membrane involved immersing it in ethanol (VWR Chemicals, 20821365) for 30 seconds, followed by 2 minutes in water and then 5 minutes in 1X transfer buffer (Santa Cruz, sc-296648). After blocking with 5% non-fat dried milk powder (Panreac, APA0830.0500) in Tris buffered saline with Tween-20 (TBS-T) buffer (Santa Cruz Biotechnology, sc-281695) or 5% BSA for 1 hour, blots were incubated in agitation at 4°C overnight with monoclonal antibodies against the protein of interest (i.e., markers associated with VM and EMT), according to the recommended dilution by the provider (**Table 2**). Proteins were detected using horseradish peroxidase-conjugated (HRP) secondary antibodies (Stressgen®) (**Table 2**) at 1:10,000 and the Enhanced Chemiluminescence Detection System ECL (GE Healthcare) was used to reveal the blot. Band intensity was analysed using computer-assisted densitometry.

Table 2. **Antibodies used for immunoblotting.** Target protein, reference, dilution, antibody type and host are shown.

Target	Reference	Dilution	Antibody type	Host
CPEB4	homemade	1:50	Primary antibody	Mouse
E-Cadherin	BD Biosciences, 610181	1:2000	Primary antibody	Mouse
N-cadherin	Abcam, ab18203	1:1000	Primary antibody	Rabbit
Twist1	Abcam, ab50887	1:50	Primary antibody	Mouse
Slug	Cell Signaling, 9585S	1:500	Primary antibody	Rabbit
VE-cadherin	R&D systems, AF938	1:1000	Primary antibody	Goat
c-myc	Cell Signaling, 9402S	1:1000	Primary antibody	Rabbit
Notch1	Abcam, ab52627	1:500	Primary antibody	Rabbit
CD133	Cell Signaling, A3G6K	1:1000	Primary antibody	Rabbit
β-actin	Sigma, A2228	1:10000	Primary antibody	Mouse
α-tubulin	Sigma, T9026	1:1000	Primary antibody	Mouse
GAPDH	Santa Cruz, sc-32233	1:10000	Primary antibody	Mouse
Goat αRabbit	Enzo Life Sciences, ADI-SAB-300-J	1:10000	Secondary antibody	Goat
Rabbit αMouse	Sigma Aldrich, A9044	1:10000	Secondary antibody	Rabbit
Mouse αGoat	Santa Cruz, sc-2354	1:10000	Secondary antibody	Mouse

RNA extraction and gene expression analysis

Total RNA was isolated and purified using the RNeasy Mini Kit (Qiagen®, 74106) in accordance with the manufacturer's instructions. The amount of RNA was measured by NanoDrop ND-1000 spectrophotometer (Thermo Scientific®). Reverse transcription was conducted using the QuantiTect Reverse Transcription kit (Qiagen®, 205311), according to the manufacturer's instructions. The synthesized cDNA was then amplified by RT-qPCR using human and murine CPEB1, CPEB2, CPEB3, CPEB4, β-actin and TaqMan Gene expression assays (Thermofisher®) (**Table 3**), in an ABI PRISM 7900 Sequence Detection System (Applied Biosystems). cDNA samples were diluted 1:2.5 in ddH_2O. Then, a premix was prepared containing 5 µL PowerUp™ SYBR™ Green Master Mix (containing DNA polymerase, dNTPs and buffer), variable volume of forward/reverse primer at 15 µM (**Table 3**) and nuclease-free water up to 8 µL total per reaction. These eight microliters were mixed with 2 µL of cDNA by centrifugation (1 minute at 2500 rpm). All PCR reactions were performed in triplicates, using nuclease-free water as control. CPEBs mRNA expression levels were normalized to endogenous control β-actin expression, which was unaffected in the different cell lines.

Table 3. **Primers used for RT-qPCR.** Hs stands for *Homo Sapiens* and Mm stands for *Mus Musculus*.

primer	Species	Primer Forward (5' to 3')	Primer Reverse (5' to 3')
β-actin	Hs and Mm	CCCAGAGCAAGAGAGG	GTCCAGACGCAGGATG
CPEB1	Hs and Mm	CCTTGGGATATTACAGAAGCTGG	CCTTTGGGAGGACACCG
CPEB2	Hs	GAGAGCTCAGTTCAGGCACTC	AGCAAGTTCCACAGCCCTTA
CPEB2	Mm	TGGAGCAACCATCAGAACAG	CGAGTGAATTTCGGTGGTG
CPEB3	Hs and Mm	GGCACTTAACAGTCGATCTTCTC	GGCAGTGATCTCATCTTCATCA
CPEB4	Hs	TGGGGATCAGCCTCTTCATA	CAATCCGCCTACAAACACCT
CPEB4	Mm	CCAGGACGTTTGACATGCACT	GGAATCCATCTTCCATCGGAAA

Co-culture of tumor and endothelial cells in matrigel with bevacizumab treatment

Tumor cells were co-cultured with murine ECs expressing cherry protein (H5V Cherry). We used the murine immortalized H5V EC line as an appropriate model of pathologic or activated EC. H5Vs are transformed and tumorigenic endothelioma cells. H5V cell line is

a murine heart EC line that has been immortalized. It was derived from the embryonic heart of a female C57BL/6 mouse. These cells are transfected with the murine polyomavirus middle T antigen to transform the ECs. H5V cells were grown on DMEM/F-12 supplemented with 10% bovine calf serum (Hyclone, SH30072.03), 100 units/mL penicillin, 100 µg/mL streptomycin, 100 µg/mL non-essential amino acids and 100 µg/mL sodium pyruvate (complete medium). Incubation of cells took place at 37ºC, 5% CO_2 and 21% O_2 in a humid atmosphere.

Prior to seeding the cells onto the matrigel, bevacizumab (Medchemexpress, HY-P9906) treatment was administered to the media at working concentrations previously documented in the literature. The working concentrations used were 0.125 mg/mL, 0.25 mg/mL and 0.5 mg/mL. Bevacizumab was diluted into the complete media to achieve the desired concentrations. To assess the efficacy and results of the treatment, the Leica AF6000 microscope was utilized. This microscope allowed for imaging of different regions at various emission wavelengths for GFP (500-540 nm) and Cherry (580-620 nm) expression. Five images were obtained from each well of a 24-well plate, captured in random fields.

To assess the impact of bevacizumab treatment on the formation of structures, Qupath software (version 0.3.2) was employed. This analysis involved evaluating the area occupied by the different cell types within the structures, utilizing the expression of GFP and Cherry fluorescent proteins.

In vivo models and protocols

Animals were maintained at the animal facility of the Medicine Faculty of the University of Barcelona, with light and dark cycles and *ad libitum* normal diet (otherwise indicated in this section) and water. Protocols were approved by the Animal Ethics Committee of the University of Barcelona and the Catalan Government.

Xenograft model of CPEB4^{SCR} and CPEB4^{KD} cells

Once HepG2 cells were tested to be Luc-GFP positive and contain the desired phenotype (being CPEB4^{SCR} or CPEB4^{KD}), xenografts were performed. Animals used were CR nod

SCID (Severe Combined Immunodeficiency) mice (Charles River) to obtain the xenograft of human HepG2 cells.

To obtain xenograft*s*, cells were detached using trypsin, counted using a Neubauer's chamber with the aid of the viability dye trypan blue and the same number of cells per condition were placed in 15 mL falcon, centrifuged 300g for 5 minutes and resuspended in a solution containing 50% matrigel and 50% PBS with the cells in suspension. Once cells were resuspended in PBS-matrigel, they were kept on ice and transported to the animal facility. Mice were anaesthetized with the inhalatory anaesthetic isoflurane (B. Braun VetCare, IsoVet®) 2% in O_2 and placed on top of an electric blanket during all the procedure to keep their body temperature constant. On the mice right flank, WT cells for CPEB4 were subcutaneously injected and on the left flank cells KD for CPEB4 were subcutaneously injected with the aid of a sterile 1 mL 25G syringe (BD Plastipak™, 303172). After cell injection, mice were placed in their cage and kept warm with an infrared light until complete recovery from anaesthesia.

Tumor growth was monitored by bioluminescence and touching the palpable tumors of the mice. Bioluminescence was measured with the IVIS 50-In Vivo Bioluminescence Imaging System (BLI) with one-week intervals prior injection of the substrate of luciferase, D-luciferin (Gold Biotechnology®, eLUCK-100) at 150 mg/kg body weight by an intraperitoneal injection in the mouse of interest (10 minutes prior to imaging), then mice were anaesthetise with isoflurane and placed in the imaging system. Anaesthesia was maintained with isoflurane (2% in O_2) during the imaging procedure. Images were acquired using a standardized exposure time, binning and field of view settings. Bioluminescent signals were quantified as the sum of all counts for all pixels within a defined region of interest (ROI) over the tumor corrected by average background ROI. The software Living Image 4.8.2 (64 bit) IVIS™ imaging systems was used for the analysis. Tumor growth was stablished plotting bioluminescent signal intensity (arbitrary units, AU) obtained in the different tumors analysed.

When tumors reached a size that posed a risk of damaging the skin of the mice, mice were anaesthetized, tumors extracted and mice were then euthanized. Two pieces of

each extracted tumor were frozen for subsequent protein and RNA extraction (using the same protocol as for cell lines). The remainder of the tumor was preserved overnight in formalin solution neutral buffered 10% (Merck, HT501320). The following morning, the tumor piece was transferred from formalin to PBS and sent to the histology facility. There, paraffin blocks were prepared and histological sections of the tissue were obtained. Histological tissue staining, immunohistochemistry (IHC) and immunofluorescence (IF) were subsequently performed.

Liver cancer protocol

A liver carcinogenesis protocol was developed to obtain liver tumoral samples. Male C57BL/6J mice, either wild type or CPEB4 knockout, were maintained under standard conditions with 12-hour light and dark cycles at 21°C and had access to food and water in cages with a maximum of five animals per cage. Food was monitored and changed weekly, maintaining 200 grams per cage. From week 6 of age, male animals were randomly assigned and divided into two groups: one subjected to a HFD (HFD: 60% fat, 20% protein and 20% carbohydrates) (Research Diets, D12492) and the other to a normal diet (ND: 13% fat, 20% protein and 67% carbohydrates) (Envigo, 2014S). At week 16, all animals were injected with the mutagen DEN (Sigma, N0756) at a concentration of 80 mg/kg via intraperitoneal administration. Phenobarbital (PB) was added to the drinking water at 0.05% from week 20 until the end of the protocol. Animals were euthanized at week 50 due to overdose of anesthesia and were fasted the day prior to necropsy.

Histological tissue staining and immunohistochemistry (IHC)

Tissues and tumors of interest were embedded in paraffin and subsequently cut into histological sections. These histological sections were first deparaffinised and hydrated under a fume hood. Histological sections were rehydrated through sequential immersions: four immersions in xylene (Panreac AppliChem, 211769.1714), each for 8 minutes; two immersions in absolute alcohol (Sigma-Aldrich, CAS 64-17-5), each for 8 minutes; followed by 96% alcohol for 5 minutes, 70% alcohol for 5 minutes and 40%

alcohol for 5 minutes. The samples were then transferred to distilled water until the next step. Diluted alcohols were prepared from absolute alcohol diluting it in distilled water.

To expose antigens for antibody recognition, antigen retrieval was performed using a steamer to minimize tissue aggression. Two different antigen revealing buffers were used depending on antibody manufacture's protocol. For citrate buffer (pH 6), antigen retrieval buffer (100X Citrate Buffer) from Abcam (Abcam, ab93678) was diluted 100 times in distilled water. For Tris-EDTA buffer (pH 9), antigen retrieval buffer 100X Tris-EDTA buffer, pH 9.0 from Abcam (Abcam, ab936849) was diluted 100 times in distilled water.

Histological sections were introduced into Sequenza Staining Rack (Thermo Scientific, 73310017) with Epredia™ Shandon™ Plastic Coverplates (Epredia™, 72110017). Next, internal peroxidase activity was inhibited by adding 100 µL Dako REAL Peroxidase-Blocking Solution (Ready-to-use) (DAKO, S202386-2), incubated for 10 minutes, followed by washing. To avoid unspecific background staining, blocking was performed using 100 µL per slide of 5% goat serum (DAKO, X0907) for 1 hour at room temperature.

Subsequently, primary antibody incubation was conducted overnight at 4ºC in the dark. 100 µL of diluted primary antibody (**Table 4**) in DAKO antibody background reducing diluent (DAKO, S3022) was applied per sample. After primary antibody incubation, samples were washed with PBS 3 times.

After washing, secondary antibody incubation was performed in the darkness during appropriate time (different according to primary antibody specifications). Secondary antibodies were EnVision+ Single Reagents (HRP Rabbit) (DAKO, K400311-2) and EnVision+ Single Reagent (HRP Mouse) (DAKO K4001) and used according to the primary antibody host species. After this incubation, samples were washed again with PBS for 3 times.

For 3,3'-diaminobenzidine (DAB) development, development solution was prepared with 20 µL liquid DAB per 1 mL Dako real substrate buffer (DAKO, K3468) and 100 µL were added per sample. The reaction was monitored under an upright bright field microscope until signal was detected and the reaction was stopped with PBS washes.

Next, counterstaining was performed with hematoxylin (Sigma-Aldrich, GHS232-1L) for 1 minute, followed by rinsing in running water for 5 minutes.

Samples were dehydrated with sequential alcohol immersions: 70% alcohol for 3 minutes, 96% alcohol for 3 minutes and three changes of 100% alcohol for 3 minutes each. This was followed by three xylene immersions for 2 minutes each.

Finally, excess xylene was removed. A drop of hydrophobic mounting medium was applied (Sigma-Aldrich, 1005790500) and the coverslip was placed on top, ensuring no air bubbles remained. Samples were allowed to dry overnight. IHC were scanned by Nanozoomer 2.0HT – Hamamatsu and Nanozoomer Digital Pathology Image Software and visualized by NDP.view 2 program.

Table 4. Primary antibodies used for IHC. Target protein, reference, dilution and host species are shown.

Antibody	Reference	Dilution	Host species
CD31	Abcam, ab28364	1:50	Rabbit
GFP	Cell signaling, 2956	1:100	Rabbit

PAS staining

For the detection of aldehyde and mucosubstances forming VM structures in tissue samples, we employed the Microscopy PAS Staining Kit (Sigma-Aldrich, 1016460001). Tissue sections were initially deparaffinized and rehydrated through a series of xylene and alcohol washes (as previously described). Following rehydration, the sections were treated with periodic acid for 10 minutes to oxidize the vicinal diols present in polysaccharides to aldehyde groups. The sections were then washed thoroughly and incubated with the Schiff's reagent for 15 minutes, which forms a magenta-colored complex with the aldehyde groups. After a series of washing steps to remove excess reagent, the sections were subsequently dehydrated through graded alcohols and xylene before being mounted with a coverslip. The resulting PAS staining was evaluated under a light microscope to visualize the presence and distribution of vasculogenic mimicry structures within the tissue samples. Stainings were scanned by Nanozoomer

2.0HT – Hamamatsu and Nanozoomer Digital Pathology Image Software and visualized by NDP.view 2 program.

Statistical analysis and reproducibility

The data shown are in mean ± standard deviation and statistics were analysed with R software. Results that followed a normal distribution (p-value > 0.05 from Kolmogorov-Smirnov test) were compared using parametric statistical procedures (Student's T-test). Significance was accepted at p-value < 0.05. All cell culture experiments were performed at least 3 times. For animal studies, aged- and sex-matched animals were used. Littermates were used whenever possible. Experiments were repeated independently with similar results as indicated in the figure legend.

Results

Generation of HepG2 CPEB4 scramble luciferase-GFP and HepG2 CPEB4 knockdown luciferase-GFP cells

Commercial tumoral HepG2 cells at 40% confluence were infected with lentivirus expressing shRNA targeting CPEB4 (5'-GCGTTATGTGTTGAACAGTAT-3') to obtain the constitutive knockdown cells for CPEB4 (HepG2 CPEB4^{KD}) or expressing shRNA targeting nowhere in the mammalian genome (commercial sequence) to obtain the scramble condition, WT for CPEB4 (HepG2 CPEB4^{SCR}). After lentiviral infection, cells underwent an antibiotic selection with puromycin (2 µg/mL). Successfully infected cells were validated by protein and RNA levels (*data not shown*). Then, these validated cells were infected by a retrovirus expressing luciferase-GFP plasmid to obtain the working cells, HepG2 CPEB4^{SCR} Luc-GFP and HepG2 CPEB4^{KD} Luc-GFP cells (**Figure 13**). Before doing any extra experiment with these cells, protein as well as RNA were extracted to validate the correct reduction of CPEB4 in these cells (**Figure 14**) by western blot (**Figure 14A**) and RT-qPCR (**Figure 14B**). Once the phenotype of the cells was validated, expression of GFP was measured by flow cytometry and positive cells were sorted (**Figure 15**). The expression of luciferase-GFP allowed us to detect tumor growth through bioluminescence, thanks to luciferase, and to analyze the structures formed by the tumor cells *in vitro* by fluorescence, as they will be GFP-positive, as described later in this "Results" section.

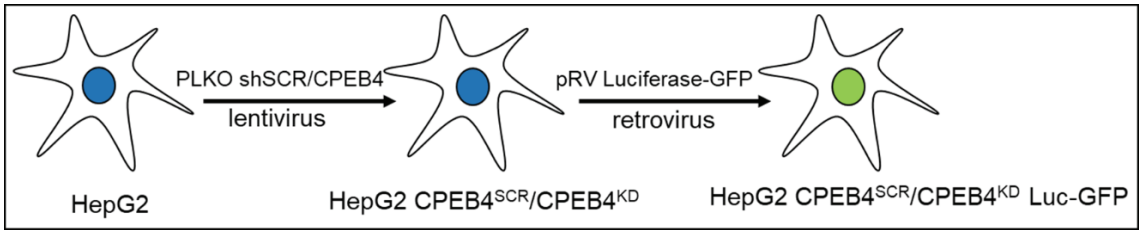

Figure 13. Generation and validation of HepG2 cells with targeted knockdown of CPEB4 and Luciferase-GFP expression. HepG2 cells were infected with lentivirus expressing shRNA targeting CPEB4 (HepG2 CPEB4^{KD}) or a control (HepG2 CPEB4^{SCR}), followed by puromycin selection. After validating knockdown efficiency, cells were further infected with a retrovirus

carrying a luciferase-GFP plasmid, producing HepG2 CPEB4^{SCR} Luc-GFP and HepG2 CPEB4^{KD} Luc-GFP cell lines.

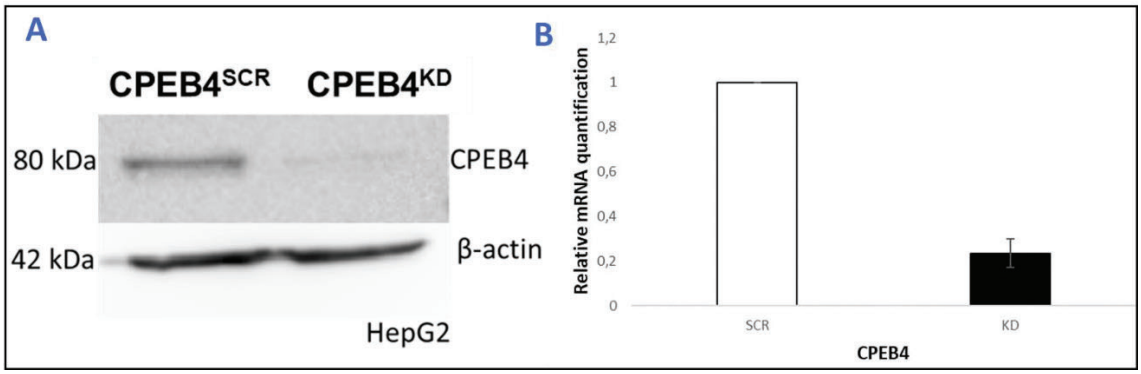

Figure 14. **Validation of CPEB4 knockdown of HepG2 CPEB4^{KD} Luc-GFP comparing to its counterpart CPEB4 wild type (HepG2 CPEB4^{SCR} Luc-GFP)**. Validation was made (**A**) by protein (40 µg of total protein were loaded in the gel, protein expression was normalized to the expression of β-actin, housekeeping gene) and (**B**) mRNA levels. Data are expressed as mean ± standard deviation.

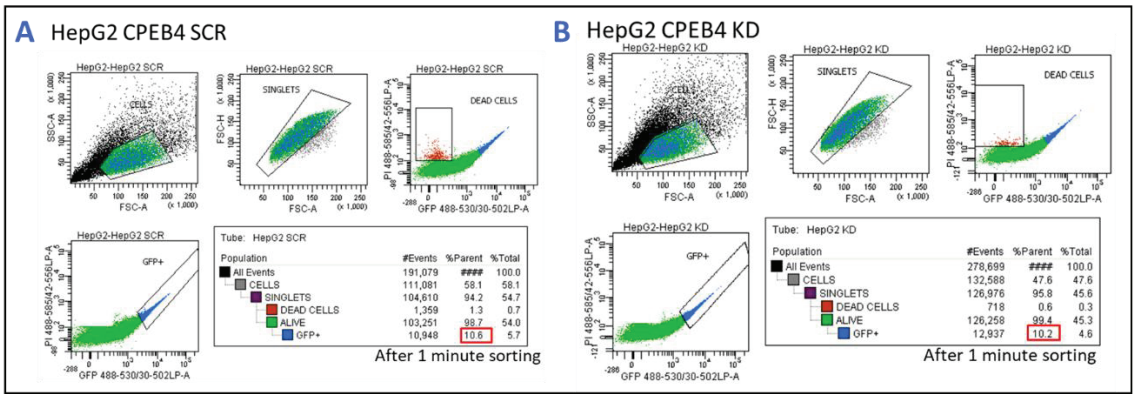

Figure 15. GFP expression in the HepG2 CPEB4^{SCR} Luc-GFP and HepG2 CPEB4^{KD} Luc-GFP cells. The percentage of GFP positive cells was analysed by flow cytometry analyses comparing the cells of interest with non-infected HepG2 cells. Then, GFP positive cells were sorted in order to obtain the same intensity of GFP positive cells (cells that passed the 10^4 power of GFP intensity) in the CPEB4^{SCR} (**A**) and CPEB4^{KD} conditions (**B**). In both cases around 10% of the initial sample (parent sample) was GFP positive in the power of intensity desired.

Generation of 2020B3 luciferase GFP CPEB4 knockout cells and wild type controls

To further validate our findings, we conducted experiments using the murine liver tumor cell line 2020B3. This cell line was derived from a liver tumor developed in a male mouse fed with HFD. The obtained cells were genetically modified to express luciferase-GFP, while also being inducible for the depletion of CPEB4 (**Figure 16**). Liver tumors in this

mouse were induced following a HFD and liver carcinogenesis protocol (DEN and phenobarbital); the mice used to generate cell lines were let in the animal facility until they showed symptoms of sickness to be sure they had liver tumors. The CPEB4 gene in this mouse was flanked with loxP sites to facilitate its knockout. Liver tumors were resected, disaggregated into individual cells and cultured. Once the cell line was established, cells were infected with a retrovirus expressing luciferase-GFP and GFP-positive cells were selected using flow cytometry (**Figure 17**). To generate CPEB4^{KO} cells, 2020B3 cells were infected with an adenovirus expressing CRE recombinase at a MOI of 1,000, resulting in CPEB4 excision through the CRE–LoxP recombination system. CPEB4 depletion was confirmed by immunoblotting (**Figure 18A**) and RT-qPCR (**Figure 18B**).

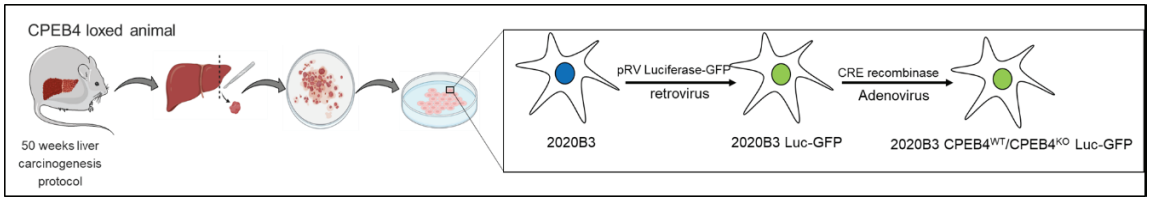

Figure 1. Generation and characterization of 2020B3 murine liver tumor cell line with CPEB4 knockout and Luciferase-GFP reporter expression. The murine liver tumor cell line 2020B3 was derived from tumors induced by a HFD and DEN carcinogen treatment in a male C57BL/6J mouse. CPEB4 was flanked by loxP sites for knockout. Cells were cultured, infected with a retrovirus expressing luciferase-GFP and sorted for GFP positivity. CPEB4 knockout was achieved by infecting with an adenovirus expressing CRE recombinase.

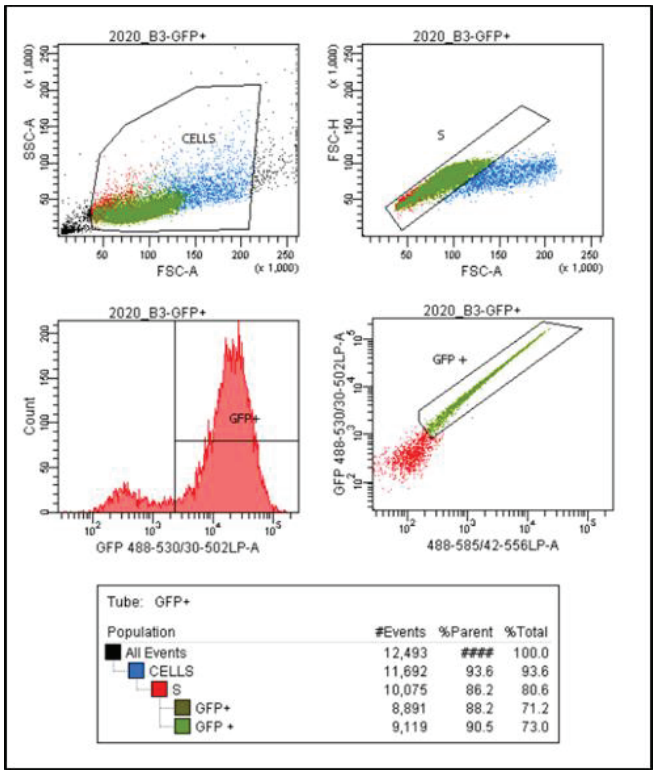

Figure 172. GFP expression in 2020B3 Luc-GFP cells. The percentage of GFP positive cells was analysed by flow cytometry analyses comparing the cells of interest with non-infected 2020B3 cells. Then, those cells were sorted to keep only GFP positive cells.

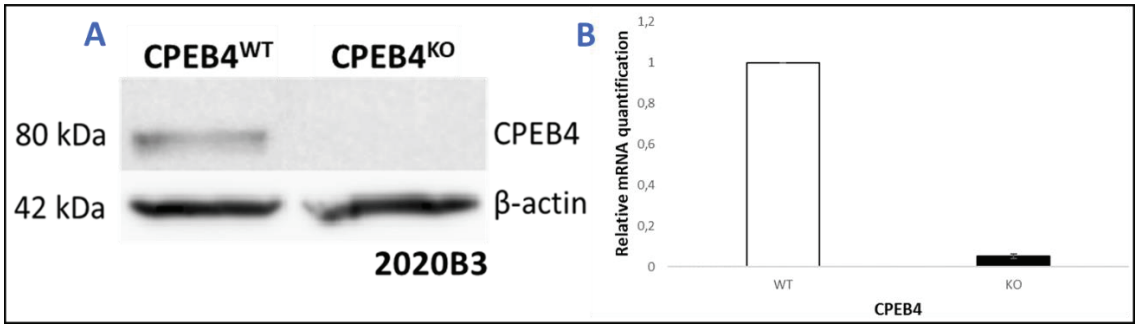

Figure 183. Validation of CPEB4 knockout of 2020B3 CPEB4^{KO} Luc-GFP comparing to its counterpart wild type (2020B3 CPEB4^{WT} Luc-GFP). Validation was performed by protein (40 µg of total protein were loaded in the gel, protein expression was normalized to the expression of β-actin, housekeeping gene) (**A**) and mRNA levels by RT-qPCR (**B**). Data are expressed as mean ± standard deviation.

Liver cancer cells demonstrate vasculogenic mimicry competence *in vitro* and CPEB4 depletion enhances their tube formation ability

To assess whether human liver cancer cells exhibit VM competence, we first evaluated their capacity to form tubular structures *in vitro* using growth factor-reduced matrigel. For this purpose, we generated a human liver cancer cell line (HepG2) with reduced CPEB4 expression by infecting the cells with a lentivirus carrying pLKO shCPEB4 to create a $CPEB4^{KD}$ condition, or with pLKO shSCR as a control ($CPEB4^{SCR}$), as previously described in the "Results" section.

We then plated human liver tumor cells (HepG2 $CPEB4^{SCR}$ and $CPEB4^{KD}$, both Luc-GFP) on growth factor-reduced matrigel (240,000 cells per well) in a 24-well plate and evaluated the formation of closed tubular structures after 22 hours. Both HepG2 $CPEB4^{SCR}$ Luc-GFP and $CPEB4^{KD}$ Luc-GFP cells were capable of forming tubular structures; however, $CPEB4^{KD}$ cells formed significantly more closed structures compared to $CPEB4^{SCR}$ cells (**Figure 19**). This suggests that CPEB4 plays a role in attenuating or preventing the formation of these structures and that a deficiency in CPEB4 enhances their development.

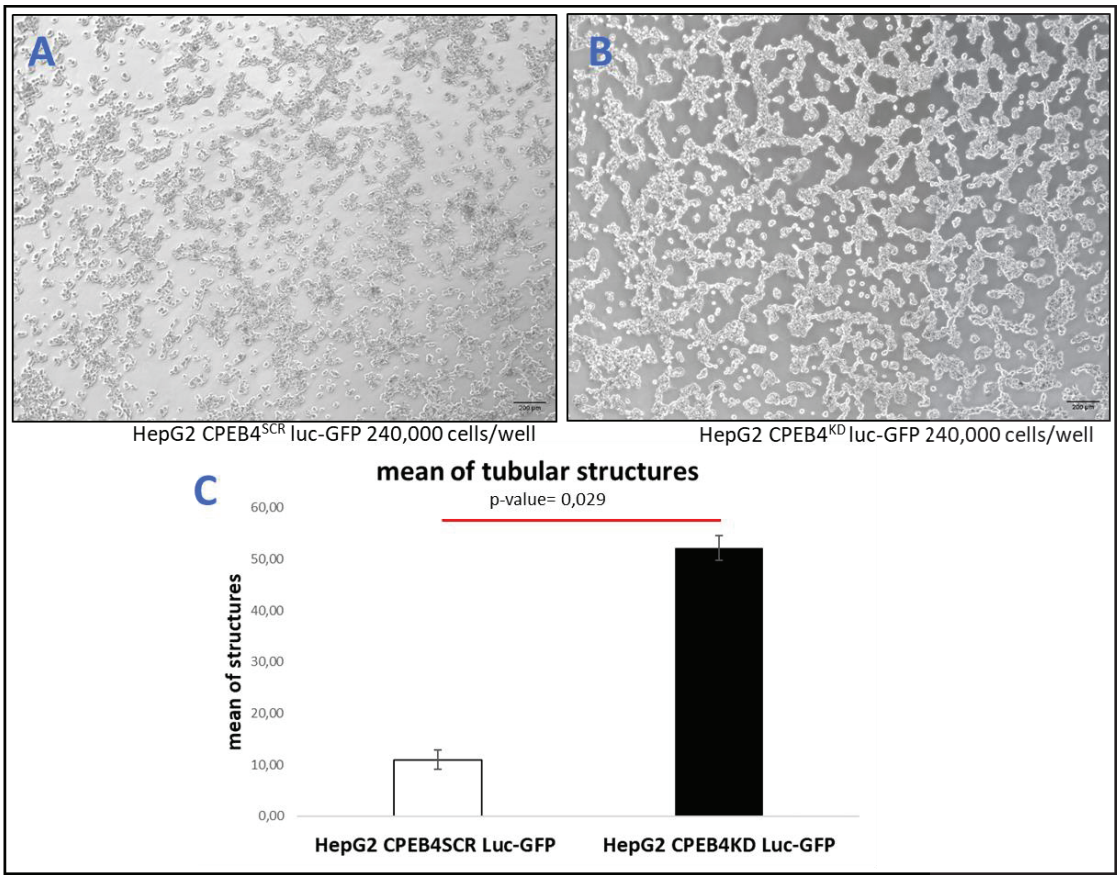

Figure 19. Enhanced tubular structure formation by HepG2 CPEB4^{KD} cells on matrigel compared to CPEB4^{SCR} cells. (**A-B**) Representative pictures of human liver tumoral HepG2 cells plated on matrigel. HepG2 CPEB4^{KD} (**A**) cells are able to form significative more tubular structures than CPEB4^{SCR} (**B**) cells (p-value = 0.029). Images were taken 22 hours post seeding in an invert microscope. (**C**) Analysis of closed tubular structures was performed with ImageJ software. The experiment was repeated 3 times with 3 wells per condition and 5 pictures per well. Data are expressed as mean ± standard deviation.

To further validate our findings, we conducted experiments with a murine liver tumor cell line, 2020B3, derived from a mouse liver tumor. Mouse liver tumor 2020B3 cells were plated on growth factor-reduced matrigel (240,000 cells per well) in 24-well plates and the formation of closed tubular structures was assessed after 22 hours. We observed that 2020B3 Luc-GFP CPEB4^{WT} cells were unable to form tubular structures, whereas 2020B3 Luc-GFP CPEB4^{KO} cells successfully formed closed tubular structures (**Figure 20**). This result confirms our hypothesis that CPEB4 depletion enhances the *in vitro* ability of liver tumor cells to form VM-like structures.

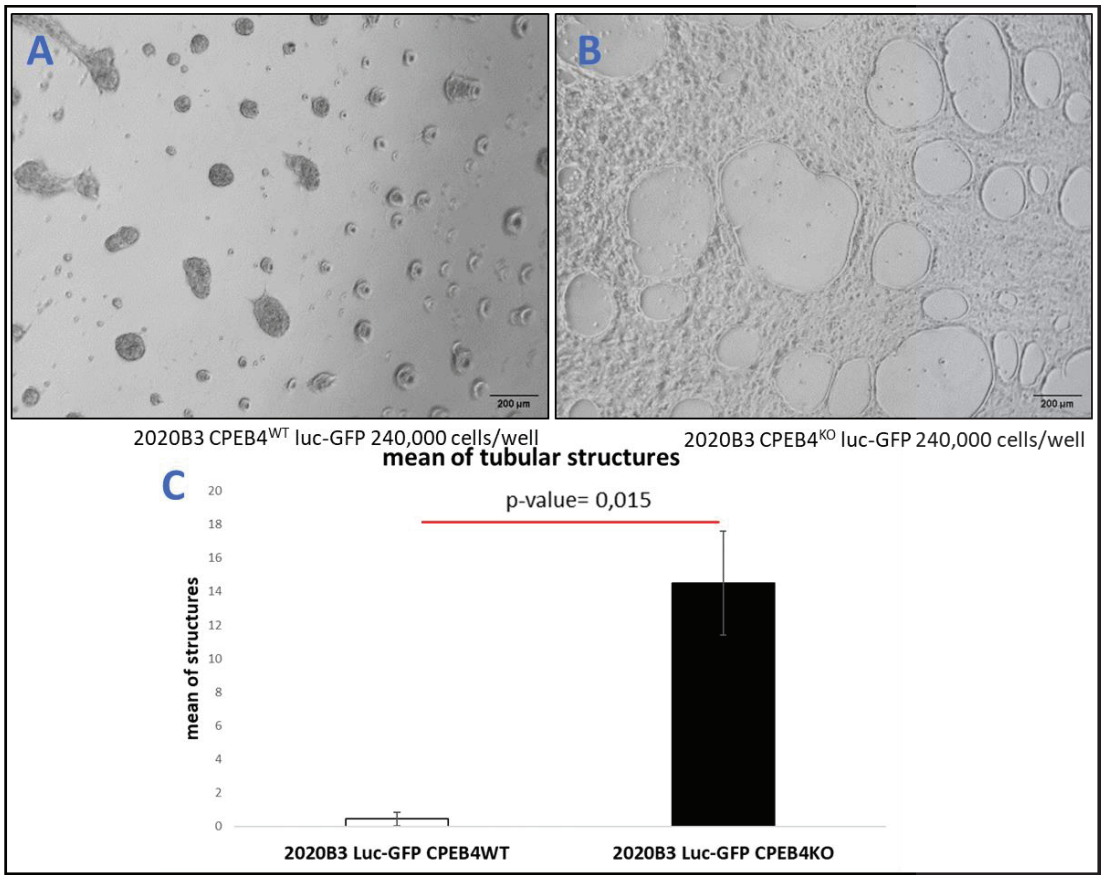

Figure 20. Tubular structure formation by 2020B3 murine liver tumor cells on matrigel: comparison of CPEB4^{WT} and CPEB4^{KO} cells. (**A-B**) Representative pictures of murine liver tumor cells 2020B3 cells plated on matrigel. 2020B3 CPEB4^{KO} (**B**) cells are able to form significative more tubular structures than CPEB4^{WT} (**A**) cells. CPEB4^{WT} cells are not able to form structures whereas CPEB4^{KO} cells do form closed tubular structures (p-value = 0.015). Images were taken 22 hours post seeding in an invert microscope. (**C**) Analysis of closed tubular structures was performed with ImageJ software. The experiment was repeated 3 times with 4 wells per condition and 5 pictures per well. Data are expressed as mean ± standard deviation.

CPEB4 reduction (CPEB4^{KD}) or depletion (CPEB4^{KO}) does not impact the proliferation capacity of liver tumor cell lines *in vitro*

To investigate how CPEB4 deficiency enhances VM competency in liver tumor cells, we examined several tumorigenic parameters, including proliferation, colony formation in soft agar, anoikis resistance and the expression of EMT markers.

Having established that liver cancer cells can form VM structures *in vitro* and that CPEB4 may influence this process, we first focused on evaluating the effect of CPEB4 on cell proliferation.

To evaluate the proliferation capacity of the human liver cancer cell line, HepG2, an initial count of 50,000 cells was seeded into 6-well plates and incubated for four days. Cell counts were performed daily over a span of four days to determine the proliferation rates of both CPEB4^{SCR} and CPEB4^{KD} cells. After four days of counting the cells under each condition, the proliferation rates were calculated. The results showed no significant differences in proliferation, p-value > 0.05, between CPEB4^{SCR} and CPEB4^{KD} cells (**Figure 21**). These findings suggest that CPEB4 reduction does not affect the proliferation capacity of human liver tumor cells, indicating that the increased aggressiveness observed *in vitro* is not due to differences in proliferation but likely arises from other tumorigenic processes influenced by CPEB4.

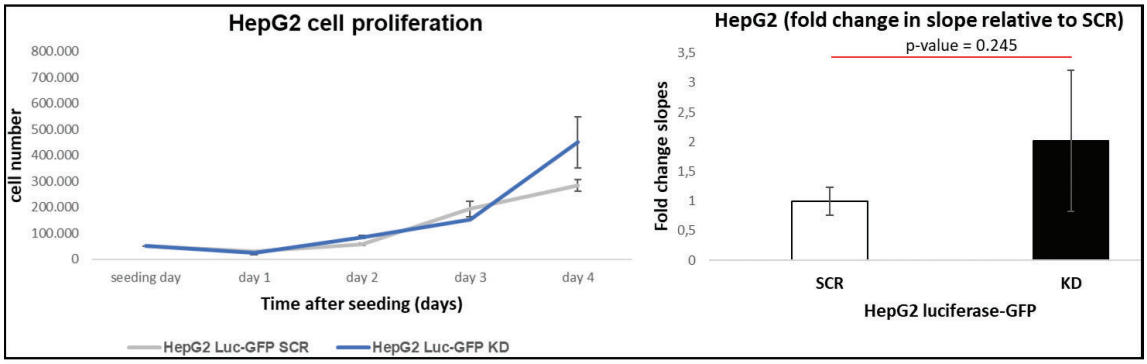

Figure 21. Cell proliferation analysis of HepG2 CPEB4^{SCR} (grey line) and CPEB4^{KD} cells (blue line) over time. To assess the proliferation capacity of the human liver cancer cell line HepG2, 50,000 cells were seeded into 6-well plates and allowed to grow for four days. Cell counts were performed on consecutive days, revealing no differences in proliferation between CPEB4^{SCR} and CPEB4^{KD} cells (p-value = 0.245). The experiment was repeated 3 times with 3 wells per condition. Data are expressed as mean ± standard deviation.

To assess the proliferation capacity of the murine tumor cell line 2020B3, we utilized the crystal violet assay. This method relies on the ability of crystal violet to intercalate with DNA, thereby staining cells that adhere to the culture plate. Following staining, the crystal violet is solubilized and its absorbance is measured at 520 nm. The intensity of the crystal violet staining is directly proportional to the cell biomass. We plated an initial density of 40,000 cells into 6-well plates and monitored cell proliferation over a period of 4 days, analysing the differences in proliferation curves (**Figure 22**). The results

indicated that the proliferation of 2020B3 cells was comparable in the absence and presence of CPEB4 (p- value > 0.05).

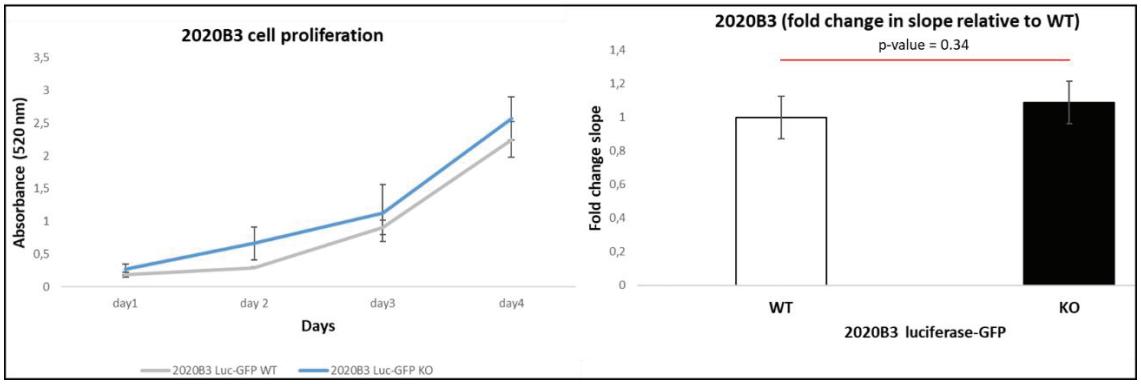

Figure 22. Proliferation analysis of 2020B3 liver tumor cells using crystal violet assay. CPEB4 may not be playing a role regarding proliferation *in vitro* of liver tumor cells in the case 2020B3 according to their proliferation curve in crystal violet assay (p-value = 0.34). The experiment was repeated 3 times with 3 wells per condition. Data are expressed as mean ± standard deviation.

The *in vitro* proliferative capacity of liver cancer cell lines, as demonstrated in 2D culture growth curves, remained unaltered upon CPEB4 reduction ($CPEB4^{KD}$) or depletion ($CPEB4^{KO}$). These results suggest that CPEB4 may not influence the proliferation of liver tumoral cells *in vitro*.

CPEB4 deficiency in murine liver tumour cells increases anchorage-independent growth *in vitro*

Next, we focused on the ability of murine transformed liver cells to grow independently of a solid surface, phenomenon known as anchorage-independent growth—a recognized hallmark of carcinogenesis.

Evidence from other cancers, such as breast cancer, suggests a correlation between VM and the ability of cancer cells to form colonies in soft agar. VM, where tumor cells form vessel-like structures without endothelial cells, is often associated with aggressive cancer phenotypes, including CSC characteristics. CSCs, known for their ability to perform VM, also display enhanced anchorage-independent growth, as demonstrated by their robust colony formation in soft agar assays. This cellular plasticity and stemness,

which enable both VM and soft agar growth, are indicative of a more aggressive and metastatic cancer phenotype (298–300).

Given these observations in other cancers, we sought to determine whether a similar correlation exists in liver cancer cells, particularly in the context of CPEB4 deficiency.

To evaluate anchorage-independent growth, we conducted soft agar colony formation assay, a well-established *in vitro* method for characterizing this capability. This assay is considered one of the most stringent tests for malignant transformation in cells and provides a semi-quantitative evaluation. Additionally, it helps predict whether these cells can grow as an allograft in mice, as successful growth in soft agar suggests a higher likelihood of development in an unverified niche.

For these experiments, murine 2020B3 either WT or KO for CPEB4 cells were utilized. Five thousand 2020B3 cells were plated in soft agar plates and allowed to grow until colonies were visible under a microscope. After three weeks, colonies were stained with iodonitrotetrazolium chloride, then scanned and counted using ImageJ software (**Figure 23**). The results demonstrated that 2020B3 cells were capable of anchorage-independent growth and the number of colonies significantly increased (p-value < 0.05) upon the removal of CPEB4 (CPEB4^{KO}).

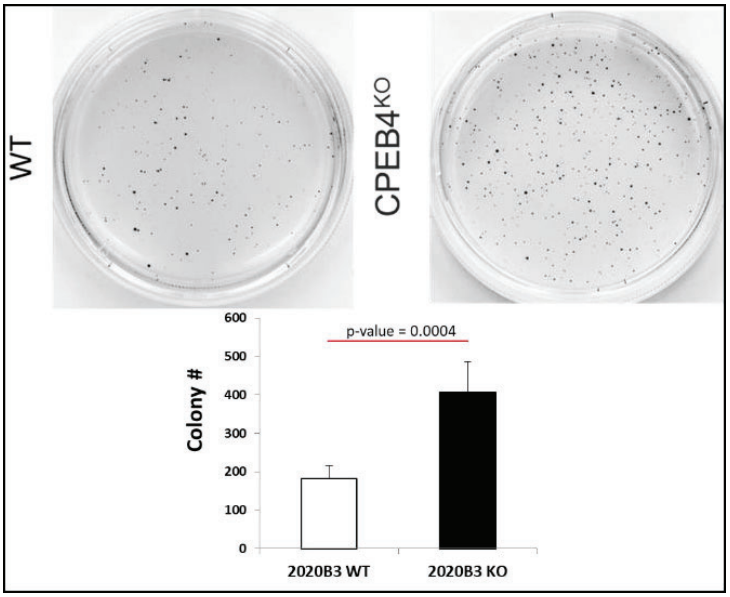

Figure 23. Impact of CPEB4 depletion on colony formation in soft agar by 2020B3 murine liver tumor cells. CPEB4 depletion provides a higher potential regarding colony formation in soft agar

in murine cell line (2020B3) regarding their ability to form more colonies when CPEB4 is depleted (p-value = 0.0004). The experiment was repeated 3 times with 6 plates per condition. Data are expressed as mean ± standard deviation.

Anoikis resistance is maintained despite absence of CPEB4 in liver tumor cell lines

Then, we wanted to check if CPEB4 deficient liver cancer cells were able to survive anoikis death. Anoikis is defined as a type of cell death triggered by the loss of contact between tumor cells and the ECM as well as with neighbouring cells. Tumor cells may develop resistance to anoikis, a trait associated with enhanced metastatic potential and increased VM capability in some tumor types (301,302). This process was first described by Frisch and Francis in 1994. Essentially, adhesion to ECM components is crucial for proper cell localization and, consequently, for the appropriate regulation of cell survival and death.

Highly aggressive tumor cells acquire resistance to anoikis, enabling them to survive even after detachment from the primary matrix. These cells disseminate throughout the body via the circulatory and lymphatic systems. EMT and resistance to anoikis are critical processes in metastasis and MV. Some factors involved in regulating these processes include Twist, Snail and Zeb1.

To determine whether CPEB4 deficiency affects anoikis resistance in liver cancer cells, we compared the viability of wild-type and CPEB4^{KO} murine liver cancer cells under non-adherent conditions. Cells were plated on ultra-low attachment plates to mimic the environment encountered during dissemination, where surface adhesion is limited. Viability was then compared to cells grown on high-adherence plates to assess the potential differences in survival. This approach allowed us to evaluate whether the loss of CPEB4 alters the anoikis resistance of liver cancer cells, contributing to their metastatic potential and aggressiveness.

2020B3 cells were detached, counted and 50,000 cells per well (in a total volume of 0.5 mL with complete medium) were plated on the different 24-well plates. After 18 hours, luminescence measurements—indicative of adenosine triphosphate (ATP) levels and, by extension, cell viability—were high in the treated high-adherence plates. A trend toward

increased cell viability was observed in the 2020B3 Luc-GFP CPEB4^{KO} population compared to the CPEB4^{WT} population. In contrast, luminescence readings were lower on the ultra-low attachment plates, indicating reduced cell viability, with no notable differences in luminescence units between the CPEB4^{WT} and CPEB4^{KO} cells (**Figure 24A**).

To assess the relative increase in ATP levels compared to the control, the difference in luminescence between the two cell types on ultra-low attachment plates was compared to that on high-adherence plates. Statistical analysis revealed no significant differences (p-value > 0.05), suggesting that neither cell type exhibited a significantly higher resistance to anoikis death than the other. However, both cell types demonstrated some capacity to survive on ultra-low attachment surfaces. After 18 hours, 66% of 2020B3 Luc-GFP CPEB4^{WT} cells and 58% of 2020B3 Luc-GFP CPEB4^{KO} cells remained viable without adherence, compared to their counterparts on treated high-adherence plates (**Figure 24B**).

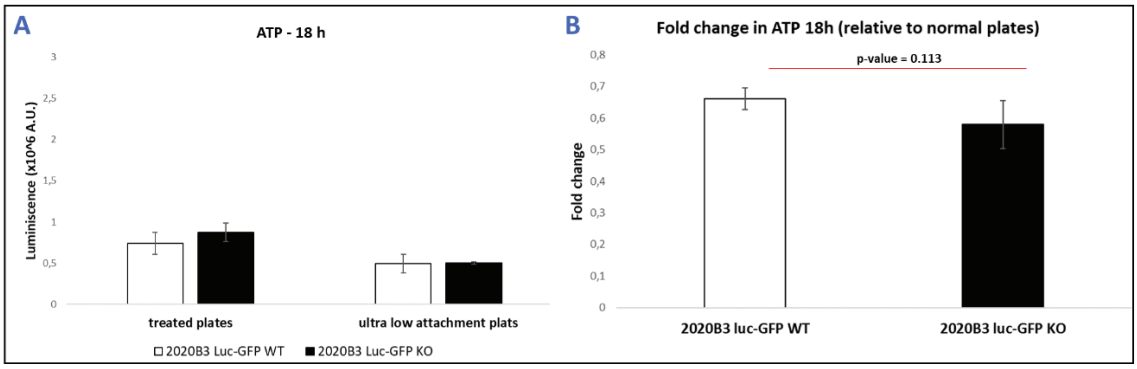

Figure 24. Quantification of ATP in 2020B3 cells in arbitrary units (x10^6 A.U.) during an anoikis resistance assay. (**A**). Luminescence in 2020B3 Luc-GFP CPEB4^{WT} and 2020B3 Luc-GFP CPEB4^{KO} cells on treated and ultra-low attachment plates at 18 hours post seeding. (**B**) ATP production on ultra-low attachment plates relative to adherent plates at 18 hours post seeding, no statistical differences were observed (p-value = 0.113). The experiment was repeated 3 times with 3 wells per condition. Data are expressed as mean ± standard deviation.

At 36 hours, ATP levels had increased in treated plates relative to 18-hour measurements, indicating continued proliferation and growth of both CPEB4^{WT} and CPEB4^{KO} cells on high-adherence plates. Consistent with the 18-hour results, the 2020B3 Luc-GFP CPEB4^{KO} cells showed higher viability compared to the 2020B3 Luc-GFP

CPEB4^{WT} cells. On ultra-low attachment plates, however, a reduction in ATP levels was observed, corresponding to decreased viability in both cell types (**Figure 25A**).

When analysing ATP levels at 36 hours relative to the control, there was a trend toward higher cell viability in CPEB4^{WT} cells compared to CPEB4^{KO} cells; however, this difference was not statistically significant (p-value > 0.05). Consequently, no significant differences in anoikis resistance were observed between the 2020B3 Luc-GFP CPEB4^{WT} and 2020B3 Luc-GFP CPEB4^{KO} cells after 36 hours of culture. At this time point, the percentage of cells that remained viable—and thus resistant to anoikis—was 24% for CPEB4^{WT} cells and 18% for CPEB4^{KO} cells (**Figure 25B**).

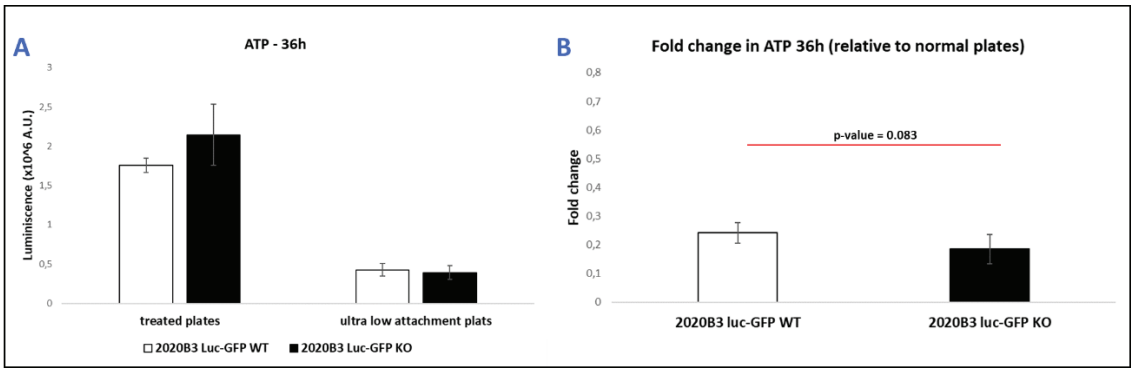

Figure 4. Quantification of ATP in 2020B3 cells in arbitrary units (x10^6 A.U.) during an anoikis resistance assay. (**A**) Luminescence in 2020B3 Luc-GFP CPEB4^{WT} and 2020B3 Luc-GFP CPEB4^{KO} cells on treated and ultra-low attachment plates at 36 hours post seeding. (**B**) ATP production on ultra-low attachment plates relative to adherent plates at 36 hours post seeding, no differences were observed between CPEB4^{WT} or CPEB4^{KO} cells, p-value = 0.083. The experiment was repeated 3 times with 3 wells per condition. Data are expressed as mean ± standard deviation.

This study evaluated the aggressiveness of murine liver cancer cells, focusing on the anoikis resistance of CPEB4^{WT} versus CPEB4^{KO} cells. By measuring cell viability on ultra-low attachment versus high-adherence plates, it was found that both cell types had similar resistance to anoikis. At 18 hours, both CPEB4^{WT} and CPEB4^{KO} cells showed reduced viability on ultra-low attachment plates compared to high-adherence plates, with no significant differences between the two types. By 36 hours, while cell viability on high-adherence plates continued to increase, both cell types demonstrated

decreased viability on ultra-low attachment surfaces, with no statistically significant differences in anoikis resistance between the CPEB4^{WT} and CPEB4^{KO} cells.

CPEB4 depletion promotes endothelial-like and epithelial-to-mesenchymal phenotype transition in liver cancer cells *in vitro*

The acquisition of VM competency in tumor cells is closely associated with the EMT, a pivotal mechanism in cancer progression. EMT induces epithelial cells to lose their cell-cell adhesion characteristics and acquire mesenchymal traits, such as enhanced migratory and invasive capabilities, alongside increased resistance to apoptosis (303). This transition is crucial for tumor progression and has been demonstrated to play a key role in facilitating VM competency across various tumor types, including melanoma and breast carcinoma (304,305). The plasticity conferred by EMT not only promotes tumor invasiveness but also contributes to the formation of VM structures, underscoring the complex interplay between EMT, CSC and VM (306,307).

Interestingly, genome-wide studies conducted in collaboration with Raúl Mendez at the Institute for Research in Biomedicine (IRB Barcelona) (*manuscript in preparation*) indicated that CPEB4 knockout cells display increased markers of both EMT and VM compared to their CPEB4 wildtype counterparts (*data not shown*).

To validate CPEB4's involvement in EMT and VM, we assessed the expression of relevant markers of both characteristics in the presence (CPEB4$^{SCR/WT}$) or absence (CPEB4$^{KD/KO}$) of CPEB4 using immunoblotting (**Figure 26**). For this purpose, we used the human (HepG2) and murine (2020B3) liver cancer cells modified as previously described in this thesis.

Figure 26A shows the successful reduction of CPEB4 protein expression in CPEB4 knockdown human liver cancer cells (HepG2) and CPEB4 knockout murine liver cancer cells (2020B3). We evaluated markers associated with EMT, including the epithelial marker epithelial-cadherin (E-cadherin) (**Figure 26B**) and mesenchymal markers such as neural cadherin (N-cadherin), Twist1 and snail family transcriptional repressor 2 (Slug) (**Figure 26C**). We also examined markers associated with, though not exclusive to, VM,

including vascular endothelial cadherin (VE-cadherin), Notch Receptor 1 (Notch1), MYC proto-oncogene (c-myc) and Prominin-1 (CD133) (**Figure 26D**).

In HepG2 cells with CPEB4 knockdown, the downregulation of E-cadherin—a key epithelial marker essential for maintaining cell-cell adhesion and epithelial integrity—suggests a shift towards a less epithelial phenotype. In contrast, E-cadherin expression in 2020B3 cells remains unchanged, which may be due to alterations in its cellular localization rather than its overall expression (**Figure 26B**). Despite this, both HepG2 and 2020B3 cells with CPEB4 reduction exhibit increased expression of mesenchymal markers N-cadherin, Twist1 and Slug, suggesting a transition to a more mesenchymal phenotype. N-cadherin disrupts epithelial adhesion, enabling EMT, while Twist1 triggers EMT by repressing epithelial markers and Slug promotes EMT by inhibiting epithelial proteins (**Figure 26C**).

Studies have identified several proteins that correlate with an increased potential for VM, including VE-cadherin, Notch1, c-myc and CD133. VE-cadherin is crucial for endothelial cell-cell adhesion and the formation of vessel-like structures in VM. Notch1 regulates angiogenesis and influences EC behaviour, affecting VM formation. C-myc, an oncogene that promotes cell proliferation and survival, is associated with enhanced VM development. CD133, a marker for CSCs, plays a role in VM by influencing cell-signalling pathways. Our data indicate that these markers are upregulated in CPEB4$^{KD/KO}$ liver tumor cells, suggesting an enhanced propensity for forming VM structures (**Figure 26D**).

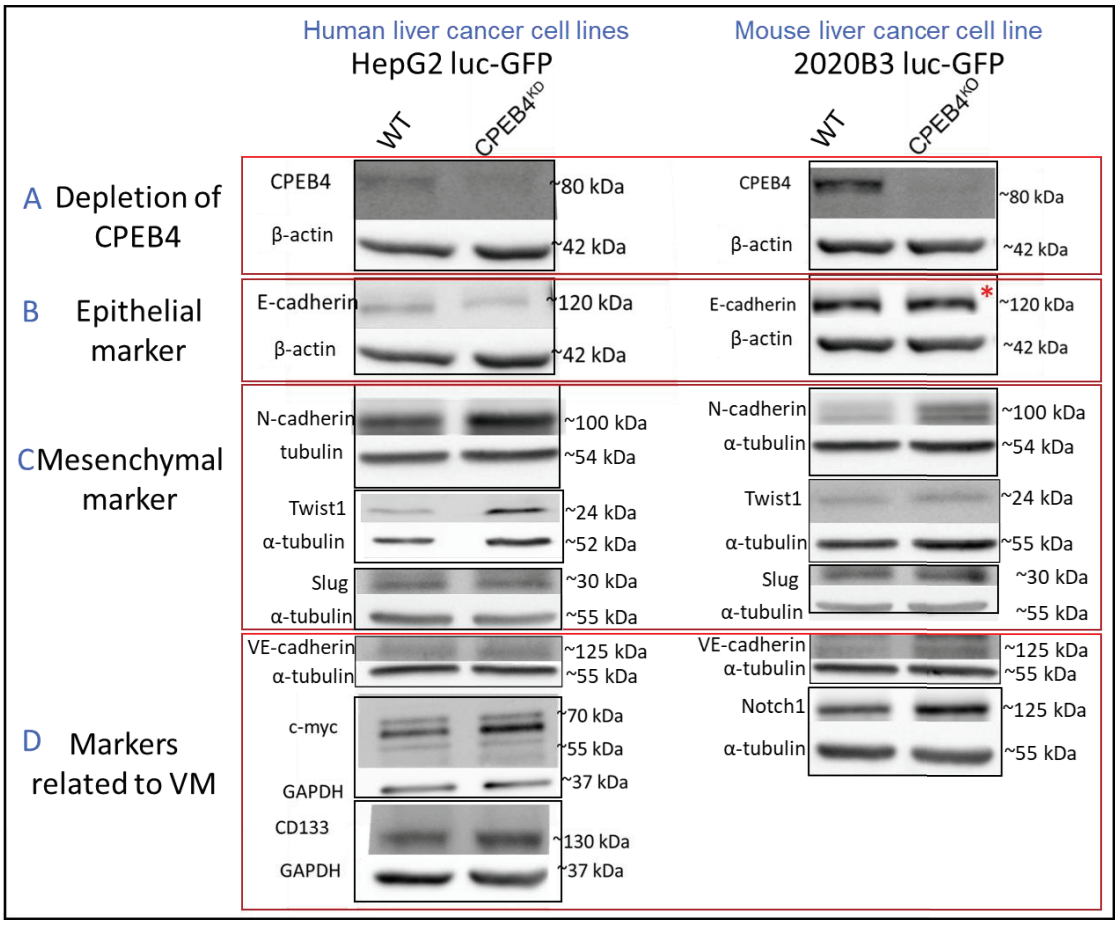

Figure 26. Western blot analysis of protein expression in HepG2 and 2020B3 cells. (**A**) Illustrates the reduction of CPEB4 protein. (**B**) Depicts proteins associated with the epithelial phenotype, (**C**) shows markers indicative of the mesenchymal phenotype and (**D**) highlights markers related to VM. The data indicate that HepG2 CPEB4^{KD} and 2020B3 CPEB4^{KO} cells exhibit a more pronounced mesenchymal phenotype and increased expression of VM-related markers than HepG2 CPEB4^{SCR} and 2020B3 CPEB4^{WT} cells.

Detection of liver tumor vasculogenic mimicry and angiogenesis *in vivo* using CD31-PAS staining

We conducted xenograft studies with human HepG2 liver cancer cells to investigate the role of CPEB4 in the vasculogenic potential of tumor cells *in vivo*. HepG2 luciferase-GFP cells, either CPEB4^{SCR} or CPEB4^{KD}, were subcutaneously injected into immunodeficient CR nod SCID mice. Specifically, eight 6-week-old SCID mice were injected with five million cells on each flank—HepG2 CPEB4^{SCR} Luc-GFP cells on the right flank and HepG2 CPEB4^{KD} Luc-GFP cells on the left flank. Tumor formation was monitored using the IVIS-50 in vivo bioluminescence imaging system. Mice were sacrificed when the tumors

reached a size that began to compromise the integrity of the skin. The tumors were embedded in paraffin and sections were prepared for IHC and IF analyses.

We observed a higher incidence of tumor formation following the injection of CPEB4^{KD} cells compared to CPEB4^{SCR} cells (**Figure 27**).

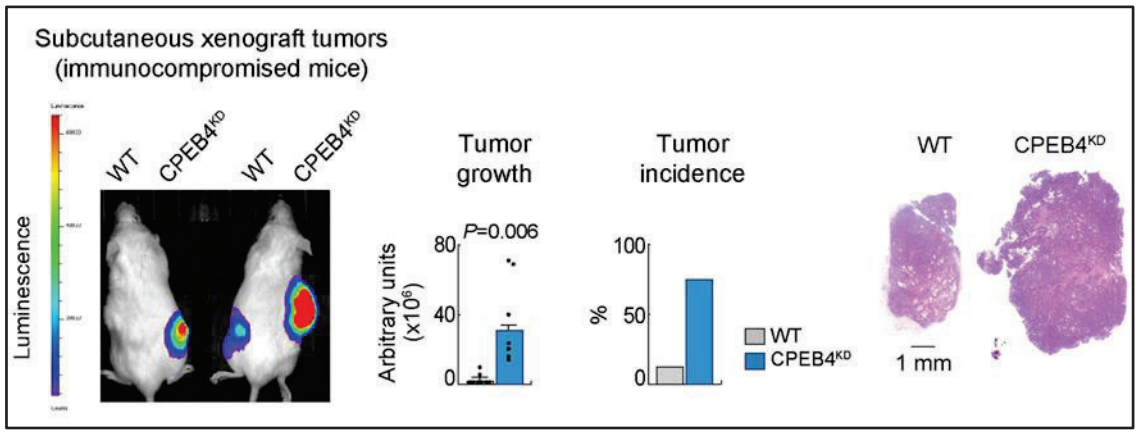

Figure 27. Tumor growth and incidence after subcutaneous implantation of CPEB4^{KD} and wild-type human HepG2 (ATCC®) liver cancer cells into immunocompromised SCID mice. Representative mouse photographs and H&E-stained microscopic photographs of CPEB4^{KD} and wild-type tumors are shown. We could observe that tumor growth and incidence were higher when CPEB4 was reduced. Scale bar, 1 mm.

To detect VM in HepG2 xenograft tumors, we performed IHC using the vascular endothelial marker CD31 in combination with PAS staining (**Figure 28**). PAS staining identifies glycoproteins typically lining VM structures, which are characterized by CD31-negative (CD31^{NEG}) and PAS-positive (PAS^{POS}) structures containing red blood cells, as validated by hematoxylin and eosin (H&E) staining (**Figure 28**).

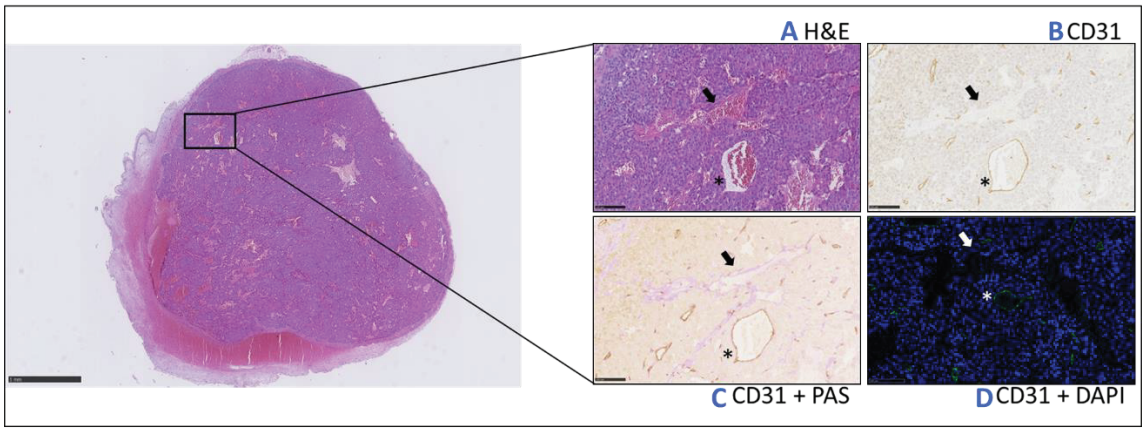

Figure 28. Histological and IHC analysis of tumors: differentiation of VM structures and endothelial vessels. Mice were sacrificed when tumors were big enough and tumors were collected for analysis. (**A**) Histological examination using H&E staining. Black arrow and asterisk pinpoint two structures that contain red blood cells inside (**B**) Immunostaining for CD31. We can observe that the structure marked with the black arrow is CD31 negative suggesting it is a VM structure. The structure marked with a black asterisk is CD31 positive, suggesting it is an endothelial vessel. (**C**) PAS staining. With PAS staining we can observe that, indeed, the structure marked with a black arrow is surrounded by PAS staining (**D**) Combined CD31 and PAS staining.

To enhance the detection and differentiate between murine and human cells, we complemented this approach with IF (**Figure 29**). This allowed simultaneous detection of CD31, GFP, DAPI, and the human nuclei marker HuNu, improving accuracy by distinguishing murine (DAPI-positive, blue) from human (DAPI+HuNu-positive, purple) cells, and enabling the assessment of tumor cell transdifferentiation into endothelial cells. This advanced IF technique offers a clearer understanding of VM and tumor vascularization.

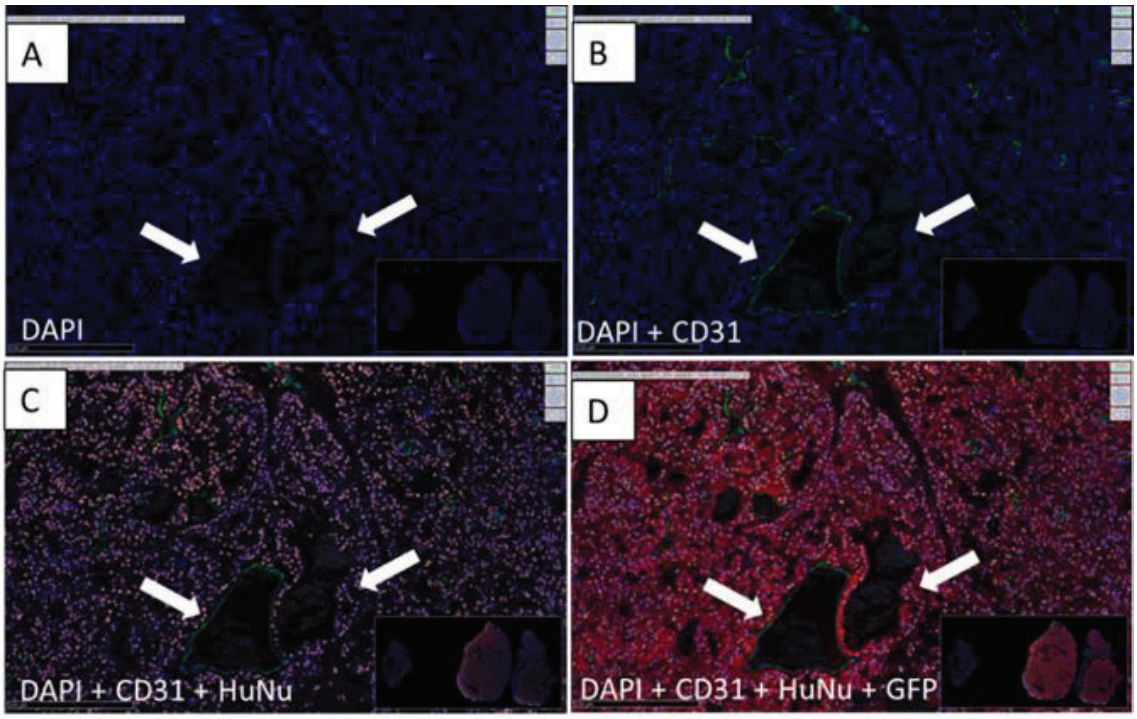

Figure 29. Representative image of IF implemented in our lab (in collaboration to IRB) to detect VM structures. (**A**) Nuclei stained with DAPI (blue) reveal two structures containing red blood cells (indicated by white arrows). (**B**) The endothelial marker CD31 (green) surrounds one of the tubular structures identified in panel **A**. (**C**) Human nuclear stain (HuNu) differentiates human nuclei (purple) from murine nuclei (blue) around the structures. (**D**) GFP staining confirms that one of the tubular structures is surrounded by GFP-positive human tumor cells, suggesting it may be a VM tube, as it is $CD31^{NEG}$.

We classified tumors into three distinct regions for analysis: viable tumor, perinecrosis and total tumor (the sum of viable and perinecrosis regions) (**Figure 30**). Within these regions, we measured the density of structures by counting the number of structures per mm^2 of tumor area. Our analysis indicates that the absence of CPEB4 promotes the formation of new angiogenic vessels, as evidenced by an increase in CD31 density across the different regions, suggesting that CPEB4 depletion in liver cancer cells affects the host's angiogenic response. However, the density of VM structures remained unchanged with CPEB4 removal. Notably, there was a tendency for increased VM in areas of the tumor where O_2 and nutrients are scarce, particularly in perinecrotic regions (p-value = 0.17), indicating a potential adaptive response by the tumor cells to their microenvironment.

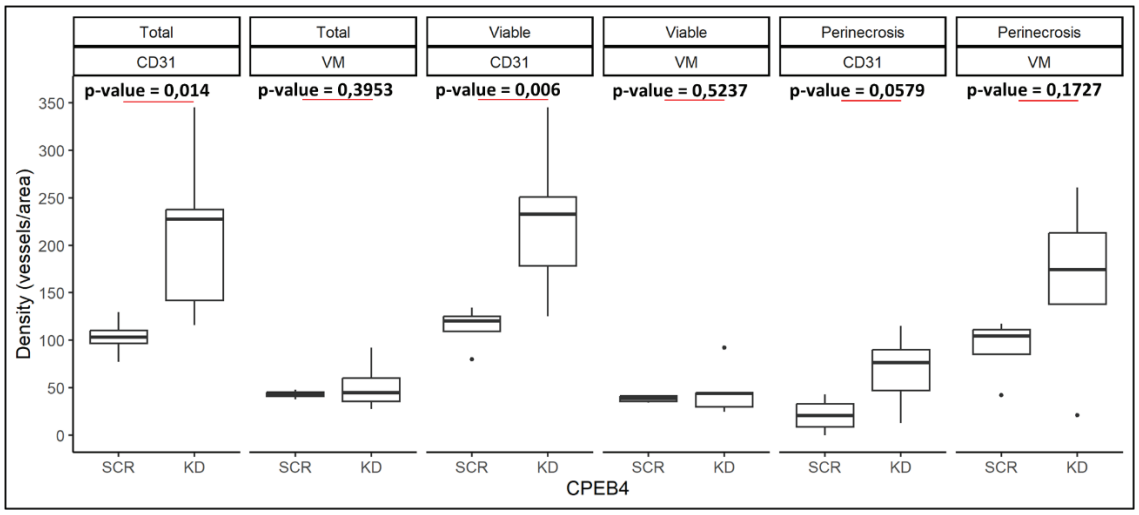

Figure 30. Tumor region categorization and endothelial and VM vessel density analysis. Tumors were classified into viable, perinecrotic and total regions for analysis. CPEB4 depletion increased CD31 endothelial vessels density, indicating enhanced angiogenesis, while VM structure density remained unchanged. A trend towards increased VM was observed in perinecrotic regions (p = 0.17), suggesting an adaptive response by the tumor cells to their microenvironment.

CPEB4-regulated vasculogenic mimicry correlates with tumor aggressiveness in an *in vivo* mouse model of HFD-induced liver cancer

To further investigate the role of VM in liver cancer *in vivo*, we used a mouse model of HFD-induced liver cancer. Male C57BL/6J mice were maintained with *ad libitum* water and a controlled diet. We utilized a global loss-of-function genetic mouse model ($CPEB4^{KO}$) and wild type ($CPEB4^{WT}$) controls to assess the impact of CPEB4 depletion on HFD-associated liver cancer.

The liver carcinogenesis protocol was a two-hit protocol (**Figure 31A**). Mice were fed either a ND (13% energy from fat) or a HFD (60% energy from fat) starting at 6 weeks of age. At 16 weeks of age, mice receive an intraperitoneal injection of 80 mg/kg DEN, a liver carcinogen. From week 20 until the end of the protocol at 50 weeks, mice received 0.05% PB in their drinking water. At the end of the 50-week protocol, mice were sacrificed and livers were collected for macroscopic and microscopic analysis.

Tumor number (**Figure 31B**) was assessed by counting the number of tumors in each group: wild-type mice on a ND, knockout mice on a ND, wild-type mice on an HFD and

knockout mice on an HFD. For evaluating tumor aggressiveness (**Figure 31C**), we consulted a pathologist who classified liver tissue into five categories according to their malignancy: normal tissue, nodular hyperplasia, adenoma, adenocarcinoma and carcinoma. We then calculated the relative incidence of each tissue classification and determined the proportion of aggressive tumors for each genotype (CPEB4^{WT} and CPEB4^{KO}). We observed a higher number of tumors (**Figure 31B**) and greater tumor aggressiveness (**Figure 31C**) in CPEB4^{KO} mice on a HFD compared to CPEB4^{WT} mice on the same diet. There was no difference considering the number of tumors in the normal diet group.

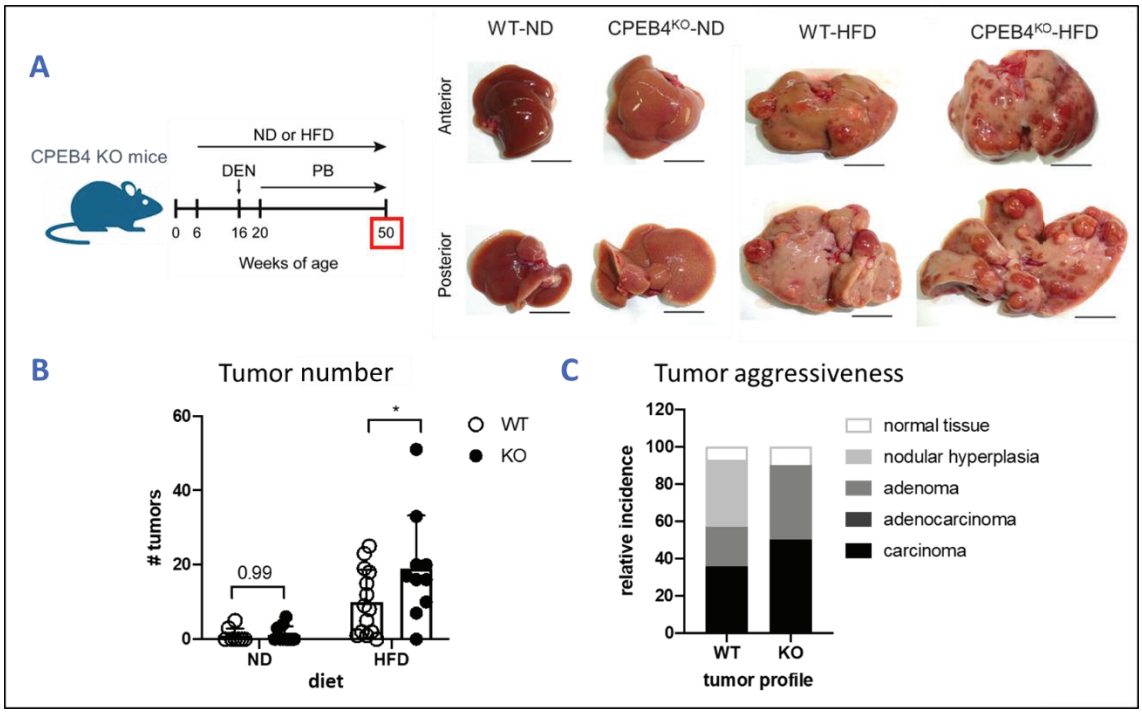

Figure 31. Liver carcinogenesis protocol and results. (**A**) Mice were placed on either a ND or a HFD at 6 weeks of age. At 16 weeks, they received an 80 mg/kg intraperitoneal injection of DEN. From week 20 to 50, they were given 0.05% PB in their drinking water. At the end of the protocol, mice were sacrificed and tumors were extracted. Macroscopically, livers from animals in HFD group had worse morphology and, from those livers, the ones from CPEB4^{KO} animals were the worst (steatosis, more tumors visible macroscopically and worsen morphology). (**B**) CPEB4^{KO} mice on HFD showed a higher tumor number of liver tumors compared to HFD-fed CPEB4^{WT} mice (p-value = 0.034). (**C**) Tumors in HFD-fed CPEB4^{KO} mice were more aggressive compared to those in HFD-fed CPEB4^{WT} mice according to their tumor type classification.

To investigate whether VM contributed to the aggressive phenotype observed in the *in vivo* liver cancer model under HFD, we performed histological analyses of liver samples (**Figure 32**). These analyses included H&E staining (**Figure 32A**), immunostaining for platelet endothelial cell adhesion molecule (CD31) (**Figure 32B**), Periodic Acid-Schiff (PAS) (**Figure 32C**) and combined CD31+PAS staining (**Figure 32D**). The gold standard for detecting VM involves immunohistochemistry targeting CD31 and PAS staining to identify glycoprotein-lined channels formed by tumor cells. VM-positive vessels are characterized by the presence of CD31-negative ($CD31^{NEG}$) and PAS-positive (PAS^{POS}) structures containing red blood cells, as validated by H&E staining.

For analysis, we categorized tumors into three size ranges: ≤ 2 mm², >2≤4 mm² and >4 mm². This categorization was based on literature indicating that tumor size is a critical determinant of liver tumor aggressiveness and clinical outcomes (200). We then assessed the density of normal endothelial vessels ($CD31^{POS}PAS^{POS}$) (**Figure 33**) and VM vessels ($CD31^{NEG}PAS^{POS}$) in these areas (**Figure 34**). For the analysis of vessel presence, we used the QuPath software. To perform the analysis, tumor area was measured considering all the region of the liver occupied by the tumor. Then, VM vessels ($CD31^{NEG}PAS^{POS}$) were counted manually considering the different characteristics: the presence of red blood cells confirmed by H&E, CD31 negativity and PAS positivity. VM density was calculated by dividing the number of VM vessels by the tumor area. Endothelial vessel density ($CD31^{POS}PAS^{POS}$) was assessed through QuPath as a percentage of staining.

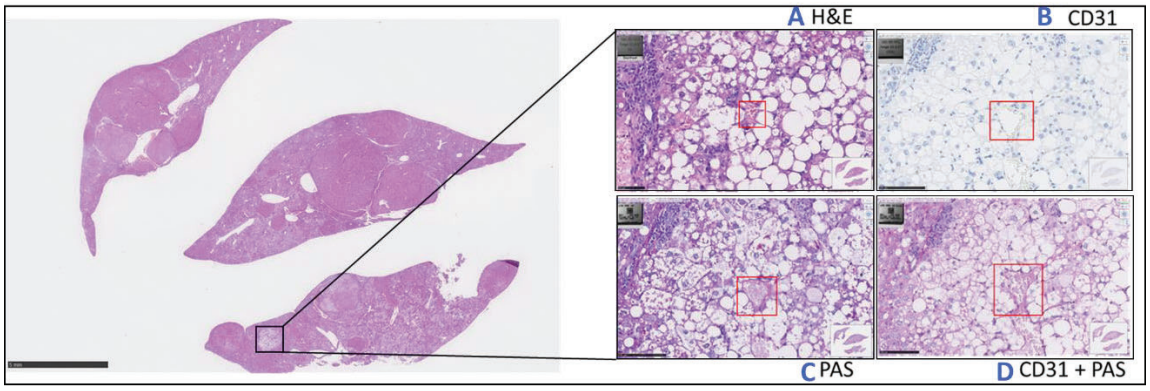

Figure 5. Liver analysis at the end of the 50-week protocol. Mice were sacrificed at the end of the 50-week protocol and livers were collected for analysis. (**A**) Histological examination using

H&E staining used to check for red blood cell presence inside the structures. (**B**) Immunostaining for CD31. (**C**) PAS staining. (**D**) Combined CD31 and PAS staining. In the red area indicated we observe a $CD31^{NEG}PAS^{POS}$ vessels with the presence of red blood cells inside in H&E. This vessel was considered VM positive.

Our data indicated that the density of normal endothelium-lined vessels was unaltered regardless of CPEB4 presence or absence in any of the area regions defined nor taking all WT and KO tumors together (**Figure 33A-B**). There was no correlation between the density of normal endothelial vessels and tumor area (p-value > 0.05) in any of CPEB4 genotypes ($CPEB4^{WT}$ nor $CPEB4^{KO}$) (**Figure 33C**).

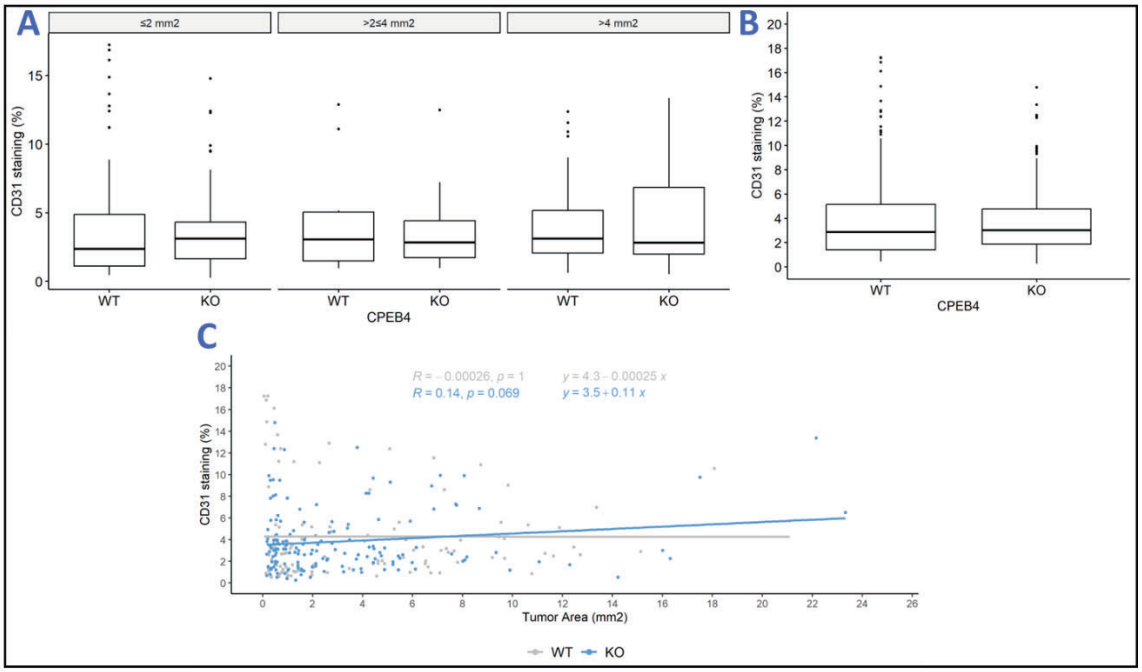

Figure 33. Tumor size categorization and endothelial vessel density. Tumors were classified into three size ranges: ≤2 mm², >2≤4 mm² and >4 mm². (**A-B**) The density of normal endothelial vessels ($CD31^{POS}PAS^{POS}$) was evaluated. No significant difference in vessel density was observed regardless of CPEB4 presence in any group (**B**) nor taking all WT and KO tumors together. (**C**) There was no correlation between vessel density and tumor size in $CPEB4^{WT}$ (p-value = 1) nor in $CPEB4^{KO}$ (p-value = 0.069).

Conversely, the density of VM vessels was significantly higher (p-value < 0.05) in $CPEB4^{KO}$ HFD animals compared to $CPEB4^{WT}$ HFD animals across all tumor size ranges (**Figure 34A**) and considering all tumors of each group together (**Figure 34B**). Notably, tumors without VM were observed more frequently in $CPEB4^{WT}$ animals, while in $CPEB4^{KO}$ animals, VM was present even in the smallest tumor size group (**Figure 34C**). In tumors ≤2 mm^2,

68.6% of tumors in CPEB4^{WT} animals presented VM structures compared to 92.2% tumors of CPEB4^{KO} animals. In the case of tumors with an area >2≤4 mm^2, all tumors in CPEB4^{KO} animals presented VM structures compared to 78.6% tumors in CPEB4^{WT} animals. In the case of big tumors, >4 mm^2, 90.48% of tumors in CPEB4^{WT} animals contained VM structures and all tumors in CPEB4^{KO} animals contained these structures.

Moreover, there was a significant (p-value < 0.05) positive correlation between VM density and tumor area, which was more pronounced in CPEB4^{KO} tumors as can be observed from the slope of the correlation. The slope for correlation of VM structures and tumor area of tumors developed in CPEB4^{WT} animals was 6.3 whereas the slope for correlation of tumors developed in CPEB4^{KO} animals was more than double of that of CPEB4^{WT} animals (13) (**Figure 34D**).

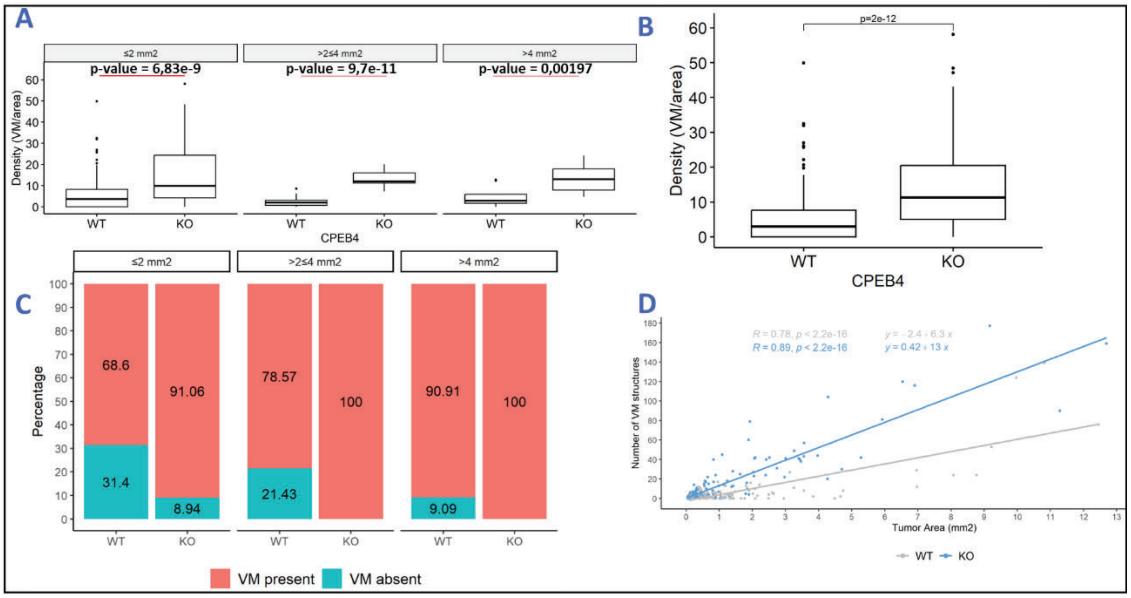

Figure 34. Vascularization and correlation with tumor area in CPEB4^{KO} versus CPEB4^{WT} mice on HFD. Tumors were categorized into three size ranges: ≤2 mm², >2≤4 mm² and >4 mm². (**A**) VM vessel density (CD31^{NEG}PAS^{POS}) was significantly higher in CPEB4^{KO} HFD mice compared to CPEB4^{WT} HFD mice across all tumor sizes (p-value = 6.83e-9 in ≤2 mm^2, p-value = 9.7e-11 in >2≤4 mm^2 and p-value = 0.00197 in >4 mm^2). (**B**) This increased VM density was observed in all tumors from each group combined (p-value = 2e-12). (**C**) CPEB4^{WT} mice presented tumors without VM more frequently, while VM was present even in the smallest tumors of CPEB4^{KO} mice. (**D**) A significant positive correlation between VM density and tumor area was observed, particularly pronounced in CPEB4^{KO} (blue line) tumors.

These findings indicate that VM development occurs even in smaller tumors in CPEB4^{KO} animals, potentially explaining their increased aggressiveness. Enhanced VM may facilitate better nourishment and growth, thereby contributing to the malignancy observed in these tumors.

Co-culture of tumoral and endothelial cells in matrigel and bevacizumab treatment

Having established that liver cancer cells can form VM structures *in vitro* we aimed to investigate whether these structures contribute to the resistance to anti-angiogenic therapy observed in liver cancer patients. To this end, we conducted *in vitro* matrigel experiments using murine liver cancer cells (2020B3) that were either wild type or knockout for CPEB4, tagged with luciferase-GFP.

To simulate a more accurate murine tumor environment, we co-cultured these liver cancer cells with murine ECs, H5V cells. H5Vs are transformed and tumorigenic endothelioma cells. Distinction between the two cell types was facilitated thanks to GFP expression by liver tumor cells (2020B3 Luc-GFP) and mCherry expression by ECs (H5V Cherry).

We first optimized the co-culture density for both cell types and assessed the expression levels of the GFP and cherry reporters *in vitro*. Tested densities were 120,000 cells (ratio 1:1 endothelial and tumoral), 240,000 cells (ratio 1:1 endothelial and tumoral) and 360,000 (ratio 1:2, endothelial and tumoral). The selected density was 240,000 cells in total in a ratio 1:1 as this was the condition in which closed tubular structures were observed. Fewer cell density plated lead to no structures and greater densities lead to a monolayer due to over growing of the cells.

Our observations indicated that the number of closed tubular structures in the co-culture assays remained consistent regardless of whether the co-cultured cells were WT or KO for CPEB4 as determined by the analysis of number of closed structures per field per condition (**Figure 35**).

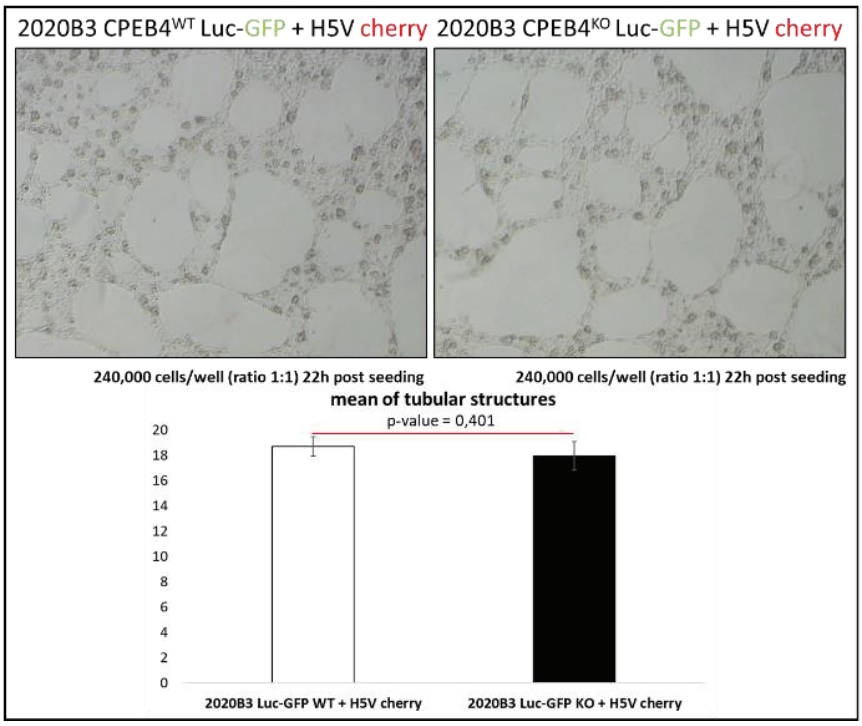

Figure 35. Co-culture of murine tumoral cells with murine ECs expressing the mCherry fluorescent protein. Analysis of co-culture assays revealed that the number of closed tubular structures per field remained consistent regardless of whether the tumor cells were WT or KO for CPEB4. Analysis was performed counting the number of closed tubular structures per field. The experiment was repeated 3 times with 4 wells per condition. Data are expressed as mean ± standard deviation.

Following the determination of optimal co-culture density (240,000 cells in a 1:1 ratio), we performed additional matrigel experiments where the co-cultured cells were treated with bevacizumab, an anti-angiogenic therapy commonly used in clinical settings. The working doses used were 0.125 mg/mL, 0.25 mg/mL, and 0.5 mg/mL. Bevacizumab was diluted into the complete media to achieve the desired concentrations. We observed a dose-dependent response: as the bevacizumab concentration increased, the proportion of tumor cells within the tubular structures also increased (**Figure 36A**). Initially, at a 0 mg/mL dose, CPEB4^{KO} cells contributed more to the formation of these structures compared to CPEB4^{WT} cells. Both cell types showed a doubling in their proportion of structure formation with increased bevacizumab treatment. When the maximum concentration of bevacizumab was added (0.5 mg/mL), the proportion of tumoral cells forming the structure was double comparing to their starting point (**Figure 36B**).

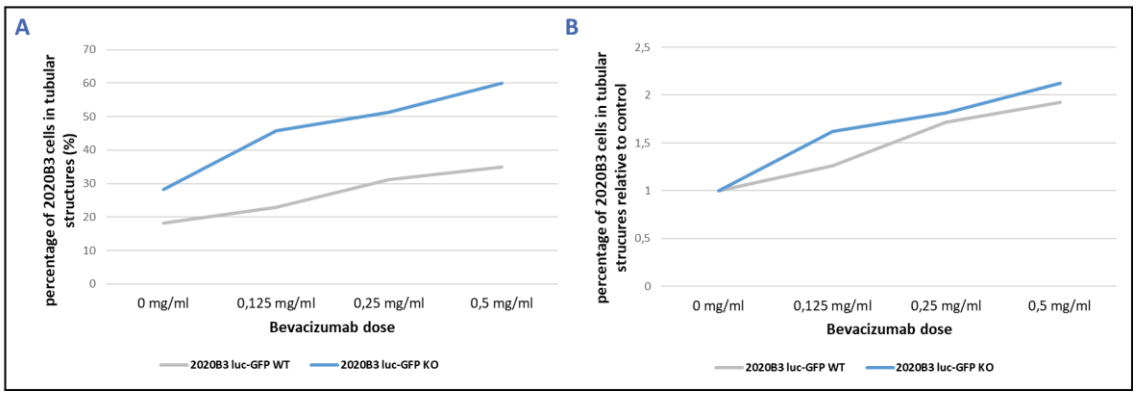

Figure 36. Co-culture of murine tumoral cells (2020B3) CPEB4^{WT} (grey line) and CPEB4^{KO} (blue line). A. We observed a dose dependent response: as bevacizumab concentration increased the proportion of tumoral cels within the tubular structures also increased. **B**. In both cell types they doubled their percentage in the VM structure when the bevacizumab dose was the maximum.

These results suggest that CPEB4-deficient liver tumor cells exhibit an enhanced ability to form tubular-like structures in response to anti-angiogenic therapy *in vitro*. This phenomenon implies a potential resistance mechanism mediated by CPEB4, highlighting its role in tumor adaptation to anti-angiogenic treatments.

Discussion

Unravelling the effects of CPEB4 depletion on liver cancer cell phenotypes

Generation and validation of HepG2 and 2020B3 cell lines

The generation of HepG2 CPEB4^{KD} and HepG2 CPEB4^{SCR} cells, alongside 2020B3 CPEB4^{KO} and CPEB4^{WT} cells, has provided a robust foundation for understanding the role of CPEB4 in liver cancer progression. Lentiviral and retroviral technologies were utilized to create stable cell lines expressing luciferase-GFP, allowing for real-time tracking of tumor growth and cellular behavior. Validation through Western blot and RT-qPCR confirmed effective CPEB4 reduction or depletion in both HepG2 and 2020B3 cell lines, ensuring that subsequent experiments could reliably assess the impact of CPEB4 deficiency on liver cancer cell phenotypes.

Enhanced vasculogenic mimicry in CPEB4-deficient liver cancer cells

Our results demonstrated that CPEB4 depletion significantly enhances the ability of liver cancer cells to form VM structures. HepG2 CPEB4^{KD} cells and 2020B3 CPEB4^{KO} cells formed more closed tubular structures *in vitro* compared to their respective controls. This observation aligns with the notion that CPEB4 functions as a suppressor of VM, a process where tumor cells mimic ECs to form vessel-like structures. The enhanced VM capability in CPEB4-deficient cells suggests that CPEB4 negatively regulates this phenomenon, which is often associated with aggressive cancer behavior and resistance to anti-angiogenic therapies.

Proliferation capacity remains unaffected by CPEB4 depletion

Contrary to the significant impact on VM formation, CPEB4 depletion did not alter the proliferation capacity of liver cancer cells *in vitro*. Both HepG2 and 2020B3 cell lines exhibited comparable proliferation rates, regardless of CPEB4 status. This finding suggests that the observed increase in VM competency is not attributed to changes in cell proliferation but rather to alterations in the cellular machinery that governs VM formation. This result highlights that CPEB4's influence on liver cancer aggressiveness is

more closely linked to its role in regulating cellular plasticity and VM rather than directly affecting cell growth.

Anchorage-independent growth and CPEB4 depletion

The assessment of anchorage-independent growth revealed that CPEB4 deficiency enhances the ability of liver cancer cells to form colonies in soft agar. This property is indicative of increased malignancy and stem-like characteristics. The higher number of colonies formed by 2020B3 CPEB4^{KO} cells compared to their wild-type counterparts underscores the role of CPEB4 in modulating cellular aggressiveness. Anchorage-independent growth is often associated with the potential for metastasis and aggressive cancer phenotypes, reinforcing the hypothesis that CPEB4 plays a crucial role in liver cancer progression through its influence on cellular plasticity.

Anoikis resistance in CPEB4-deficient liver cancer cells

Both murine liver cancer 2020B3 CPEB4^{WT} and CPEB4^{KO} cells showed similar viability on ultra-low attachment plates, indicating that CPEB4 does not critically influence the ability of liver cancer cells to survive in conditions of low adhesion. This finding suggests that, while CPEB4 affects VM and anchorage-independent growth, it does not have a substantial impact on anoikis resistance. The absence of observable differences in anoikis resistance between the two cell types may be attributable to several factors. First, both cell types might inherently possess similar levels of key molecules involved in the anoikis signaling pathways independent on CPEB4 regulation, resulting in comparable responses to detachment-induced apoptosis. Additionally, the experimental conditions used, such as the time of exposure to non-adherent conditions or the specific assays employed, may not be sensitive enough to detect subtle variations in anoikis resistance. Moreover, compensatory survival mechanisms, such as activation of alternative survival pathways, may be equivalently activated in both cell types, thereby masking potential differences in anoikis susceptibility. These factors collectively could contribute to the observed lack of significant distinction in anoikis resistance between the cell types under investigation.

EMT and VM: an interconnected mechanism

The results presented in this study underscore the pivotal role of CPEB4 in modulating cellular phenotypes crucial for liver cancer progression. Our data reveal that CPEB4 depletion promotes significant changes in liver cancer cells, specifically enhancing EMT and VM. This observation aligns with well-established mechanisms in cancer biology, where EMT facilitates tumor progression by conferring increased migratory and invasive capabilities to cancer cells. EMT induces a loss of epithelial characteristics and acquisition of mesenchymal traits, including enhanced migration, invasiveness, and resistance to apoptosis. Our findings extend these insights by demonstrating that CPEB4 depletion accelerates this transition, as evidenced by decreased expression of the epithelial marker E-cadherin and increased expression of mesenchymal markers such as N-cadherin, Twist1 and Slug.

The elevated levels of mesenchymal markers in CPEB4-depleted cells support the hypothesis that CPEB4 functions as a suppressor of EMT. N-cadherin, known for its role in inducing EMT, disrupts epithelial adhesion and facilitates this transition. Meanwhile, Twist1 and Slug further promote the process by repressing epithelial markers and enhancing the mesenchymal phenotype. This transition is suggested to be crucial for facilitating VM. Our data show increased expression of VM-associated proteins such as VE-cadherin, Notch1, c-myc and CD133 in CPEB4-depleted cells, corroborating the role of CPEB4 in regulating VM competency.

Validation through immunoblotting and phenotypic analysis confirmed successful CPEB4 reduction in both HepG2 and 2020B3 liver cancer cells, providing a basis for further investigation into the phenotypic changes associated with CPEB4 depletion. HepG2 cells with reduced CPEB4 levels exhibited decreased E-cadherin, indicative of a transition towards a mesenchymal phenotype. Interestingly, 2020B3 cells retained E-cadherin expression, likely due to alterations in its cellular localization rather than overall expression. Despite this, both cell types with reduced CPEB4 levels demonstrated increased expression of mesenchymal markers and VM-associated proteins, suggesting that CPEB4 depletion enhances the cells' propensity for VM formation and a mesenchymal phenotype. These findings collectively indicate that CPEB4 acts as a

negative regulator of both EMT and VM, both essential for the aggressive behaviour of liver cancer cells.

Xenograft models: tumor formation and vascularization

Our xenograft studies with HepG2 liver cancer cells provide *in vivo* evidence supporting the role of CPEB4 in liver cancer progression. The increased incidence derived from $CPEB4^{KD}$ cells compared to $CPEB4^{SCR}$ cells, along with the observation of more aggressive tumor characteristics, align with our hypothesis that CPEB4 depletion contributes to enhanced tumor aggressiveness. The use of CD31 IHC and PAS staining to detect VM structures in xenograft tumors demonstrated that, while CPEB4 depletion promoted the formation of new angiogenic vessels, the density of VM structures remained unchanged. This suggests that CPEB4 affects the host's angiogenic response but does not necessarily increase the formation of VM structures in this context. However, a tendency for increased VM in perinecrotic regions of $CPEB4^{KD}$ tumors indicates an adaptive response to the hypoxic TME.

As part of this thesis, we also implemented and advanced IF approach to assess VM in xenograft tumors. Our optimized IF assay incorporates CD31, GFP, DAPI and HuNu markers, allowing for precise differentiation between human tumor cells and murine host cells.

Role of VM in liver cancer: insights from whole-body $CPEB4^{KO}$ models

Our study utilizing an HFD-induced liver cancer mouse model further elucidates the role of CPEB4 in tumor aggressiveness. The higher number and greater aggressiveness of tumors in $CPEB4^{KO}$ mice on an HFD compared to $CPEB4^{WT}$ mice suggest that CPEB4 depletion enhances tumor progression. In the whole-body $CPEB4^{KO}$ mice, we observed a significant increase in VM vessel density ($CD31^{NEG}PAS^{POS}$) in liver tumors compared to WT controls across all tumor area groups. This finding indicates that VM development occurs even in smaller tumors in $CPEB4^{KO}$ animals, potentially contributing to their malignancy by facilitating improved nourishment and growth. This finding suggests that CPEB4 acts as a suppressor of VM. The absence of CPEB4 appears to remove a critical regulatory checkpoint, leading to enhanced VM as an alternative mechanism for tumor

vascularization. Notably, the density of traditional angiogenic vessels ($CD31^{POS}PAS^{POS}$) did not show significant differences between WT and KO tumors, indicating that CPEB4's regulatory role may be more specifically targeted at VM rather than conventional angiogenesis.

Contrasting findings from xenograft models

In contrast, xenograft studies involving subcutaneous injection of $CPEB4^{KD}$ HepG2 and control cells revealed different patterns of vascularization. Tumors derived from $CPEB4^{KD}$ cells exhibited a higher density of angiogenic vessels ($CD31^{POS}PAS^{POS}$) compared to tumors from WT cells. However, VM density remained unchanged between the two groups. This result suggests that in the xenograft context, the loss of CPEB4 primarily stimulates angiogenesis rather than VM.

The increased angiogenesis observed in $CPEB4^{KD}$ tumors may be attributed to the loss of CPEB4's regulatory effect on pro-angiogenic factors, leading to upregulation of endothelial cell-driven vessel formation. However, the unchanged VM density in these models indicates that VM formation is not significantly affected by $CPEB4^{KD}$ in this specific experimental setup. This discrepancy could be due to differences in the TME between xenografts and the systemic context of KO mice. The localized microenvironment of xenografts might drive angiogenesis more prominently, while VM could be more influenced by systemic factors in KO models.

Context-dependent regulation of CPEB4

The observed differences between the whole-body KO and xenograft models underscore the context-dependent role of CPEB4 in tumor vascularization. In the whole-body KO model, CPEB4 deficiency promotes VM, reflecting an intrinsic adaptation of tumor cells to the absence of CPEB4. Conversely, in the xenograft model, $CPEB4^{KD}$ enhances angiogenesis without significant changes in VM, indicating that tumor cells adapt differently based on the experimental conditions.

These findings highlight the importance of considering both systemic and localized contexts when evaluating CPEB4's role in cancer progression. The increased

angiogenesis in xenograft models with CPEB4^{KD} suggests potential therapeutic implications for targeting angiogenesis in liver cancer. Conversely, the prominent role of VM in KO animal models points to the need for understanding CPEB4's impact on alternative vascularization mechanisms to address resistance to anti-angiogenic therapies.

Resistance to anti-angiogenic therapy: *in vitro* evidence

To investigate the role of VM in resistance to anti-angiogenic therapy, we conducted *in vitro* matrigel experiments with CPEB4^{WT} and CPEB4^{KO} liver cancer cells co-cultured with ECs. Our results show that both cell types formed tubular structures regardless of CPEB4 status. However, in the presence of bevacizumab, an anti-angiogenic therapy, the proportion of tumor cells within these structures increased compared to ECs and even more in the case of CPEB4^{KO} cells. These results indicate enhanced VM in response to treatment. Furthermore, this phenomenon suggests that CPEB4 could mediate resistance to anti-angiogenic therapies by promoting the formation of VM structures, highlighting its role in tumor adaptation and therapy resistance.

Impact of bevacizumab treatment and co-culture with endothelial cells

The observation that the formation of tubular structures by CPEB4-deficient tumor cells increases in response to bevacizumab treatment and when co-cultured with endothelial cells provides additional insights into the role of CPEB4 and the effects of anti-angiogenic therapy.

Bevacizumab, an anti-angiogenic agent targeting VEGF, aims to inhibit new blood vessel formation. However, its treatment appears to paradoxically increase the VM formation by CPEB4-deficient tumor cells. This phenomenon could be explained by: adaptive resistance mechanisms and compensatory pathways. In adaptive resistance mechanisms tumor cells may adapt to bevacizumab treatment by enhancing VM as an alternative method to ensure adequate nutrient and oxygen supply. CPEB4-deficient cells, with their increased capacity for VM, might exploit this adaptive pathway more effectively. If it is compensatory pathways, bevacizumab-induced inhibition of VEGF signaling could lead to the activation of compensatory pathways that promote VM.

CPEB4-deficient cells might be particularly adept at leveraging these pathways due to their intrinsic VM capability.

The observation that increasing bevacizumab doses further enhance the tubular structure formation by CPEB4-deficient cells suggests a dose-dependent relationship where higher doses of the drug might intensify the selection pressure for VM. This effect could be indicative of a robust adaptive response by the tumor cells to counteract the anti-angiogenic effects of bevacizumab.

CPEB4 and tumor response to bevacizumab

The presence or absence of CPEB4 in tumor cells significantly impacts their response to bevacizumab treatment, highlighting CPEB4 potential role as a biomarker for tailoring HCC therapies. CPEB4-deficient tumor cells show an increased ability to form VM structures compared to their wild-type counterparts.

The enhanced VM observed in CPEB4-deficient cells could correlate with reduced sensitivity to bevacizumab. Bevacizumab, by targeting VEGF, primarily affects endothelial cell-driven angiogenesis. Tumors with high VM capability might bypass the need for VEGF-mediated angiogenesis, rendering bevacizumab less effective. Consequently, CPEB4-deficient tumors might be less responsive to bevacizumab treatment due to their increased reliance on VM for blood supply.

Potential biomarker role of CPEB4

CPEB4 expression levels could serve as a predictive biomarker for the efficacy of bevacizumab treatment in HCC patients. High CPEB4 expression might indicate a greater likelihood of benefiting from bevacizumab therapy, as CPEB4 presence is associated with reduced VM and better response to anti-angiogenic agents. Conversely, low CPEB4 levels could predict resistance to bevacizumab, suggesting that alternative or additional therapeutic strategies may be required.

Assessing CPEB4 levels in tumors could help in personalizing treatment plans. Patients with CPEB4-deficient tumors, or with reduced levels, might benefit from combination therapies that target both VM and VEGF pathways. Given the potential resistance of

CPEB4-deficient tumors to bevacizumab, exploring combination therapies that address both VM and VEGF pathways could improve treatment outcomes. For example, drugs targeting VM-specific pathways or other angiogenic factors could be combined with bevacizumab to overcome resistance.

Validating CPEB4 as a biomarker involves developing reliable assays for its detection and quantification in clinical samples. This could include immunohistochemistry, RT-qPCR, or other molecular techniques to assess CPEB4 expression in tumor biopsies. Implementing CPEB4 as a biomarker in clinical practice could involve stratifying patients based on their CPEB4 status. This would enable more precise treatment regimens, potentially improving patient outcomes and reducing unnecessary exposure to less effective therapies. Further research and clinical validation are essential to fully realize the potential of CPEB4 as a predictive biomarker and to develop optimized treatment approaches based on individual tumor profiles.

Strengths and contributions of this study

This research offers a series of strengths and valuable contributions to the field of HCC biology and tumor vascularization. Through a multifaceted approach that combines different *in vivo* models and cutting-edge methodologies this work expands the current understanding of VM and angiogenesis in liver cancer.

Comprehensive exploration of CPEB4 in HCC

This study represents one of the first comprehensive investigations into the role of CPEB4 in vascularization of HCC. Prior to this work, CPEB4 had been studied in various cancers, but its specific involvement in HCC vascularization had not been addressed in detail. By identifying CPEB4 as a key regulator of both VM and angiogenesis, this research significantly advances our understanding of the molecular pathways that influence tumor vascularization in liver cancer. It contributes to a growing body of literature suggesting that translational control plays a pivotal role in cancer biology.

Identification of CPEB4 as a context-dependent regulator

A significant contribution of this study is the identification of CPEB4 as a context-dependent regulator. The results show that CPEB4 has distinct effects on VM and angiogenesis depending on the experimental model used. In whole-body KO mice, the absence of CPEB4 leads to increased VM, while in xenografts with CPEB4^{KD}, angiogenesis is elevated. This finding suggests that CPEB4 plays a multifaceted role, potentially interacting with different molecular pathways or environmental cues in distinct contexts. Understanding these context-dependent effects of CPEB4 adds depth to the current knowledge of tumor biology and highlights the complexity of molecular regulation in cancer.

Insight into the mechanistic role of translational control in tumor vascularization

This research underscores the importance of translational control in tumor vascularization by highlighting the regulatory role of CPEB4. While most cancer research has focused on transcriptional changes and genetic mutations, this study provides novel evidence that post-transcriptional regulation, particularly translational control, can significantly affect tumor vascularization strategies. The link between CPEB4-dependent translational control and VM and angiogenesis represents a critical step forward in understanding how cancer cells orchestrate vascularization under stress conditions.

Pioneering VM research in HCC

This thesis advances the limited body of research on VM in HCC. The observation that VM is more pronounced in tumors from CPEB4^{KO} animals provides crucial evidence that VM can be modulated by specific molecular regulators in liver cancer. This is the first study to directly link CPEB4 to VM in HCC, which fills an important gap in the literature and challenges the conventional focus on angiogenesis alone. These findings suggest that VM may be an underappreciated factor in HCC progression and resistance to therapy, opening new avenues for research and therapeutic development.

Robust use of multiple *in vivo* models

The use of both whole-body CPEB4^{KO} models and xenograft models is a significant strength of this study. The combination of these models allows for a broader

investigation of CPEB4's role in tumor vascularization in different biological contexts. The whole-body KO model provides insights into how systemic loss of CPEB4 affects tumor development, while the xenograft model, with specific KD in tumor cells, isolates the tumor-intrinsic effects. This dual approach provides a robust framework for understanding how CPEB4 impacts HCC in different physiological environments, strengthening the study's conclusions.

Detailed regional tumor analysis

A major methodological strength of this research is the detailed analysis of different tumor regions, specifically distinguishing between total tumor, viable tumor and perinecrotic regions. This regional segmentation allowed for the observation that VM is more prominent in the perinecrotic regions of tumors with $CPEB4^{KD}$. This insight highlights the importance of spatial heterogeneity in tumor biology and demonstrates that VM may be particularly relevant in hypoxic or stressed tumor regions. This type of detailed analysis adds a new layer of complexity to the understanding of TME and sets the stage for future research into how different regions within tumors respond to molecular and environmental factors.

Use of IF to study tumor vascularization

The employment of IF to study vascularization and VM represents a key strength of this work. Unlike traditional histological methods, IF enables precise detection and differentiation of cell types and vessel structures. This technique allows for a more nuanced analysis of vascularization in tumors, providing more reliable and detailed data on the nature and density of VM structures. The ability to detect subtle differences in tumor vascularization enhances the validity of the findings and their potential applicability to the clinic.

Potential therapeutic implications

The findings of this study have significant therapeutic implications. By showing that CPEB4 modulates both VM and angiogenesis, the research identifies CPEB4 as a potential therapeutic target and biomarker. Restoring or enhancing CPEB4 function

could inhibit VM, a process associated with poor prognosis and resistance to anti-angiogenic therapies. Furthermore, the increased angiogenesis observed in CPEB4^{KD} xenografts suggests that targeting CPEB4 in combination with anti-angiogenic therapies could enhance treatment efficacy. These insights provide a foundation for future studies aimed at exploring CPEB4 as a therapeutic target in HCC, with the potential to improve treatment outcomes for patients.

Addressing a gap in the literature on HCC vascularization

By focusing on VM and angiogenesis in HCC, this study addresses a critical gap in the literature. While VM has been studied in other tumor types, its relevance in HCC has been relatively underexplored. This research, therefore, makes an important contribution by demonstrating that VM is present and regulated in HCC, particularly in the absence of CPEB4. This fills a knowledge gap and suggests that VM should be considered in the development of therapeutic strategies for liver cancer. The study's findings will likely encourage further investigation into the mechanisms of VM in HCC, which could ultimately lead to new therapeutic approaches.

Future directions

While this thesis has explored the role of VM in liver cancer and its regulation by CPEB4, several avenues for further investigation could deepen our understanding and expand the current body of knowledge. In this section, I outline potential experiments, approaches, and unanswered questions that were beyond the scope of this study but hold the potential to significantly advance the field. By addressing these gaps, future research may uncover new insights, refine methodologies and open avenues for therapeutic innovation in liver cancer.

Additional *in vivo* studies

***In vivo* bevacizumab treatment experiments**

Future *in vivo* experiments with bevacizumab or other anti-angiogenic agents would directly test whether CPEB4 affects resistance to such therapies. Moreover, examining

how CPEB4^{KO} and KD tumors respond to these treatments would provide insights into the clinical relevance of CPEB4's role in tumor vascularization.

Tissue-specific insights

Future experiments could utilize conditional KO models or tissue-specific KO approaches to isolate the effects of CPEB4 within the tumor itself, without influencing systemic physiology. For example, liver-specific KO models would allow for a more focused investigation of CPEB4's role in HCC while minimizing confounding variables. Additionally, the use of reporter mice could help differentiate between host- and tumor-derived vascular components, enhancing the ability to track the cellular origins of VM and angiogenic vessels.

Longitudinal studies on tumor evolution

Longitudinal studies tracking changes in tumor vascularization and VM over time could provide valuable insights into how CPEB4 influences tumor progression and response to treatment. By monitoring tumor dynamics at different stages of growth and treatment, the role of CPEB4 in tumor evolution could be better understood and identify potential windows for therapeutic intervention.

Mechanisms

Future research should focus on identifying the specific mechanisms through which CPEB4 regulates both VM and angiogenesis in HCC. Techniques such as ribosome profiling, RNA immunoprecipitation sequencing and proteomics could be employed to pinpoint direct translational targets of CPEB4 and map the regulatory networks it modulates. This comprehensive approach would provide deeper insights into the molecular pathways influenced by CPEB4, helping to explain the observed differences in vascularization between whole-body knockout and knockdown xenografts models. Additionally, understanding these pathways could reveal new therapeutic targets for disrupting VM in HCC.

To validate the molecular mechanisms underlying CPEB4's role, further experiments using RT-qPCR or functional assays such as siRNA knockdown or overexpression of key

target genes should be conducted. Additionally, chromatin immunoprecipitation or ribosome profiling could be employed to identify direct translational targets of CPEB4 in both tumor cells and ECs, providing deeper insights into the regulatory networks governed by CPEB4.

Building on these insights, *in vivo* experiments are essential to confirm CPEB4's role across different experimental settings. Employing genetic and pharmacological tools to manipulate CPEB4 activity in various mouse models of HCC could help confirm the observed effects and explore potential off-target effects. Additionally, using inducible knockout or conditional knockdown systems could provide more precise control over CPEB4 expression and elucidate its role in specific stages of tumor progression.

Finally, future research should explore how CPEB4 interacts with key signaling pathways involved in tumor vascularization, such as the VEGF pathway, Wnt/β-catenin signaling or the mTOR pathway. Co-immunoprecipitation, mass spectrometry and reporter assays could elucidate the integration of CPEB4 within these broader tumor biology networks, providing insights into its functional impact and potential therapeutic synergy with other cancer treatments.

Therapies, biomarkers and patient contexts

Future research into therapies, biomarkers and patient-specific contexts is crucial to fully harness the therapeutic potential of CPEB4 in HCC. Given its role in both VM and angiogenesis, combination therapies targeting CPEB4 along with established anti-angiogenic agents offer a promising avenue. Preclinical studies in mouse models of HCC could evaluate the efficacy of combining CPEB4 modulators with angiogenesis inhibitors, potentially overcoming resistance mechanisms and improving therapeutic outcomes. These studies would not only explore the synergy between these pathways but also assess how modulating CPEB4 affects tumor vascularization and resistance to current therapies.

Another essential direction for future research is the development of novel CPEB4 modulators. Identifying small molecules that specifically modulate CPEB4 activity could provide targeted therapeutic options for HCC. High-throughput screening and structure-

based drug design could lead to the discovery of such modulators, while RNA-based therapies, like RNA interference or antisense oligonucleotides targeting CPEB4, could offer alternative approaches to manipulating its function in tumors.

To translate these findings into clinical practice, a deeper understanding of how CPEB4 expression correlates with patient outcomes is necessary. Analysing clinical samples from HCC patients to determine the association between CPEB4 expression levels, VM, angiogenesis and treatment response could establish CPEB4 as a relevant biomarker. This could pave the way for clinical trials to evaluate CPEB4's potential as a prognostic or predictive biomarker, allowing for more personalized treatment strategies based on its expression in tumors.

Furthermore, patient-derived xenograft models of HCC represent a valuable tool for studying the clinical relevance of CPEB4. These models, which more accurately replicate human tumor biology and vascularization processes, could provide insights into how varying levels of CPEB4 modulate VM in a patient-specific context. Such studies would not only deepen our understanding of CPEB4's role in tumor vascularization but also help identify individualized responses to therapies targeting this protein, ultimately guiding more tailored treatment approaches in HCC.

Through this integrated exploration of combination therapies, novel modulators, biomarker development, and patient-specific models, the therapeutic potential of CPEB4 in HCC can be better realized, advancing both basic research and clinical application.

Conclusions

The findings presented in this doctoral thesis led to the following key conclusions:

CPEB4 as a regulator of vasculogenic mimicry: Human liver cancer cells (HepG2) demonstrate the ability to form VM structures *in vitro*, with this capacity significantly enhanced in the absence of CPEB4. This suggests that CPEB4 may act as a suppressor of VM in liver cancer. Conversely, murine liver cancer cells (2020B3) do not form VM structures unless CPEB4 is removed, further supporting the hypothesis that CPEB4 regulates the formation of these tubular structures.

Role of CPEB4 in epithelial-to-mesenchymal transition: The mechanism by which CPEB4 influences VM may involve its regulation of EMT in tumor cells. In the absence of CPEB4, liver cancer cells adopt a more mesenchymal phenotype, which is often associated with increased tumor invasiveness. Given CPEB4's role in mRNA translation, it is hypothesized that CPEB4 may regulate the expression of epithelial markers at the translational level. While CPEB4 primarily affects translation, it may also stabilize mRNA levels. Future experiments using RT-qPCR to target candidate genes identified in this thesis will help clarify whether CPEB4 modulates these markers at the protein level without significantly altering mRNA levels.

Impact of CPEB4 on tumor aggressiveness *in vivo*: Xenografts of human liver cancer cells (HepG2) lacking CPEB4 exhibit more aggressive tumor behavior, with faster and larger tumor growth compared to CPEB4-sufficient ($CPEB4^{SCR}$) tumors. Increased aggressiveness is also linked to changes in vasculature, with CPEB4-deficient tumors recruiting host vessels ($CD31^{POS}PAS^{POS}$) more effectively. Additionally, these tumors show a tendency for increased VM ($CD31^{NEG}PAS^{POS}$), particularly in perinecrotic regions, where angiogenesis is insufficient to meet tumor needs.

CPEB4 and *in vivo* liver carcinogenesis: In a liver carcinogenesis model, $CPEB4^{KO}$ animals subjected to a HFD develop more aggressive tumors compared to $CPEB4^{WT}$ animals. This aggressive phenotype is accompanied by a higher density of VM structures, while

endothelial-lined CD31 vessel density remains unchanged. This suggests that CPEB4 deficiency promotes tumor aggressiveness through increased VM, which compensates for insufficient traditional angiogenesis in these tumors.

CPEB4 and resistance to anti-angiogenic therapies: VM, which is associated with more aggressive tumors, may also play a role in mediating resistance to anti-angiogenic therapies. *In vitro* studies reveal that liver tumor cells increase their formation of VM structures when treated with the anti-angiogenic agent bevacizumab. These findings suggest that CPEB4 may influence tumor responses to such therapies and highlight the importance of considering VM as a potential mechanism of resistance in liver cancer treatment strategies.

In summary, this thesis underscores the critical role of CPEB4 in regulating VM and angiogenesis in liver cancer. The results suggest that targeting CPEB4 could enhance therapeutic approaches, particularly in overcoming resistance to anti-angiogenic treatments, and emphasize the need for further research into the molecular pathways underlying its effects.

References

1. Fernandez M. Molecular pathophysiology of portal hypertension. Hepatology. 2015 Apr 9;61(4):1406–15.
2. Abdel-Misih SRZ, Bloomston M. Liver Anatomy. Surg Clin North Am. 2010 Aug;90(4):643–53.
3. Kruepunga N, Hakvoort TBM, Hikspoors JPJM, Köhler SE, Lamers WH. Anatomy of rodent and human livers: What are the differences? Biochim Biophys Acta - Mol Basis Dis. 2019 May;1865(5):869–78.
4. Smedsrod B, De Bleser PJ, Braet F, Lovisetti P, Vanderkerken K, Wisse E, et al. Cell biology of liver endothelial and Kupffer cells Endothelial. Gut. 1994;35(11):1509–16.
5. Iwakiri Y, Shah V, Rockey DC. Vascular pathobiology in chronic liver disease and cirrhosis – Current status and future directions. J Hepatol. 2014 Oct;61(4):912–24.
6. Friedman SL. Hepatic Stellate Cells: Protean, Multifunctional, and Enigmatic Cells of the Liver. Physiol Rev. 2008 Jan;88(1):125–72.
7. Blachier F. Physiological and Metabolic Functions of the Intestinal Epithelium: From the Small to the Large Intestine. In: Metabolism of Alimentary Compounds by the Intestinal Microbiota and Health. Cham: Springer International Publishing; 2023. p. 1–26.
8. D'Antiga L, editor. Pediatric Hepatology and Liver Transplantation. Cham: Springer International Publishing; 2019.
9. Ke P-Y. Diverse Functions of Autophagy in Liver Physiology and Liver Diseases. Int J Mol Sci. 2019 Jan 13;20(2):300.
10. Schulze RJ, Schott MB, Casey CA, Tuma PL, McNiven MA. The cell biology of the hepatocyte: A membrane trafficking machine. J Cell Biol. 2019 Jul 1;218(7):2096–112.
11. Gissen P, Arias IM. Structural and functional hepatocyte polarity and liver disease. J Hepatol. 2015 Oct;63(4):1023–37.
12. Guidotti J-E, Brégerie O, Robert A, Debey P, Brechot C, Desdouets C. Liver Cell Polyploidization: A Pivotal Role for Binuclear Hepatocytes. J Biol Chem. 2003 May;278(21):19095–101.

13. Margall-Ducos G, Celton-Morizur S, Couton D, Brégerie O, Desdouets C. Liver tetraploidization is controlled by a new process of incomplete cytokinesis. J Cell Sci. 2007 Oct 15;120(20):3633–9.

14. Wakabayashi Y, Dutt P, Lippincott-Schwartz J, Arias IM. Rab11a and myosin Vb are required for bile canalicular formation in WIF-B9 cells. Proc Natl Acad Sci. 2005 Oct 18;102(42):15087–92.

15. Levitt D, Levitt M. Human serum albumin homeostasis: a new look at the roles of synthesis, catabolism, renal and gastrointestinal excretion, and the clinical value of serum albumin measurements. Int J Gen Med. 2016 Jul;Volume 9:229–55.

16. Kaksonen M, Roux A. Mechanisms of clathrin-mediated endocytosis. Nat Rev Mol Cell Biol. 2018 May 7;19(5):313–26.

17. Treyer A, Müsch A. Hepatocyte Polarity. In: Comprehensive Physiology. Wiley; 2013. p. 243–87.

18. Shen W-J, Azhar S, Kraemer FB. SR-B1: A Unique Multifunctional Receptor for Cholesterol Influx and Efflux. Annu Rev Physiol. 2018 Feb 10;80(1):95–116.

19. Santos AJM, Nogueira C, Ortega-Bellido M, Malhotra V. TANGO1 and Mia2/cTAGE5 (TALI) cooperate to export bulky pre-chylomicrons/VLDLs from the endoplasmic reticulum. J Cell Biol. 2016 May 9;213(3):343–54.

20. Raote I, Malhotra V. Protein transport by vesicles and tunnels. J Cell Biol. 2019 Mar 4;218(3):737–9.

21. Zanoni P, Velagapudi S, Yalcinkaya M, Rohrer L, von Eckardstein A. Endocytosis of lipoproteins. Atherosclerosis. 2018 Aug;275:273–95.

22. Fedoseienko A, Wijers M, Wolters JC, Dekker D, Smit M, Huijkman N, et al. The COMMD Family Regulates Plasma LDL Levels and Attenuates Atherosclerosis Through Stabilizing the CCC Complex in Endosomal LDLR Trafficking. Circ Res. 2018 Jun 8;122(12):1648–60.

23. Olzmann JA, Carvalho P. Dynamics and functions of lipid droplets. Nat Rev Mol Cell Biol. 2019 Mar 6;20(3):137–55.

24. Yang L, Yang C, Thomes PG, Kharbanda KK, Casey CA, McNiven MA, et al. Lipophagy and Alcohol-Induced Fatty Liver. Front Pharmacol. 2019 May 9;10(MAY):1–13.

25. Morita K, Hama Y, Izume T, Tamura N, Ueno T, Yamashita Y, et al. Genome-wide CRISPR screen identifies TMEM41B as a gene required for autophagosome formation. J Cell Biol. 2018 Nov 5;217(11):3817–28.

26. Zhou Z, Xu M-J, Gao B. Hepatocytes: a key cell type for innate immunity. Cell Mol Immunol. 2016 May 21;13(3):301–15.

27. Xu M, Feng D, Wu H, Wang H, Chan Y, Kolls J, et al. Liver is the major source of elevated serum lipocalin-2 levels after bacterial infection or partial hepatectomy: A critical role for IL-6/STAT3. Hepatology. 2015 Feb 20;61(2):692–702.

28. Schrem H, Klempnauer J, Borlak J. Liver-Enriched Transcription Factors in Liver Function and Development. Part II: the C/EBPs and D Site-Binding Protein in Cell Cycle Control, Carcinogenesis, Circadian Gene Regulation, Liver Regeneration, Apoptosis, and Liver-Specific Gene Regulation. Pharmacol Rev. 2004 Jun;56(2):291–330.

29. Holers VM. Complement and Its Receptors: New Insights into Human Disease. Annu Rev Immunol. 2014 Mar 21;32(1):433–59.

30. Endo Y, Nakazawa N, Iwaki D, Takahashi M, Matsushita M, Fujita T. Interactions of Ficolin and Mannose-Binding Lectin with Fibrinogen/Fibrin Augment the Lectin Complement Pathway. J Innate Immun. 2010;2(1):33–42.

31. Armstrong PB. Proteases and protease inhibitors: a balance of activities in host–pathogen interaction. Immunobiology. 2006 Jun;211(4):263–81.

32. Chang B, Xu M, Zhou Z, Cai Y, Li M, Wang W, et al. Short- or long-term high-fat diet feeding plus acute ethanol binge synergistically induce acute liver injury in mice: An important role for CXCL1. Hepatology. 2015 Oct 3;62(4):1070–85.

33. Krenkel O, Tacke F. Liver macrophages in tissue homeostasis and disease. Nat Rev Immunol. 2017 May 20;17(5):306–21.

34. De Kleer I, Willems F, Lambrecht B, Goriely S. Ontogeny of Myeloid Cells. Front Immunol. 2014 Sep 3;5(AUG):1–11.

35. Gomez Perdiguero E, Klapproth K, Schulz C, Busch K, Azzoni E, Crozet L, et al. Tissue-resident macrophages originate from yolk-sac-derived erythro-myeloid progenitors. Nature. 2015 Feb 26;518(7540):547–51.

36. Guillot A, Tacke F. Liver Macrophages: Old Dogmas and New Insights. Hepatol Commun. 2019 Jun 22;3(6):730–43.

37. Reynolds G, Haniffa M. Human and Mouse Mononuclear Phagocyte Networks: A Tale of Two Species? Front Immunol. 2015 Jun 25;6(JUN):1–15.

38. Toll-like N. Regulation of endosomal TLRs Kupffer cells : finding their niche. Nat Rev Immunol. 2019;19(11):660–1.

39. Harty MW, Muratore CS, Papa EF, Gart MS, Ramm GA, Gregory SH, et al. Neutrophil Depletion Blocks Early Collagen Degradation in Repairing Cholestatic Rat Livers. Am J Pathol. 2010 Mar;176(3):1271–81.

40. Pellicoro A, Ramachandran P, Iredale JP, Fallowfield JA. Liver fibrosis and repair: immune regulation of wound healing in a solid organ. Nat Rev Immunol. 2014 Mar 25;14(3):181–94.

41. Wree A, McGeough MD, Inzaugarat ME, Eguchi A, Schuster S, Johnson CD, et al. NLRP3 inflammasome driven liver injury and fibrosis: Roles of IL-17 and TNF in mice. Hepatology. 2018 Feb 28;67(2):736–49.

42. Duffield JS, Forbes SJ, Constandinou CM, Clay S, Partolina M, Vuthoori S, et al. Selective depletion of macrophages reveals distinct, opposing roles during liver injury and repair. J Clin Invest. 2005 Jan 3;115(1):56–65.

43. Hernandez-Gea V, Friedman SL. Pathogenesis of Liver Fibrosis. Annu Rev Pathol Mech Dis. 2011 Feb 28;6(1):425–56.

44. Bandyopadhyay K, Marrero I, Kumar V. NKT cell subsets as key participants in liver physiology and pathology. Cell Mol Immunol. 2016 May 14;13(3):337–46.

45. Bertoletti A. T cell fitness in the liver: How can T cells keep it up? J Hepatol. 2016 Jun;64(6):1208–10.

46. Zisser A, Ipsen DH, Tveden-Nyborg P. Hepatic Stellate Cell Activation and Inactivation in NASH-Fibrosis—Roles as Putative Treatment Targets? Biomedicines. 2021 Mar 31;9(4):365.

47. Wake K. “Sternzellen” in the liver: Perisinusoidal cells with special reference to storage of vitamin A. Am J Anat. 1971 Dec 3;132(4):429–61.

48. Rohn F, Kordes C, Buschmann T, Reichert D, Wammers M, Poschmann G, et al. Impaired integrin α 5 /β 1 -mediated hepatocyte growth factor release by stellate cells of the aged liver. Aging Cell. 2020 Apr 11;19(4):1–17.

49. Trivedi P, Wang S, Friedman SL. The Power of Plasticity—Metabolic Regulation of Hepatic Stellate Cells. Cell Metab. 2021 Feb;33(2):242–57.

50. Saeed A, Dullaart R, Schreuder T, Blokzijl H, Faber K. Disturbed Vitamin A Metabolism in Non-Alcoholic Fatty Liver Disease (NAFLD). Nutrients. 2017 Dec 29;10(1):29.

51. Shirakami Y, Lee S-A, Clugston RD, Blaner WS. Hepatic metabolism of retinoids and disease associations. Biochim Biophys Acta - Mol Cell Biol Lipids. 2012 Jan;1821(1):124–36.

52. D'Ambrosio DN, Clugston RD, Blaner WS. Vitamin A Metabolism: An Update. Nutrients. 2011 Jan 12;3(1):63–103.

53. Blomhoff R, Holte K, Næss L, Berg T. Newly administered [3H]retinol is transferred from hepatocytes to stellate cells in liver for storage. Exp Cell Res. 1984 Jan;150(1):186–93.

54. Blomhoff R, Helgerud P, Rasmussen M. In vivo uptake of chylomicron [3H]retinyl ester by rat liver: Evidence for retinol transfer from parenchymal to nonparenchymal cells. Proc Natl Acad Sci U S A. 1982;7326–7330(December):7326–30.

55. Gajendiran P, Vega LI, Itoh K, Sesaki H, Vakili MR, Lavasanifar A, et al. Elevated mitochondrial activity distinguishes fibrogenic hepatic stellate cells and sensitizes for selective inhibition by mitotropic doxorubicin. J Cell Mol Med. 2018 Apr 4;22(4):2210–9.

56. Molenaar MR, Vaandrager AB, Helms JB. Some Lipid Droplets Are More Equal Than Others: Different Metabolic Lipid Droplet Pools in Hepatic Stellate Cells. Lipid Insights. 2017 Jan 1;10:117863531774728.

57. Tuohetahuntila M, Molenaar MR, Spee B, Brouwers JF, Wubbolts R, Houweling M, et al. Lysosome-mediated degradation of a distinct pool of lipid droplets during hepatic stellate cell activation. J Biol Chem. 2017 Jul;292(30):12436–48.

58. Hou W, Syn W-K. Role of Metabolism in Hepatic Stellate Cell Activation and Fibrogenesis. Front Cell Dev Biol. 2018 Nov 12;6(NOV):1–10.

59. Lee TF, Mak KM, Rackovsky O, Lin Y, Kwong AJ, Loke JC, et al. Downregulation of hepatic stellate cell activation by retinol and palmitate mediated by adipose differentiation-related protein (ADRP). J Cell Physiol. 2010 Jun 8;223(3):648–57.

60. Friedman SL. Mechanisms of Hepatic Fibrogenesis. Gastroenterology. 2008 May;134(6):1655–69.

61. Davies PF. Flow-mediated endothelial mechanotransduction. Physiol Rev. 1995 Jul 1;75(3):519–60.

62. DeLeve LD. Liver sinusoidal endothelial cells in hepatic fibrosis. Hepatology. 2015 May 23;61(5):1740–6.

63. DeLeve LD. Liver sinusoidal endothelial cells and liver regeneration. J Clin Invest. 2013 May 1;123(5):1861–6.

64. Poisson J, Lemoinne S, Boulanger C, Durand F, Moreau R, Valla D, et al. Liver sinusoidal endothelial cells: Physiology and role in liver diseases. J Hepatol. 2017

Jan;66(1):212–27.

65. Sørensen KK, McCourt P, Berg T, Crossley C, Couteur D Le, Wake K, et al. The scavenger endothelial cell: a new player in homeostasis and immunity. Am J Physiol Integr Comp Physiol. 2012 Dec 15;303(12):R1217–30.

66. Böttcher JP, Schanz O, Garbers C, Zaremba A, Hegenbarth S, Kurts C, et al. IL-6 trans-Signaling-Dependent Rapid Development of Cytotoxic CD8+ T Cell Function. Cell Rep. 2014 Sep;8(5):1318–27.

67. Lohse A, Knolle P, Bilo K, Uhrig A, Waldmann C, Ibe M, et al. Antigen-presenting function and B7 expression of murine sinusoidal endothelial cells and Kupffer cells. Gastroenterology. 1996 Apr;110(4):1175–81.

68. Eslam M, Newsome PN, Sarin SK, Anstee QM, Targher G, Romero-Gomez M, et al. A new definition for metabolic dysfunction-associated fatty liver disease: An international expert consensus statement. J Hepatol. 2020 Jul;73(1):202–9.

69. Marchesini G, Day CP, Dufour JF, Canbay A, Nobili V, Ratziu V, et al. EASL–EASD–EASO Clinical Practice Guidelines for the management of non-alcoholic fatty liver disease. J Hepatol. 2016 Jun;64(6):1388–402.

70. Estes C, Anstee QM, Arias-Loste MT, Bantel H, Bellentani S, Caballeria J, et al. Modeling NAFLD disease burden in China, France, Germany, Italy, Japan, Spain, United Kingdom, and United States for the period 2016–2030. J Hepatol. 2018 Oct;69(4):896–904.

71. Kanwar P, Kowdley K V. The Metabolic Syndrome and Its Influence on Nonalcoholic Steatohepatitis. Clin Liver Dis. 2016 May;20(2):225–43.

72. Simoes ICM, Janikiewicz J, Bauer J, Karkucinska-Wieckowska A, Kalinowski P, Dobrzyń A, et al. Fat and Sugar—A Dangerous Duet. A Comparative Review on Metabolic Remodeling in Rodent Models of Nonalcoholic Fatty Liver Disease. Nutrients. 2019 Nov 24;11(12):2871.

73. Friedman SL. Liver fibrosis – from bench to bedside. J Hepatol. 2003 Jan;38:38–53.

74. Afratis NA, Selman M, Pardo A, Sagi I. Emerging insights into the role of matrix metalloproteases as therapeutic targets in fibrosis. Matrix Biol. 2018 Aug;68–69(1):167–79.

75. Roehlen N, Crouchet E, Baumert TF. Liver Fibrosis: Mechanistic Concepts and Therapeutic Perspectives. Cells. 2020 Apr 3;9(4):875.

76. Kisseleva T, Brenner D. Molecular and cellular mechanisms of liver fibrosis and its

regression. Nat Rev Gastroenterol Hepatol. 2021 Mar 30;18(3):151–66.

77. Sung H, Ferlay J, Siegel RL, Laversanne M, Soerjomataram I, Jemal A, et al. Global Cancer Statistics 2020: GLOBOCAN Estimates of Incidence and Mortality Worldwide for 36 Cancers in 185 Countries. CA Cancer J Clin. 2021 May 4;71(3):209–49.

78. Ferlay J, Colombet M, Soerjomataram I, Parkin DM, Piñeros M, Znaor A, et al. Cancer statistics for the year 2020: An overview. Int J Cancer. 2021 Aug 15;149(4):778–89.

79. Agarwal R, Narayan J, Bhattacharyya A, Saraswat M, Tomar AK. Gene expression profiling, pathway analysis and subtype classification reveal molecular heterogeneity in hepatocellular carcinoma and suggest subtype specific therapeutic targets. Cancer Genet. 2017 Oct;216–217:37–51.

80. Younossi ZM, Koenig AB, Abdelatif D, Fazel Y, Henry L, Wymer M. Global epidemiology of nonalcoholic fatty liver disease—Meta-analytic assessment of prevalence, incidence, and outcomes. Hepatology. 2016 Jul 22;64(1):73–84.

81. Michelotti GA, Machado M V., Diehl AM. NAFLD, NASH and liver cancer. Nat Rev Gastroenterol Hepatol. 2013 Nov 1;10(11):656–65.

82. Ipsen DH, Lykkesfeldt J, Tveden-Nyborg P. Molecular mechanisms of hepatic lipid accumulation in non-alcoholic fatty liver disease. Cell Mol Life Sci. 2018 Sep 23;75(18):3313–27.

83. Mayo R, Crespo J, Martínez-Arranz I, Banales JM, Arias M, Mincholé I, et al. Metabolomic-based noninvasive serum test to diagnose nonalcoholic steatohepatitis: Results from discovery and validation cohorts. Hepatol Commun. 2018 Jul 4;2(7):807–20.

84. Marchisello S, Di Pino A, Scicali R, Urbano F, Piro S, Purrello F, et al. Pathophysiological, Molecular and Therapeutic Issues of Nonalcoholic Fatty Liver Disease: An Overview. Int J Mol Sci. 2019 Apr 20;20(8):1948.

85. Khomich O, Ivanov A V., Bartosch B. Metabolic Hallmarks of Hepatic Stellate Cells in Liver Fibrosis. Cells. 2019 Dec 20;9(1):24.

86. Wobser H, Dorn C, Weiss TS, Amann T, Bollheimer C, Büttner R, et al. Lipid accumulation in hepatocytes induces fibrogenic activation of hepatic stellate cells. Cell Res. 2009 Aug 23;19(8):996–1005.

87. Botchlett R, Woo S-L, Liu M, Pei Y, Guo X, Li H, et al. Nutritional approaches for managing obesity-associated metabolic diseases. J Endocrinol. 2017

Jun;233(3):R145–71.

88. Malehmir M, Pfister D, Gallage S, Szydlowska M, Inverso D, Kotsiliti E, et al. Platelet GPIbα is a mediator and potential interventional target for NASH and subsequent liver cancer. Nat Med. 2019 Apr 1;25(4):641–55.

89. Sepanlou SG, Safiri S, Bisignano C, Ikuta KS, Merat S, Saberifiroozi M, et al. The global, regional, and national burden of cirrhosis by cause in 195 countries and territories, 1990–2017: a systematic analysis for the Global Burden of Disease Study 2017. Lancet Gastroenterol Hepatol. 2020 Mar;5(3):245–66.

90. Ibrahim SH, Hirsova P, Gores GJ. Non-alcoholic steatohepatitis pathogenesis: sublethal hepatocyte injury as a driver of liver inflammation. Gut. 2018 May;67(5):963–72.

91. Huang DQ, El-Serag HB, Loomba R. Global epidemiology of NAFLD-related HCC: trends, predictions, risk factors and prevention. Nat Rev Gastroenterol Hepatol. 2021 Apr 21;18(4):223–38.

92. Yamamura S, Eslam M, Kawaguchi T, Tsutsumi T, Nakano D, Yoshinaga S, et al. MAFLD identifies patients with significant hepatic fibrosis better than NAFLD. Liver Int. 2020 Dec 30;40(12):3018–30.

93. Sharma B, John S. Hepatic Cirrhosis. StatPearls. 2024.

94. Gomes RN, Manuel F, Nascimento DS. The bright side of fibroblasts: molecular signature and regenerative cues in major organs. npj Regen Med. 2021 Aug 10;6(1):43.

95. Rockey DC, Friedman SL. Fibrosis Regression After Eradication of Hepatitis C Virus: From Bench to Bedside. Gastroenterology. 2021 Apr;160(5):1502-1520.e1.

96. Iredale JP, Pellicoro A, Fallowfield JA. Liver Fibrosis: Understanding the Dynamics of Bidirectional Wound Repair to Inform the Design of Markers and Therapies. Dig Dis. 2017;35(4):310–3.

97. Ellis EL, Mann DA. Clinical evidence for the regression of liver fibrosis. J Hepatol. 2012 May;56(5):1171–80.

98. Dufour J-F. Reversibility of Hepatic Fibrosis in Autoimmune Hepatitis. Ann Intern Med. 1997 Dec 1;127(11):981.

99. Rockey DC. Translating an Understanding of the Pathogenesis of Hepatic Fibrosis to Novel Therapies. Clin Gastroenterol Hepatol. 2013 Mar;11(3):224-231.e5.

100. Galle PR, Forner A, Llovet JM, Mazzaferro V, Piscaglia F, Raoul J-L, et al. EASL

Clinical Practice Guidelines: Management of hepatocellular carcinoma. J Hepatol. 2018 Jul;69(1):182–236.

101. Trinchet J, Bourcier V, Chaffaut C, Ait Ahmed M, Allam S, Marcellin P, et al. Complications and competing risks of death in compensated viral cirrhosis (ANRS CO12 CirVir prospective cohort). Hepatology. 2015 Sep 20;62(3):737–50.

102. Llovet JM, Willoughby CE, Singal AG, Greten TF, Heikenwälder M, El-Serag HB, et al. Nonalcoholic steatohepatitis-related hepatocellular carcinoma: pathogenesis and treatment. Nat Rev Gastroenterol Hepatol. 2023 Aug 17;20(8):487–503.

103. Singal AG, Kanwal F, Llovet JM. Global trends in hepatocellular carcinoma epidemiology: implications for screening, prevention and therapy. Nat Rev Clin Oncol. 2023 Dec 26;20(12):864–84.

104. Murray CJL, Aravkin AY, Zheng P, Abbafati C, Abbas KM, Abbasi-Kangevari M, et al. Global burden of 87 risk factors in 204 countries and territories, 1990–2019: a systematic analysis for the Global Burden of Disease Study 2019. Lancet. 2020 Oct;396(10258):1223–49.

105. Okunogbe A, Nugent R, Spencer G, Powis J, Ralston J, Wilding J. Economic impacts of overweight and obesity: current and future estimates for 161 countries. BMJ Glob Heal. 2022 Sep 20;7(9):e009773.

106. Zucman-Rossi J, Villanueva A, Nault J-C, Llovet JM. Genetic Landscape and Biomarkers of Hepatocellular Carcinoma. Gastroenterology. 2015 Oct;149(5):1226-1239.e4.

107. Akinyemiju T, Abera S, Ahmed M, Alam N, Alemayohu MA, Allen C, et al. The Burden of Primary Liver Cancer and Underlying Etiologies From 1990 to 2015 at the Global, Regional, and National Level. JAMA Oncol. 2017 Dec 1;3(12):1683.

108. Wang J, Chenivesse X, Henglein B, Bréchot C. Hepatitis B virus integration in a cyclin A gene in a hepatocellular carcinoma. Nature. 1990 Feb;343(6258):555–7.

109. Chang M-H, You S-L, Chen C-J, Liu C-J, Lai M-W, Wu T-C, et al. Long-term Effects of Hepatitis B Immunization of Infants in Preventing Liver Cancer. Gastroenterology. 2016 Sep;151(3):472-480.e1.

110. Kanwal F, Kramer J, Asch SM, Chayanupatkul M, Cao Y, El-Serag HB. Risk of Hepatocellular Cancer in HCV Patients Treated With Direct-Acting Antiviral Agents. Gastroenterology. 2017 Oct;153(4):996-1005.e1.

111. Ioannou GN, Beste LA, Green PK, Singal AG, Tapper EB, Waljee AK, et al. Increased Risk for Hepatocellular Carcinoma Persists Up to 10 Years After HCV Eradication

in Patients With Baseline Cirrhosis or High FIB-4 Scores. Gastroenterology. 2019 Nov;157(5):1264-1278.e4.

112. Llovet JM, Villanueva A. Effect of HCV clearance with direct-acting antiviral agents on HCC. Nat Rev Gastroenterol Hepatol. 2016 Oct 1;13(10):561–2.

113. Puigvehí M, Moctezuma-Velázquez C, Villanueva A, Llovet JM. The oncogenic role of hepatitis delta virus in hepatocellular carcinoma. JHEP Reports. 2019 Aug;1(2):120–30.

114. Lin C-W, Lin C-C, Mo L-R, Chang C-Y, Perng D-S, Hsu C-C, et al. Heavy alcohol consumption increases the incidence of hepatocellular carcinoma in hepatitis B virus-related cirrhosis. J Hepatol. 2013 Apr;58(4):730–5.

115. Jepsen P, Ott P, Andersen PK, Sørensen HT, Vilstrup H. Risk for Hepatocellular Carcinoma in Patients With Alcoholic Cirrhosis. Ann Intern Med. 2012 Jun 19;156(12):841.

116. Estes C, Razavi H, Loomba R, Younossi Z, Sanyal AJ. Modeling the epidemic of nonalcoholic fatty liver disease demonstrates an exponential increase in burden of disease. Hepatology. 2018 Jan 1;67(1):123–33.

117. Welzel TM, Graubard BI, Quraishi S, Zeuzem S, Davila JA, El-Serag HB, et al. Population-Attributable Fractions of Risk Factors for Hepatocellular Carcinoma in the United States. Am J Gastroenterol. 2013 Aug;108(8):1314–21.

118. Kanwal F, Kramer JR, Mapakshi S, Natarajan Y, Chayanupatkul M, Richardson PA, et al. Risk of Hepatocellular Cancer in Patients With Non-Alcoholic Fatty Liver Disease. Gastroenterology. 2018 Dec;155(6):1828-1837.e2.

119. Mittal S, El-Serag HB, Sada YH, Kanwal F, Duan Z, Temple S, et al. Hepatocellular Carcinoma in the Absence of Cirrhosis in United States Veterans Is Associated With Nonalcoholic Fatty Liver Disease. Clin Gastroenterol Hepatol. 2016 Jan;14(1):124-131.e1.

120. Rich NE, Yopp AC, Singal AG, Murphy CC. Hepatocellular Carcinoma Incidence Is Decreasing Among Younger Adults in the United States. Clin Gastroenterol Hepatol. 2020 Jan;18(1):242-248.e5.

121. Bray F, Ferlay J, Soerjomataram I, Siegel RL, Torre LA, Jemal A. Global cancer statistics 2018: GLOBOCAN estimates of incidence and mortality worldwide for 36 cancers in 185 countries. CA Cancer J Clin. 2018 Nov 12;68(6):394–424.

122. Rich NE, Hester C, Odewole M, Murphy CC, Parikh ND, Marrero JA, et al. Racial and Ethnic Differences in Presentation and Outcomes of Hepatocellular

Carcinoma. Clin Gastroenterol Hepatol. 2019 Feb;17(3):551-559.e1.

123. Lee Y-CA, Cohet C, Yang Y-C, Stayner L, Hashibe M, Straif K. Meta-analysis of epidemiologic studies on cigarette smoking and liver cancer. Int J Epidemiol. 2009 Dec;38(6):1497–511.

124. Bravi F, Bosetti C, Tavani A, Gallus S, La Vecchia C. Coffee Reduces Risk for Hepatocellular Carcinoma: An Updated Meta-analysis. Clin Gastroenterol Hepatol. 2013 Nov;11(11):1413-1421.e1.

125. Simon TG, Duberg A-S, Aleman S, Chung RT, Chan AT, Ludvigsson JF. Association of Aspirin with Hepatocellular Carcinoma and Liver-Related Mortality. N Engl J Med. 2020 Mar 12;382(11):1018–28.

126. Singal AG, Lampertico P, Nahon P. Epidemiology and surveillance for hepatocellular carcinoma: New trends. J Hepatol. 2020 Feb;72(2):250–61.

127. Papatheodoridis G, Dalekos G, Sypsa V, Yurdaydin C, Buti M, Goulis J, et al. PAGE-B predicts the risk of developing hepatocellular carcinoma in Caucasians with chronic hepatitis B on 5-year antiviral therapy. J Hepatol. 2016 Apr;64(4):800–6.

128. Marrero JA, Kulik LM, Sirlin CB, Zhu AX, Finn RS, Abecassis MM, et al. Diagnosis, Staging, and Management of Hepatocellular Carcinoma: 2018 Practice Guidance by the American Association for the Study of Liver Diseases. Clin Liver Dis. 2019 Jan 21;13(1):1–1.

129. van der Pol CB, Lim CS, Sirlin CB, McGrath TA, Salameh J-P, Bashir MR, et al. Accuracy of the Liver Imaging Reporting and Data System in Computed Tomography and Magnetic Resonance Image Analysis of Hepatocellular Carcinoma or Overall Malignancy—A Systematic Review. Gastroenterology. 2019 Mar;156(4):976–86.

130. Papatheodoridis G V., Chan HL-Y, Hansen BE, Janssen HLA, Lampertico P. Risk of hepatocellular carcinoma in chronic hepatitis B: Assessment and modification with current antiviral therapy. J Hepatol. 2015 Apr;62(4):956–67.

131. Chang M-H, Chen C-J, Lai M-S, Hsu H-M, Wu T-C, Kong M-S, et al. Universal Hepatitis B Vaccination in Taiwan and the Incidence of Hepatocellular Carcinoma in Children. N Engl J Med. 1997 Jun 26;336(26):1855–9.

132. Singh S, Singh PP, Singh AG, Murad MH, Sanchez W. Statins Are Associated With a Reduced Risk of Hepatocellular Cancer: A Systematic Review and Meta-analysis. Gastroenterology. 2013 Feb;144(2):323–32.

133. Kennedy OJ, Roderick P, Buchanan R, Fallowfield JA, Hayes PC, Parkes J. Coffee,

including caffeinated and decaffeinated coffee, and the risk of hepatocellular carcinoma: a systematic review and dose–response meta-analysis. BMJ Open. 2017 May;7(5):e013739.

134. Llovet JM, Kelley RK, Villanueva A, Singal AG, Pikarsky E, Roayaie S, et al. Hepatocellular carcinoma. Nat Rev Dis Prim. 2021 Jan 21;7(1):6.

135. Schulze K, Imbeaud S, Letouzé E, Alexandrov LB, Calderaro J, Rebouissou S, et al. Exome sequencing of hepatocellular carcinomas identifies new mutational signatures and potential therapeutic targets. Nat Genet. 2015 May 30;47(5):505–11.

136. Llovet JM, Montal R, Sia D, Finn RS. Molecular therapies and precision medicine for hepatocellular carcinoma. Nat Rev Clin Oncol. 2018 Oct 30;15(10):599–616.

137. Hyman DM, Taylor BS, Baselga J. Implementing Genome-Driven Oncology. Cell. 2017 Feb;168(4):584–99.

138. Anstee QM, Reeves HL, Kotsiliti E, Govaere O, Heikenwalder M. From NASH to HCC: current concepts and future challenges. Nat Rev Gastroenterol Hepatol. 2019 Jul 26;16(7):411–28.

139. Friedman SL, Neuschwander-Tetri BA, Rinella M, Sanyal AJ. Mechanisms of NAFLD development and therapeutic strategies. Nat Med. 2018 Jul 2;24(7):908–22.

140. Sia D, Villanueva A, Friedman SL, Llovet JM. Liver Cancer Cell of Origin, Molecular Class, and Effects on Patient Prognosis. Gastroenterology. 2017 Mar;152(4):745–61.

141. Pikarsky E. Neighbourhood deaths cause a switch in cancer subtype. Nature. 2018 Oct 12;562(7725):45–6.

142. Seehawer M, Heinzmann F, D'Artista L, Harbig J, Roux P-F, Hoenicke L, et al. Necroptosis microenvironment directs lineage commitment in liver cancer. Nature. 2018 Oct 12;562(7725):69–75.

143. Guichard C, Amaddeo G, Imbeaud S, Ladeiro Y, Pelletier L, Maad I Ben, et al. Integrated analysis of somatic mutations and focal copy-number changes identifies key genes and pathways in hepatocellular carcinoma. Nat Genet. 2012 Jun 6;44(6):694–8.

144. Paterlini-Bréchot P, Saigo K, Murakami Y, Chami M, Gozuacik D, Mugnier C, et al. Hepatitis B virus-related insertional mutagenesis occurs frequently in human liver cancers and recurrently targets human telomerase gene. Oncogene. 2003 Jun 19;22(25):3911–6.

145. Nault J-C, Ningarhari M, Rebouissou S, Zucman-Rossi J. The role of telomeres and telomerase in cirrhosis and liver cancer. Nat Rev Gastroenterol Hepatol. 2019 Sep 28;16(9):544–58.

146. Bayard Q, Meunier L, Peneau C, Renault V, Shinde J, Nault J-C, et al. Cyclin A2/E1 activation defines a hepatocellular carcinoma subclass with a rearrangement signature of replication stress. Nat Commun. 2018 Dec 7;9(1):5235.

147. Nault J-C, Datta S, Imbeaud S, Franconi A, Mallet M, Couchy G, et al. Recurrent AAV2-related insertional mutagenesis in human hepatocellular carcinomas. Nat Genet. 2015 Oct 24;47(10):1187–93.

148. Letouzé E, Shinde J, Renault V, Couchy G, Blanc J-F, Tubacher E, et al. Mutational signatures reveal the dynamic interplay of risk factors and cellular processes during liver tumorigenesis. Nat Commun. 2017 Nov 3;8(1):1315.

149. Ng AWT, Poon SL, Huang MN, Lim JQ, Boot A, Yu W, et al. Aristolochic acids and their derivatives are widely implicated in liver cancers in Taiwan and throughout Asia. Sci Transl Med. 2017 Oct 18;9(412).

150. Alexandrov LB, Nik-Zainal S, Wedge DC, Aparicio SAJR, Behjati S, Biankin A V., et al. Signatures of mutational processes in human cancer. Nature. 2013 Aug 22;500(7463):415–21.

151. Zhu AX, Duda DG, Sahani D V., Jain RK. HCC and angiogenesis: possible targets and future directions. Nat Rev Clin Oncol. 2011 May 8;8(5):292–301.

152. Sherwood LM, Parris EE, Folkman J. Tumor Angiogenesis: Therapeutic Implications. N Engl J Med. 1971 Nov 18;285(21):1182–6.

153. Fang J, Zhou H, Zhang C, Shang L, Zhang L, Xu J, et al. A novel vascular pattern promotes metastasis of hepatocellular carcinoma in an epithelial–mesenchymal transition–independent manner. Hepatology. 2015 Aug 22;62(2):452–65.

154. Pang RWC, Joh JW, Johnson PJ, Monden M, Pawlik TM, Poon RTP. Biology of Hepatocellular Carcinoma. Ann Surg Oncol. 2008 Apr;15(4):962–71.

155. Goel S, Duda DG, Xu L, Munn LL, Boucher Y, Fukumura D, et al. Normalization of the Vasculature for Treatment of Cancer and Other Diseases. Physiol Rev. 2011 Jul;91(3):1071–121.

156. Krishna Priya S, Nagare RP, Sneha VS, Sidhanth C, Bindhya S, Manasa P, et al. Tumour angiogenesis—Origin of blood vessels. Int J Cancer. 2016 Aug 15;139(4):729–35.

157. Qian C, Pezzella F. Tumor vasculature: a sally port for inhibiting cancer cell

spreading. Cancer Commun. 2018 Dec 3;38(1):1–3.

158. Coultas L, Chawengsaksophak K, Rossant J. Endothelial cells and VEGF in vascular development. Nature. 2005 Dec 15;438(7070):937–45.

159. Jászai J, Schmidt M. Trends and Challenges in Tumor Anti-Angiogenic Therapies. Cells. 2019 Sep 18;8(9):1102.

160. Carmeliet P, Jain RK. Molecular mechanisms and clinical applications of angiogenesis. Nature. 2011 May 18;473(7347):298–307.

161. Katayama Y, Uchino J, Chihara Y, Tamiya N, Kaneko Y, Yamada T, et al. Tumor Neovascularization and Developments in Therapeutics. Cancers (Basel). 2019 Mar 6;11(3):316.

162. Luo Q, Wang J, Zhao W, Peng Z, Liu X, Li B, et al. Vasculogenic mimicry in carcinogenesis and clinical applications. J Hematol Oncol. 2020 Dec 14;13(1):19.

163. Carmeliet P. Mechanisms of angiogenesis and arteriogenesis. Nat Med. 2000;6(3):389–95.

164. Semela D, Dufour J-F. Angiogenesis and hepatocellular carcinoma. J Hepatol. 2004 Nov;41(5):864–80.

165. Donnem T, Hu J, Ferguson M, Adighibe O, Snell C, Harris AL, et al. Vessel co-option in primary human tumors and metastases: an obstacle to effective anti-angiogenic treatment? Cancer Med. 2013 Aug 8;2(4):427–36.

166. Kuczynski EA, Vermeulen PB, Pezzella F, Kerbel RS, Reynolds AR. Vessel co-option in cancer. Nat Rev Clin Oncol. 2019 Aug 28;16(8):469–93.

167. Frentzas S, Simoneau E, Bridgeman VL, Vermeulen PB, Foo S, Kostaras E, et al. Vessel co-option mediates resistance to anti-angiogenic therapy in liver metastases. Nat Med. 2016 Nov 17;22(11):1294–302.

168. Maniotis AJ, Folberg R, Hess A, Seftor EA, Gardner LMG, Pe'er J, et al. Vascular Channel Formation by Human Melanoma Cells in Vivo and in Vitro: Vasculogenic Mimicry. Am J Pathol. 1999 Sep;155(3):739–52.

169. Yang JP, Liao YD, Mai DM, Xie P, Qiang YY, Zheng LS, et al. Tumor vasculogenic mimicry predicts poor prognosis in cancer patients: a meta-analysis. Angiogenesis. 2016 Apr 22;19(2):191–200.

170. Liu R, Yang K, Meng C, Zhang Z, Xu Y. Vasculogenic mimicry is a marker of poor prognosis in prostate cancer. Cancer Biol Ther. 2012 May 5;13(7):527–33.

171. Delgado-Bellido D, Serrano-Saenz S, Fernández-Cortés M, Oliver FJ. Vasculogenic

mimicry signaling revisited: focus on non-vascular VE-cadherin. Mol Cancer. 2017 Dec 21;16(1):65.

172. Wang W, Lin P, Sun B, Zhang S, Cai W, Han C, et al. Epithelial-Mesenchymal Transition Regulated by EphA2 Contributes to Vasculogenic Mimicry Formation of Head and Neck Squamous Cell Carcinoma. Biomed Res Int. 2014;2014:1–10.

173. Zhang, Jingxin, Lili Qiao, Ning Liang, Jian Xie, Hui Luo, Guodong Deng J, Zhang. Vasculogenic mimicry and tumor metastasis. JBUON. 2016;21(3):533–41.

174. Mao X -g., Xue X -y., Wang L, Zhang X, Yan M, Tu Y -y., et al. CDH5 is specifically activated in glioblastoma stemlike cells and contributes to vasculogenic mimicry induced by hypoxia. Neuro Oncol. 2013 Jul 1;15(7):865–79.

175. Comito G, Calvani M, Giannoni E, Bianchini F, Calorini L, Torre E, et al. HIF-1α stabilization by mitochondrial ROS promotes Met-dependent invasive growth and vasculogenic mimicry in melanoma cells. Free Radic Biol Med. 2011 Aug;51(4):893–904.

176. Schnegg CI, Yang MH, Ghosh SK, Hsu M-Y. Induction of Vasculogenic Mimicry Overrides VEGF-A Silencing and Enriches Stem-like Cancer Cells in Melanoma. Cancer Res. 2015 Apr 15;75(8):1682–90.

177. Camorani S, Crescenzi E, Gramanzini M, Fedele M, Zannetti A, Cerchia L. Aptamer-mediated impairment of EGFR-integrin αvβ3 complex inhibits vasculogenic mimicry and growth of triple-negative breast cancers. Sci Rep. 2017 Apr 20;7(1):46659.

178. Wu S, Yu L, Wang D, Zhou L, Cheng Z, Chai D, et al. Aberrant expression of CD133 in non-small cell lung cancer and its relationship to vasculogenic mimicry. BMC Cancer. 2012 Dec 21;12(1):535.

179. Williamson SC, Metcalf RL, Trapani F, Mohan S, Antonello J, Abbott B, et al. Vasculogenic mimicry in small cell lung cancer. Nat Commun. 2016 Nov 9;7(1):13322.

180. Li W, Zong S, Shi Q, Li H, Xu J, Hou F. Hypoxia-induced vasculogenic mimicry formation in human colorectal cancer cells: Involvement of HIF-1a, Claudin-4, and E-cadherin and Vimentin. Sci Rep. 2016 Nov 21;6(1):37534.

181. Wang H, Huang B, Li BM, Cao KY, Mo CQ, Jiang SJ, et al. ZEB1-mediated vasculogenic mimicry formation associates with epithelial–mesenchymal transition and cancer stem cell phenotypes in prostate cancer. J Cell Mol Med. 2018 Aug 12;22(8):3768–81.

182. Li Y, Wu Z, Yuan J, Sun L, Lin L, Huang N, et al. Long non-coding RNA MALAT1 promotes gastric cancer tumorigenicity and metastasis by regulating vasculogenic mimicry and angiogenesis. Cancer Lett. 2017 Jun;395:31–44.

183. Yang Z, Sun B, Li Y, Zhao X, Zhao X, Gu Q, et al. ZEB2 promotes vasculogenic mimicry by TGF-β1 induced epithelial-to-mesenchymal transition in hepatocellular carcinoma. Exp Mol Pathol. 2015 Jun;98(3):352–9.

184. Yu W, Ding J, He M, Chen Y, Wang R, Han Z, et al. Estrogen receptor β promotes the vasculogenic mimicry (VM) and cell invasion via altering the lncRNA-MALAT1/miR-145-5p/NEDD9 signals in lung cancer. Oncogene. 2019 Feb 24;38(8):1225–38.

185. FOLBERG R, MANIOTIS AJ. Vasculogenic mimicry. APMIS. 2004 Jul 22;112(7–8):508–25.

186. El Hallani S, Boisselier B, Peglion F, Rousseau A, Colin C, Idbaih A, et al. A new alternative mechanism in glioblastoma vascularization: tubular vasculogenic mimicry. Brain. 2010 Apr 1;133(4):973–82.

187. Xiang T, Lin Y-X, Ma W, Zhang H-J, Chen K-M, He G-P, et al. Vasculogenic mimicry formation in EBV-associated epithelial malignancies. Nat Commun. 2018 Nov 27;9(1):5009.

188. Liu Y, Li F, Yang YT, Xu XD, Chen JS, Chen TL, et al. IGFBP2 promotes vasculogenic mimicry formation via regulating CD144 and MMP2 expression in glioma. Oncogene. 2019 Mar 27;38(11):1815–31.

189. Ruf W, Seftor EA, Petrovan RJ, Weiss RM, Gruman LM, Margaryan N V, et al. Differential role of tissue factor pathway inhibitors 1 and 2 in melanoma vasculogenic mimicry. Cancer Res. 2003 Sep 1;63(17):5381–9.

190. Sood AK, Seftor EA, Fletcher MS, Gardner LMG, Heidger PM, Buller RE, et al. Molecular Determinants of Ovarian Cancer Plasticity. Am J Pathol. 2001 Apr;158(4):1279–88.

191. Ge H, Luo H. Overview of advances in vasculogenic mimicry-a potential target for tumor therapy. Cancer Manag Res. 2018;10:2429–37.

192. Nieto MA, Huang RY-J, Jackson RA, Thiery JP. EMT: 2016. Cell. 2016 Jun;166(1):21–45.

193. Wang Y, Sun H, Zhang D, Fan D, Zhang Y, Dong X, et al. TP53INP1 inhibits hypoxia-induced vasculogenic mimicry formation via the ROS/snail signalling axis in breast cancer. J Cell Mol Med. 2018 Jul 14;22(7):3475–88.

194. Sun D, Sun B, Liu T, Zhao X, Che N, Gu Q, et al. Slug promoted vasculogenic mimicry in hepatocellular carcinoma. J Cell Mol Med. 2013 Aug;17(8):1038–47.

195. Zhu Q-Q, Ma C, Wang Q, Song Y, Lv T. The role of TWIST1 in epithelial-mesenchymal transition and cancers. Tumor Biol. 2016 Jan 24;37(1):185–97.

196. Zhang Y, Xu L, Li A, Han X. The roles of ZEB1 in tumorigenic progression and epigenetic modifications. Biomed Pharmacother. 2019 Feb;110(September 2018):400–8.

197. Sun B, Zhang D, Zhang S, Zhang W, Guo H, Zhao X. Hypoxia influences vasculogenic mimicry channel formation and tumor invasion-related protein expression in melanoma. Cancer Lett. 2007 May;249(2):188–97.

198. Cheng R, Wang B, Cai X, Chen Z, Du Q, Zhou L, et al. CD276 Promotes Vasculogenic Mimicry Formation in Hepatocellular Carcinoma via the PI3K/AKT/MMPs Pathway. Onco Targets Ther. 2020 Nov;Volume 13:11485–98.

199. Xu J, Zhang Y, Wang Y, Tao X, Cheng L, Wu S, et al. Correlation of KAI1, CD133 and vasculogenic mimicry with the prediction of metastasis and prognosis in hepatocellular carcinoma. Int J Clin Exp Pathol. 2018;11(7):3638–46.

200. Forner A, Reig M, Bruix J. Hepatocellular carcinoma. Lancet. 2018 Mar;391(10127):1301–14.

201. Saffo S, Taddei TH. Systemic Management for Advanced Hepatocellular Carcinoma: A Review of the Molecular Pathways of Carcinogenesis, Current and Emerging Therapies, and Novel Treatment Strategies. Dig Dis Sci. 2019 Apr 18;64(4):1016–29.

202. Lencioni R, de Baere T, Soulen MC, Rilling WS, Geschwind JH. Lipiodol transarterial chemoembolization for hepatocellular carcinoma: A systematic review of efficacy and safety data. Hepatology. 2016 Jul 7;64(1):106–16.

203. Park J, Chen M, Colombo M, Roberts LR, Schwartz M, Chen P, et al. Global patterns of hepatocellular carcinoma management from diagnosis to death: the BRIDGE Study. Liver Int. 2015 Sep 25;35(9):2155–66.

204. Chen S, Cao Q, Wen W, Wang H. Targeted therapy for hepatocellular carcinoma: Challenges and opportunities. Cancer Lett. 2019 Sep;460(May):1–9.

205. Yang Y, Nagano H, Ota H, Morimoto O, Nakamura M, Wada H, et al. Patterns and clinicopathologic features of extrahepatic recurrence of hepatocellular carcinoma after curative resection. Surgery. 2007 Feb;141(2):196–202.

206. Llovet JM, Villanueva A, Marrero JA, Schwartz M, Meyer T, Galle PR, et al. Trial

Design and Endpoints in Hepatocellular Carcinoma: AASLD Consensus Conference. Hepatology. 2021 Jan 22;73(S1):158–91.

207. Llovet J, Brú C, Bruix J. Prognosis of Hepatocellular Carcinoma: The BCLC Staging Classification. Semin Liver Dis. 1999 Mar 17;19(03):329–38.

208. Heimbach JK, Kulik LM, Finn RS, Sirlin CB, Abecassis MM, Roberts LR, et al. AASLD guidelines for the treatment of hepatocellular carcinoma. Hepatology. 2018 Jan 19;67(1):358–80.

209. Vogel A, Cervantes A, Chau I, Daniele B, Llovet JM, Meyer T, et al. Hepatocellular carcinoma: ESMO Clinical Practice Guidelines for diagnosis, treatment and follow-up. Ann Oncol. 2018 Oct;29:iv238–55.

210. Meyer T, Fox R, Ma YT, Ross PJ, James MW, Sturgess R, et al. Sorafenib in combination with transarterial chemoembolisation in patients with unresectable hepatocellular carcinoma (TACE 2): a randomised placebo-controlled, double-blind, phase 3 trial. Lancet Gastroenterol Hepatol. 2017 Aug;2(8):565–75.

211. Kudo M, Han G, Finn RS, Poon RTP, Blanc J-F, Yan L, et al. Brivanib as adjuvant therapy to transarterial chemoembolization in patients with hepatocellular carcinoma: A randomized phase III trial. Hepatology. 2014 Nov;60(5):1697–707.

212. Okusaka T, Kasugai H, Shioyama Y, Tanaka K, Kudo M, Saisho H, et al. Transarterial chemotherapy alone versus transarterial chemoembolization for hepatocellular carcinoma: A randomized phase III trial. J Hepatol. 2009 Dec;51(6):1030–6.

213. Chau I, Park JO, Ryoo B-Y, Yen C-J, Poon R, Pastorelli D, et al. Alpha-fetoprotein kinetics in patients with hepatocellular carcinoma receiving ramucirumab or placebo: an analysis of the phase 3 REACH study. Br J Cancer. 2018 Jul 3;119(1):19–26.

214. Lammer J, Malagari K, Vogl T, Pilleul F, Denys A, Watkinson A, et al. Prospective Randomized Study of Doxorubicin-Eluting-Bead Embolization in the Treatment of Hepatocellular Carcinoma: Results of the PRECISION V Study. Cardiovasc Intervent Radiol. 2010 Feb 12;33(1):41–52.

215. Varela M, Real MI, Burrel M, Forner A, Sala M, Brunet M, et al. Chemoembolization of hepatocellular carcinoma with drug eluting beads: Efficacy and doxorubicin pharmacokinetics. J Hepatol. 2007 Mar;46(3):474–81.

216. Vincenzi B, Di Maio M, Silletta M, D'Onofrio L, Spoto C, Piccirillo MC, et al. Prognostic Relevance of Objective Response According to EASL Criteria and mRECIST Criteria in Hepatocellular Carcinoma Patients Treated with Loco-Regional Therapies: A Literature-Based Meta-Analysis. Kim SU, editor. PLoS One.

2015 Jul 31;10(7):e0133488.

217. Salem R, Gordon AC, Mouli S, Hickey R, Kallini J, Gabr A, et al. Y90 Radioembolization Significantly Prolongs Time to Progression Compared With Chemoembolization in Patients With Hepatocellular Carcinoma. Gastroenterology. 2016 Dec;151(6):1155-1163.e2.

218. Hilgard P, Hamami M, Fouly A El, Scherag A, Müller S, Ertle J, et al. Radioembolization with yttrium-90 glass microspheres in hepatocellular carcinoma: European experience on safety and long-term survival. Hepatology. 2010 Nov;52(5):1741–9.

219. Salem R, Lewandowski RJ, Mulcahy MF, Riaz A, Ryu RK, Ibrahim S, et al. Radioembolization for Hepatocellular Carcinoma Using Yttrium-90 Microspheres: A Comprehensive Report of Long-term Outcomes. Gastroenterology. 2010 Jan;138(1):52–64.

220. Vilgrain V, Pereira H, Assenat E, Guiu B, Ilonca AD, Pageaux G-P, et al. Efficacy and safety of selective internal radiotherapy with yttrium-90 resin microspheres compared with sorafenib in locally advanced and inoperable hepatocellular carcinoma (SARAH): an open-label randomised controlled phase 3 trial. Lancet Oncol. 2017 Dec;18(12):1624–36.

221. Chow PKH, Gandhi M, Tan S-B, Khin MW, Khasbazar A, Ong J, et al. SIRveNIB: Selective Internal Radiation Therapy Versus Sorafenib in Asia-Pacific Patients With Hepatocellular Carcinoma. J Clin Oncol. 2018 Jul 1;36(19):1913–21.

222. Ricke J, Klümpen HJ, Amthauer H, Bargellini I, Bartenstein P, de Toni EN, et al. Impact of combined selective internal radiation therapy and sorafenib on survival in advanced hepatocellular carcinoma. J Hepatol. 2019 Dec;71(6):1164–74.

223. Attallah AM, Omran MM, Attallah AA, Abdallah SO, Farid K, Darwish H, et al. HCC-ART score, a simple, highly sensitive and specific test for early diagnosis of hepatocellular carcinoma: a large-scale, multicentre study. Br J Cancer. 2013 Sep 27;109(6):1657–65.

224. Hiraoka A, Kumada T, Kariyama K, Toyoda H, Yasuda S, Tsuji K, et al. Simple Scoring System for Predicting TACE Unsuitable among Intermediate-Stage Hepatocellular Carcinoma Patients in the Multiple Systemic Treatment Era. Oncology. 2022;100(2):65–73.

225. Singal AG, Llovet JM, Yarchoan M, Mehta N, Heimbach JK, Dawson LA, et al. AASLD Practice Guidance on prevention, diagnosis, and treatment of hepatocellular carcinoma. Hepatology. 2023 May 22;

226. Kudo M, Han K-H, Ye S-L, Zhou J, Huang Y-H, Lin S-M, et al. A Changing Paradigm for the Treatment of Intermediate-Stage Hepatocellular Carcinoma: Asia-Pacific Primary Liver Cancer Expert Consensus Statements. Liver Cancer. 2020;9(3):245–60.

227. Zhang S, Zhong B-Y, Zhang L, Wang W-S, Ni C-F. Transarterial chemoembolization failure/refractoriness: A scientific concept or pseudo-proposition. World J Gastrointest Surg. 2022 Jun 27;14(6):528–37.

228. Finn RS, Qin S, Ikeda M, Galle PR, Ducreux M, Kim T-Y, et al. Atezolizumab plus Bevacizumab in Unresectable Hepatocellular Carcinoma. N Engl J Med. 2020 May 14;382(20):1894–905.

229. Abou-Alfa GK, Lau G, Kudo M, Chan SL, Kelley RK, Furuse J, et al. Tremelimumab plus Durvalumab in Unresectable Hepatocellular Carcinoma. NEJM Evid. 2022 Jul 26;1(8).

230. Kudo M, Finn RS, Qin S, Han K-H, Ikeda K, Piscaglia F, et al. Lenvatinib versus sorafenib in first-line treatment of patients with unresectable hepatocellular carcinoma: a randomised phase 3 non-inferiority trial. Lancet. 2018 Mar;391(10126):1163–73.

231. Llovet JM, Ricci S, Mazzaferro V, Hilgard P, Gane E, Blanc J-F, et al. Sorafenib in Advanced Hepatocellular Carcinoma. N Engl J Med. 2008 Jul 24;359(4):378–90.

232. Bruix J, Cheng A-L, Meinhardt G, Nakajima K, De Sanctis Y, Llovet J. Prognostic factors and predictors of sorafenib benefit in patients with hepatocellular carcinoma: Analysis of two phase III studies. J Hepatol. 2017 Nov;67(5):999–1008.

233. Bruix J, Qin S, Merle P, Granito A, Huang Y-H, Bodoky G, et al. Regorafenib for patients with hepatocellular carcinoma who progressed on sorafenib treatment (RESORCE): a randomised, double-blind, placebo-controlled, phase 3 trial. Lancet. 2017 Jan;389(10064):56–66.

234. Abou-Alfa GK, Meyer T, Cheng A-L, El-Khoueiry AB, Rimassa L, Ryoo B-Y, et al. Cabozantinib in Patients with Advanced and Progressing Hepatocellular Carcinoma. N Engl J Med. 2018 Jul 5;379(1):54–63.

235. Zhu AX, Kang Y-K, Yen C-J, Finn RS, Galle PR, Llovet JM, et al. Ramucirumab after sorafenib in patients with advanced hepatocellular carcinoma and increased α-fetoprotein concentrations (REACH-2): a randomised, double-blind, placebo-controlled, phase 3 trial. Lancet Oncol. 2019 Feb;20(2):282–96.

236. Finn RS, Qin S, Ikeda M, Galle PR, Ducreux M, Kim T-Y, et al. IMbrave150: Updated overall survival (OS) data from a global, randomized, open-label phase III study of

atezolizumab (atezo) + bevacizumab (bev) versus sorafenib (sor) in patients (pts) with unresectable hepatocellular carcinoma (HCC). J Clin Oncol. 2021 Jan 20;39(3_suppl):267–267.

237. Kelley RK, Sangro B, Harris WP, Ikeda M, Okusaka T, Kang Y-K, et al. Efficacy, tolerability, and biologic activity of a novel regimen of tremelimumab (T) in combination with durvalumab (D) for patients (pts) with advanced hepatocellular carcinoma (aHCC). J Clin Oncol. 2020 May 20;38(15_suppl):4508–4508.

238. Treps L, Faure S, Clere N. Vasculogenic mimicry, a complex and devious process favoring tumorigenesis – Interest in making it a therapeutic target. Pharmacol Ther. 2021 Jul;223:107805.

239. Zheng N, Zhang S, Wu W, Zhang N, Wang J. Regulatory mechanisms and therapeutic targeting of vasculogenic mimicry in hepatocellular carcinoma. Pharmacol Res. 2021 Apr;166(February):105507.

240. Chen Q, Lin W, Yin Z, Zou Y, Liang S, Ruan S, et al. Melittin Inhibits Hypoxia-Induced Vasculogenic Mimicry Formation and Epithelial-Mesenchymal Transition through Suppression of HIF-1 <math id="M1"> <mrow> <mtext mathvariant="bold">α</mtext> </mrow> </math> /Akt Pathway in Liver Cancer. Evidence-Based Complement Altern Med. 2019 Apr 1;2019:1–10.

241. Zang M, Hu L, Zhang B, Zhu Z, Li J, Zhu Z, et al. Luteolin suppresses angiogenesis and vasculogenic mimicry formation through inhibiting Notch1-VEGF signaling in gastric cancer. Biochem Biophys Res Commun. 2017 Aug;490(3):913–9.

242. Jue C, Min Z, Zhisheng Z, Lin C, Yayun Q, Xuanyi W, et al. COE inhibits vasculogenic mimicry in hepatocellular carcinoma via suppressing Notch1 signaling. J Ethnopharmacol. 2017 Aug;208(November 2016):165–73.

243. Gupta PB, Onder TT, Jiang G, Tao K, Kuperwasser C, Weinberg RA, et al. Identification of Selective Inhibitors of Cancer Stem Cells by High-Throughput Screening. Cell. 2009 Aug;138(4):645–59.

244. Xiao T, Zhong W, Zhao J, Qian B, Liu H, Chen S, et al. Polyphyllin I suppresses the formation of vasculogenic mimicry via Twist1/VE-cadherin pathway. Cell Death Dis. 2018 Sep 5;9(9):906.

245. Moore MJ. From Birth to Death: The Complex Lives of Eukaryotic mRNAs. Science (80-). 2005 Sep 2;309(5740):1514–8.

246. McManus J, Cheng Z, Vogel C. Next-generation analysis of gene expression regulation – comparing the roles of synthesis and degradation. Mol Biosyst. 2015;11(10):2680–9.

247. Schwanhäusser B, Busse D, Li N, Dittmar G, Schuchhardt J, Wolf J, et al. Global quantification of mammalian gene expression control. Nature. 2011 May 19;473(7347):337–42.

248. Hellen CUT. Translation Termination and Ribosome Recycling in Eukaryotes. Cold Spring Harb Perspect Biol. 2018 Oct;10(10):a032656.

249. Halbeisen RE, Galgano A, Scherrer T, Gerber AP. Post-transcriptional gene regulation: From genome-wide studies to principles. Cell Mol Life Sci. 2008 Mar 26;65(5):798.

250. Parker R, Song H. The enzymes and control of eukaryotic mRNA turnover. Nat Struct Mol Biol. 2004 Feb;11(2):121–7.

251. Fernández-Miranda G, Méndez R. The CPEB-family of proteins, translational control in senescence and cancer. Ageing Res Rev. 2012 Sep;11(4):460–72.

252. Ruggero D, Shimamura A. Marrow failure: a window into ribosome biology. Blood. 2014 Oct 30;124(18):2784–92.

253. Shi Z, Fujii K, Kovary KM, Genuth NR, Röst HL, Teruel MN, et al. Heterogeneous Ribosomes Preferentially Translate Distinct Subpools of mRNAs Genome-wide. Mol Cell. 2017 Jul;67(1):71-83.e7.

254. Huggins HP, Keiper BD. Regulation of Germ Cell mRNPs by eIF4E:4EIP Complexes: Multiple Mechanisms, One Goal. Front Cell Dev Biol. 2020 Jul 7;8.

255. Hake LE, Richter JD. CPEB is a specificity factor that mediates cytoplasmic polyadenylation during Xenopus oocyte maturation. Cell. 1994 Nov;79(4):617–27.

256. Drisaldi B, Colnaghi L, Fioriti L, Rao N, Myers C, Snyder AM, et al. SUMOylation Is an Inhibitory Constraint that Regulates the Prion-like Aggregation and Activity of CPEB3. Cell Rep. 2015 Jun;11(11):1694–702.

257. Mendez R, Murthy KGK, Ryan K, Manley JL, Richter JD. Phosphorylation of CPEB by Eg2 Mediates the Recruitment of CPSF into an Active Cytoplasmic Polyadenylation Complex. Mol Cell. 2000 Nov;6(5):1253–9.

258. Theis M, Si K, Kandel ER. Two previously undescribed members of the mouse CPEB family of genes and their inducible expression in the principal cell layers of the hippocampus. Proc Natl Acad Sci. 2003 Aug 5;100(16):9602–7.

259. Hu W, Yuan B, Lodish HF. Cpeb4-Mediated Translational Regulatory Circuitry Controls Terminal Erythroid Differentiation. Dev Cell. 2014 Sep;30(6):660–72.

260. Igea A, Méndez R. Meiosis requires a translational positive loop where CPEB1 ensues its replacement by CPEB4. EMBO J. 2010 Jul 7;29(13):2182–93.

261. Pavlopoulos E, Trifilieff P, Chevaleyre V, Fioriti L, Zairis S, Pagano A, et al. Neuralized1 Activates CPEB3: A Function for Nonproteolytic Ubiquitin in Synaptic Plasticity and Memory Storage. Cell. 2011 Dec;147(6):1369–83.

262. Belloc E, Méndez R. A deadenylation negative feedback mechanism governs meiotic metaphase arrest. Nature. 2008 Apr 2;452(7190):1017–21.

263. Ivshina M, Lasko P, Richter JD. Cytoplasmic Polyadenylation Element Binding Proteins in Development, Health, and Disease. Annu Rev Cell Dev Biol. 2014 Oct 11;30(1):393–415.

264. Wang X, Cooper NGF. comparative in Silico Analyses of Cpeb1–4 with Functional predictions. Bioinform Biol Insights. 2010;4:61–83.

265. Kim JH, Richter JD. RINGO/cdk1 and CPEB mediate poly(A) tail stabilization and translational regulation by ePAB. Genes Dev. 2007 Oct 15;21(20):2571–9.

266. Novoa I, Gallego J, Ferreira PG, Mendez R. Mitotic cell-cycle progression is regulated by CPEB1 and CPEB4-dependent translational control. Nat Cell Biol. 2010 May 4;12(5):447–56.

267. Burns DM, Richter JD. CPEB regulation of human cellular senescence, energy metabolism, and p53 mRNA translation. Genes Dev. 2008 Dec 15;22(24):3449–60.

268. Nagaoka K, Fujii K, Zhang H, Usuda K, Watanabe G, Ivshina M, et al. CPEB1 mediates epithelial-to-mesenchyme transition and breast cancer metastasis. Oncogene. 2016 Jun 2;35(22):2893–901.

269. Udagawa T, Swanger SA, Takeuchi K, Kim JH, Nalavadi V, Shin J, et al. Bidirectional Control of mRNA Translation and Synaptic Plasticity by the Cytoplasmic Polyadenylation Complex. Mol Cell. 2012 Jul;47(2):253–66.

270. Alexandrov IM, Ivshina M, Jung DY, Friedline R, Ko HJ, Xu M, et al. Cytoplasmic Polyadenylation Element Binding Protein Deficiency Stimulates PTEN and Stat3 mRNA Translation and Induces Hepatic Insulin Resistance. Ogawa W, editor. PLoS Genet. 2012 Jan 12;8(1):e1002457.

271. Chen P-J, Huang Y-S. CPEB2-eEF2 interaction impedes HIF-1α RNA translation. EMBO J. 2012 Feb 15;31(4):959–71.

272. Hägele S, Kühn U, Böning M, Katschinski DM. Cytoplasmic polyadenylation-element-binding protein (CPEB)1 and 2 bind to the HIF-1 α mRNA 3’-UTR and

modulate HIF-1α protein expression. Biochem J. 2009 Jan 1;417(1):235–46.

273. Turimella SL, Bedner P, Skubal M, Vangoor VR, Kaczmarczyk L, Karl K, et al. Characterization of cytoplasmic polyadenylation element binding 2 protein expression and its RNA binding activity. Hippocampus. 2015 May 23;25(5):630–42.

274. Fioriti L, Myers C, Huang Y-Y, Li X, Stephan JS, Trifilieff P, et al. The Persistence of Hippocampal-Based Memory Requires Protein Synthesis Mediated by the Prion-like Protein CPEB3. Neuron. 2015 Jun;86(6):1433–48.

275. Stephan JS, Fioriti L, Lamba N, Colnaghi L, Karl K, Derkatch IL, et al. The CPEB3 Protein Is a Functional Prion that Interacts with the Actin Cytoskeleton. Cell Rep. 2015 Jun;11(11):1772–85.

276. Zhang H, Zou C, Qiu Z, E F, Li Q, Chen M, et al. CPEB3-mediated MTDH mRNA translational suppression restrains hepatocellular carcinoma progression. Cell Death Dis. 2020 Sep 23;11(9):792.

277. Kojima S, Sher-Chen EL, Green CB. Circadian control of mRNA polyadenylation dynamics regulates rhythmic protein expression. Genes Dev. 2012 Dec 15;26(24):2724–36.

278. Maillo C, Martín J, Sebastián D, Hernández-Alvarez M, García-Rocha M, Reina O, et al. Circadian- and UPR-dependent control of CPEB4 mediates a translational response to counteract hepatic steatosis under ER stress. Nat Cell Biol. 2017 Feb 16;19(2):94–105.

279. Fernández-Alfara M, Sibilio A, Martin J, Tusquets Uxó E, Malumbres M, Alcalde V, et al. Antitumor T-cell function requires CPEB4-mediated adaptation to chronic endoplasmic reticulum stress. EMBO J. 2023 May 2;42(9):1–14.

280. Riechert E, Kmietczyk V, Stein F, Schwarzl T, Sekaran T, Jürgensen L, et al. Identification of dynamic RNA-binding proteins uncovers a Cpeb4-controlled regulatory cascade during pathological cell growth of cardiomyocytes. Cell Rep. 2021 May;35(6):109100.

281. Ortiz-Zapater E, Pineda D, Martínez-Bosch N, Fernández-Miranda G, Iglesias M, Alameda F, et al. Key contribution of CPEB4-mediated translational control to cancer progression. Nat Med. 2012 Jan 4;18(1):83–90.

282. Boustani MR, Mehrabi F, Yahaghi E, Khoshnood RJ, Shahmohammadi M, Darian EK, et al. Somatic CPEB4 and CPEB1 genes mutations spectrum on the prognostic predictive accuracy in patients with high-grade glioma and their clinical significance. J Neurol Sci. 2016 Apr;363:80–3.

283. Han T, Sun H, Wen X, Liu Z, Li S, WANG J-G, et al. Expression of CPEB4 in invasive ductal breast carcinoma and its prognostic significance. Onco Targets Ther. 2015 Nov;8:3499.

284. Hu W, Yang Y, Xi S, Sai K, Su D, Zhang X, et al. Expression of CPEB4 in Human Glioma and Its Correlations With Prognosis. Medicine (Baltimore). 2015 Jul;94(27):e979.

285. Zhong X, Xiao Y, Chen C, Wei X, Hu C, Ling X, et al. MicroRNA-203-mediated posttranscriptional deregulation of CPEB4 contributes to colorectal cancer progression. Biochem Biophys Res Commun. 2015 Oct;466(2):206–13.

286. Peng F, Xiao X, Jiang Y, Luo K, Tian Y, Peng M, et al. HBx Down-Regulated Gld2 Plays a Critical Role in HBV-Related Dysregulation of miR-122. Shih C, editor. PLoS One. 2014 Mar 25;9(3):e92998.

287. Giangarrà V, Igea A, Castellazzi CL, Bava F-A, Mendez R. Global Analysis of CPEBs Reveals Sequential and Non-Redundant Functions in Mitotic Cell Cycle. Jan E, editor. PLoS One. 2015 Sep 23;10(9):e0138794.

288. Pérez-Guijarro E, Karras P, Cifdaloz M, Martínez-Herranz R, Cañón E, Graña O, et al. Lineage-specific roles of the cytoplasmic polyadenylation factor CPEB4 in the regulation of melanoma drivers. Nat Commun. 2016 Nov 18;7(1):13418.

289. Lu R, Zhou Z, Yu W, Xia Y, Zhi X. CPEB4 promotes cell migration and invasion via upregulating Vimentin expression in breast cancer. Biochem Biophys Res Commun. 2017 Jul;489(2):135–41.

290. Sibilio A, Suñer C, Fernández-Alfara M, Martín J, Berenguer A, Calon A, et al. Immune translational control by CPEB4 regulates intestinal inflammation resolution and colorectal cancer development. iScience. 2022 Feb;25(2):103790.

291. Parras A, Anta H, Santos-Galindo M, Swarup V, Elorza A, Nieto-González JL, et al. Autism-like phenotype and risk gene mRNA deadenylation by CPEB4 mis-splicing. Nature. 2018 Aug 15;560(7719):441–6.

292. Kan M-C, Oruganty-Das A, Cooper-Morgan A, Jin G, Swanger SA, Bassell GJ, et al. CPEB4 Is a Cell Survival Protein Retained in the Nucleus upon Ischemia or Endoplasmic Reticulum Calcium Depletion. Mol Cell Biol. 2010 Dec 1;30(24):5658–71.

293. Suñer C, Sibilio A, Martín J, Castellazzi CL, Reina O, Dotu I, et al. Macrophage inflammation resolution requires CPEB4-directed offsetting of mRNA degradation. Elife. 2022 Apr 20;11:1–23.

294. Pell N, Garcia-Pras E, Gallego J, Naranjo-Suarez S, Balvey A, Suñer C, et al. Targeting the cytoplasmic polyadenylation element-binding protein CPEB4 protects against diet-induced obesity and microbiome dysbiosis. Mol Metab. 2021 Dec;54(November):101388.

295. Calderone V, Gallego J, Fernandez-Miranda G, Garcia-Pras E, Maillo C, Berzigotti A, et al. Sequential Functions of CPEB1 and CPEB4 Regulate Pathologic Expression of Vascular Endothelial Growth Factor and Angiogenesis in Chronic Liver Disease. Gastroenterology. 2016 Apr;150(4):982-997.e30.

296. Garcia-Pras E, Gallego J, Coch L, Mejias M, Fernandez-Miranda G, Pardal R, et al. Role and therapeutic potential of vascular stem/progenitor cells in pathological neovascularisation during chronic portal hypertension. Gut. 2017 Jul;66(7):1306–20.

297. Mejias M, Gallego J, Naranjo-Suarez S, Ramirez M, Pell N, Manzano A, et al. CPEB4 Increases Expression of PFKFB3 to Induce Glycolysis and Activate Mouse and Human Hepatic Stellate Cells, Promoting Liver Fibrosis. Gastroenterology. 2020 Jul;159(1):273–88.

298. Wei X, Chen Y, Jiang X, Peng M, Liu Y, Mo Y, et al. Mechanisms of vasculogenic mimicry in hypoxic tumor microenvironments. Mol Cancer. 2021 Jan 4;20(1):7.

299. Morales-Guadarrama G, García-Becerra R, Méndez-Pérez EA, García-Quiroz J, Avila E, Díaz L. Vasculogenic Mimicry in Breast Cancer: Clinical Relevance and Drivers. Cells. 2021 Jul 12;10(7):1758.

300. Andonegui-Elguera MA, Alfaro-Mora Y, Cáceres-Gutiérrez R, Caro-Sánchez CHS, Herrera LA, Díaz-Chávez J. An Overview of Vasculogenic Mimicry in Breast Cancer. Front Oncol. 2020 Feb 27;10.

301. Kim Y-N, Koo KH, Sung JY, Yun U-J, Kim H. Anoikis Resistance: An Essential Prerequisite for Tumor Metastasis. Int J Cell Biol. 2012;2012:1–11.

302. Wang D, Zhang L, Hu A, Wang Y, Liu Y, Yang J, et al. Loss of 4.1N in epithelial ovarian cancer results in EMT and matrix-detached cell death resistance. Protein Cell. 2021 Feb 25;12(2):107–27.

303. Kalluri R, Weinberg RA. The basics of epithelial-mesenchymal transition. J Clin Invest. 2009 Jun 1;119(6):1420–8.

304. Mani SA, Guo W, Liao M-J, Eaton EN, Ayyanan A, Zhou AY, et al. The Epithelial-Mesenchymal Transition Generates Cells with Properties of Stem Cells. Cell. 2008 May;133(4):704–15.

305. Hendrix MJC, Seftor EA, Hess AR, Seftor REB. Vasculogenic mimicry and tumour-cell plasticity: lessons from melanoma. Nat Rev Cancer. 2003 Jun 1;3(6):411–21.

306. Liu Q, Qiao L, Liang N, Xie J, Zhang J, Deng G, et al. The relationship between vasculogenic mimicry and epithelial-mesenchymal transitions. J Cell Mol Med. 2016 Sep 29;20(9):1761–9.

307. Sun B, Zhang D, Zhao N, Zhao X. Epithelial-to-endothelial transition and cancer stem cells: two cornerstones of vasculogenic mimicry in malignant tumors. Oncotarget. 2017 May 2;8(18):30502–10.

308. McDonald DM, Munn L, Jain RK. Vasculogenic Mimicry: How Convincing, How Novel, and How Significant? Am J Pathol. 2000 Feb;156(2):383–8.

UNIVERSITAT DE
BARCELONA